CHARACTERIZATION OF SPRAY DEPOSITED COLD ROLLED Al-Si-Pb ALLOYS

Ph.D. THESIS

by

RASHMI MITTAL

DEPARTMENT OF METALLURGICAL & MATERIALS ENGINEERING
INDIAN INSTITUTE OF TECHNOLOGY ROORKEE
ROORKEE-247667 INDIA
JULY, 2014

CHARACTERIZATION OF SPRAY DEPOSITED COLD ROLLED Al-Si-Pb ALLOYS

A THESIS
submitted in partial fulfilment of the
requirements for the award of the Degree
of
DOCTOR OF PHILOSOPHY
in
METALLURGICAL & MATERIALS ENGINEERING

by
RASHMI MITTAL

DEPARTMENT OF METALLURGICAL & MATERIALS ENGINEERING
INDIAN INSTITUTE OF TECHNOLOGY ROORKEE
ROORKEE-247667 INDIA
JULY, 2014

INDIAN INSTITUTE OF TECHNOLOGY ROORKEE
ROORKEE

CANDIDATE'S DECLARATION

I hereby certify that the work which is being presented in the thesis entitled "**Characterization of spray deposited cold rolled Al-Si-Pb alloys**" in partial fulfilment of the requirement for the award of the Degree of Doctor of Philosophy and submitted in the Department of Metallurgical & Materials Engineering of the Indian Institute of Technology Roorkee, Roorkee is an authentic record of my own work carried out during a period from July, 2010 to July, 2014 under the supervision of **Dr. Devendra Singh**, Associate Professor, Department of Metallurgical and Materials Engineering, Indian Institute of Technology Roorkee, Roorkee.

The matter presented in this thesis has not been submitted by me for the award of any other degree of this or any other Institute.

(RASHMI MITTAL)

This is to certify that the above statement made by the candidate is correct to the best of my knowledge.

(Devendra Singh)
Supervisor

Date:_____

The Ph.D. Viva-Voce Examination of **Miss Rashmi Mittal**, Research Scholar, has been held on……

Signature of Supervisor **Chairman, SRC** Signature of External Examiner

Head of the Deptt./Chairman, ODC

ABSTRACT

Al-Si-Pb systems are potential materials for bearing alloys because they possess superior performance like high hardness, good thermal conductivity, low wear rate, high corrosion resistance and low cost of production than other aluminum bearing alloys. Processing of these alloys by the conventional casting techniques is difficult due to liquid immiscibility and segregation of lead during melt solidification. To overcome these problems, spray deposition technique can be used which possesses several advantages like microstructural control together with producing a preform in a less number of processing steps. However, the major drawback of this technique is lower densification with poor mechanical properties. Therefore, the preform prepared by spray deposition technique must be further densified and deformed plastically in order to prepare fully dense metal sheets with improved mechanical properties. Rolling is most effective method used to densify the material because of having both hydrostatic and deviatoric components of the applied stress field. In present study Al-Si-Pb alloys were spray deposited in the form of a disc shape and then cold rolled to various percentages of thickness reductions. Further, their characteristics such as microstructure, porosity, hardness, wear and corrosion rate were studied.

The porosity, hardness, corrosion, wear and microstructural studies of the Al-Si-Pb spray deposited alloys were conducted from centre to periphery of the preform, for different lead content and for different percentage of thickness reduction. Microstructural analysis of worn surfaces and worn debris were also performed. Samples from the central and peripheral regions of the preform were cut down and then cold rolled to different thickness reductions for its microstructural study. The size of the aluminum grains was almost same at the top and centre regions of the deposit whereas it was lower at the peripheral region. The lead was uniformly dispersed in the deposit and higher fraction of lead was distributed along the grain boundaries. The size of lead particles was found to increase linearly with the increase in lead content. The size of these particles was also higher at the centre as compared to that of periphery of the preform. Grains were observed to be elongated in the rolling direction after 60 and 80 % thickness reductions and aspect ratio of Al-grains was increased with the increase in thickness reduction. Pore size was reduced with the increase in thickness reduction and it was almost eliminated after 80 % thickness reduction. However, it was increased with the increase in Pb content.

The porosity was measured for different percentage of thickness reductions at different locations of the preform. Two types of porosity were found in the samples, one was called as casting porosity and the other as crack porosity. The total porosity was decreased with the increase in thickness reduction however it was increased where the rate of increase in crack porosity was higher than the rate of decrease in casting porosity with the increase in thickness reduction. The porosity of the spray deposited alloy was found to decrease with the decrease in lead content and from centre to periphery of the preform. Also, it was unaffected along the thickness of the preform.

The hardness of the spray deposit was observed to increase with the increase in thickness reduction and it was decreased with the increase in lead content. Preform hardness was increased from centre to periphery of the deposit. Hardness was affected by the grain size and porosity of the preform. It was found to decrease with the increase in porosity and grain size of the deposit.

Friction and wear testing of spray deposited cold rolled samples were investigated using a pin on disk type wear testing machine. The spray deposited cold rolled samples with different lead content were machined into cylindrical pins having 5 mm diameter and 3 or 2.5 or 2 mm height. Wear rate behavior with applied load was observed to depict three stages, in the second stage rate of increase in wear rate was the lowest and in the third stage it was the highest. Also, the wear rate was decreased with the increase in thickness reduction irrespective of Pb content however it was increased where the porosity was increased. A linear relationship was found between wear rate and porosity of the samples. The wear rate was decreased from centre to periphery of the preform. It was decreased linearly with the increase in lead content up to 20 % and after that it was increased. The coefficient of friction was decreased rapidly up to the load of 30 N and beyond this load the friction coefficient was almost constant. The coefficient of friction was lowest for 20 % Pb content and it was decreased with the increase in thickness reduction. A linear relationship was observed between hardness and coefficient of friction of the samples.

Corrosion tests were performed in aqueous 3.5 % NaCl (analytical grade, 99.5% purity) solution. A conventional electrochemical flat bottom cell was used for electrochemical investigations and all potentiodynamic polarisation tests were performed in a potentiostat at ambient temperature at a scan rate of 0.166 mV/s. A Teflon O-ring sealed the sample to the cell exposing an area of 1 cm^2 to the solution. Corrosion rate was found to decrease with the

increase in thickness reduction however it was increased where the porosity was increased. Also, it was decreased with the increase in Pb content and also from centre to periphery of the preform.

ACKNOWLEDGEMENTS

I would like to extend my sincere gratitude to Dr. Devendra Singh, Associate Prof. for suggesting an interesting study, for his able guidance, for the informative discussions and for his assistance which made this work possible and successful.

I special vote of thank to all faculty and staff members for their kind cooperation given to me during my work.

I would like to express my gratitude for my parents, brother and sister for their encouragement, continuous and unconditional support throughout of my work.

My gratitude also goes to all my friends and colleagues who were always with me to support and encouragement.

I would also like to thank all those who directly and indirectly attached to me for their kind support given to me during my Ph.D.

Above all I want to dedicate my thesis to my Grandfather.

(RASHMI MITTAL)

CONTENTS

List of figures

List of tables

CHAPTER -1

INTRODUCTION

Finding out the suitable materials (alloy) with light in weight and low in cost of production for bearing applications is the need of today's research. It is necessary that a bearing material should have the following features [1]: (1) to allow hard particles to embed in the bearing material, (2) to accommodate slight misalignment in the bearing system, (3) to avoid damaging the counterface, (4) to support applied loads and (5) corrosion resistance for a longer service life [1, 2]. Most of the bearing materials contain two phases, one is a hard and strong phase and the other is a soft and ductile phase to satisfy these incompatible demands. Usually, hard metal elements such as Al and Cu are incorporated by soft metal elements such as Pb, Sn, Bi and In to produce the alloys for bearing applications [2]. Also, it is desirable that one of the constituent used in the bearing material should have a relatively low melting point [3]. Therefore, the majority of bearing alloys contain tin or lead. Al–Pb and Al–Sn bearing alloys have superior friction properties, low cost of production, high corrosion resistance and high thermal conductivity than other bearing alloys [4–7]. At present, Pb-containing Al alloys is verified as a promising candidate for replacing Al–Sn alloys because lead is soft, much cheaper and more freely available than tin. The wearing properties of Al-Pb alloy improved by adding the alloying elements such as Si, Cu, Sn and Mg [8]. But, a wide miscibility gap between Al and Pb arise a problem for the preparation of Al-Pb alloys using the conventional casting technique [9, 10]. Also, the presence of large density difference in a constituent phases of Al-Pb alloys are the additional issue [6,7].

The processing techniques effect on microstructure, density and stability of materials. Therefore, in the past several techniques like, powder metallurgy [11, 12], stir casting [13-17], rheocasting [18-20], melt spinning [21], strip casting [22] and spray deposition [23- 56] have been employed to prevent the segregation of Pb during melt solidification. These processing techniques have their own unique characteristics and influence over structures and properties of alloy. Out of these, the spray deposition technique has been widely used to produce tube, billet, plate, ring, etc. preforms with fine-grained, equiaxed and cellular microstructure. Rapid

solidification [57], less or no composition segregation in a less number of processing steps are the other advantages [23]. This technique was firstly developed by A. E. Singer at the university of Swansea in the 1970s [26]. Spray deposition is a method of casting metal components with homogeneous microstructure which are beyond the reach of conventional casting technique [58–64], via the deposition of semi-solid sprayed droplets on to a substrate. The resulting part exhibits a rapidly solidified microstructure with very refined grain sizes and greatly reduced levels of segregation [4]. Almost same steps are used in thermal spraying [65, 66] and metal spraying [67] process. There are few advantages arises through the rapid solidification process:

(1) Elimination of macro-segregation: Macrosegregation refers to variations in composition that occur in alloy castings or ingots having the range in scale from several millimeters to centimeters or even meters. These compositional variations have a detrimental impact on the subsequent processing behavior and properties of cast materials.

(2) Refined equiaxed grain structures: The mechanisms of grain refinement increases equiaxed grain proportion in the matrix alloys.

(3) Enhanced workability: workability related with the ability of alloy to be deformed.

There are two disadvantages of the spray deposition process.

(1) Relatively low process yield: The probability that a process will produce a defect free unit with typical losses of ~30%.

(2) Porosity: Porosity is a fraction of the volume of voids over the total volume.

The major drawback of spray deposited method is lower densification (porous) with poor mechanical properties [68]. In order to prepare fully dense metal sheets or alloy with high mechanical properties, the porous preform must be further densified and deformed plastically. The effective methods used to densify the material as well as to achieve the required mechanical properties are rolling [69-77], forging [78, 79], hot pressing [80], extrusion [81-85] etc. Out of these rolling is most effective method because of having both hydrostatic and deviatoric components of the applied stress field. The application of these components on porous materials causes flattening of pores and brings about rapid densification by collapsing the pores at a faster rate [56]. Deviatoric component of the applied stress field is more effective to remove the porosity from a porous part. In case of deviatoric or shear components of the stress, the pores finally collapses and even can disappear [86-88].

The rolling process is classified according to the temperature, if the temperature of the metal is above recrystallization temperature, then the process is called as hot rolling and if the

temperature of the metal is below recrystallization temperature, the process is termed as cold rolling. Among these two, cold rolling [89-95] is used to produce a smooth surface, reduces the yield point, improve the densification and provide a uniform thickness.

In the present work Al-Si-Pb alloys was spray deposited in a disc shape preform and then it was cold rolled. Characteristics such as microstructure, porosity, hardness, wear and corrosion were studied for different percentage reduction in thickness of this alloy. The entire work is divided into several chapters from 1 to 8. Next chapter (chapter-2) deals with the literature survey related to the work. Chapter-3 comprises of the problem formulation. Chapter-4 covers the experimental set-up and procedure carried out to attain aims of the present study. Chapter-5 consists of the results obtained and chapter-6 is on the discussion of the work. The conclusions and scope for future work are reported in chapter-7 and 8, respectively.

CHAPTER -2

LITERATURE REVIEW

This chapter is divided into the several sections to review on microstructural features, porosity, hardness, wear and corrosion behaviour of spray deposited and mechanically worked aluminum alloys.

2.1 Microstructural features of spray deposited Al alloys

Srivastava et al. [96] have investigated the microstructural characteristics and mechanical properties of spray deposited Al-Si alloys. The results invariably exhibited considerable microstructural refinement in spray deposited Al-6.5Si and Al-18Si alloys. The primary α-phase in Al-6.5Si alloy revealed spherical morphology in contrast to its dendritic morphology in the as cast alloy. The size of the primary Si phase varied from 3 to 7 μm in the spray deposited Al-18Si alloy against their size of 100-130 μm in the as cast alloy. Also, further refinement in the microstructure with reduced porosity of the preform achieved by hot extrusion. Spray deposited alloys exhibited high strength and ductility after hot extrusion compared to their counterparts as cast and extruded alloys. Ojha et al. [27] have also studied the microstructure of spray deposited Al-Si alloys. The grain size of the primary α-Al phase was 5-25 μm and Si particles size was 2-5 μm.

Anand et al. [31] spray deposit Al-Si alloy. They observed that the microstructure of a conventional ingot metallurgy processed alloy exhibited coarse Si particulates, of varying size, distributed randomly through the microstructure whereas the spray deposited alloy revealed fine particulate shaped Si dispersoids distributed uniformly through the microstructure and equiaxed shaped grains. Kaur et al. [97] prepared zircon sand reinforced spray deposited LM13 alloy. Wide difference in the morphology was observed for as cast alloy and spray processed composite. Equiaxed α-Al grains of 25-50 μm size was obtained in spray deposited composite, despite of dendritic growth of α-Al grains in ingot casted alloy. Moreover, hardness value was found to increase in spray processing route due to microstructural refinement of the composite by rapid solidification.

However, to observe the effect of Si and Sn content on Al, Anil et al. [98] also spray deposit Al-6.5Si, Al-12.5Si and Al-12.5Si-25Sn alloys in an environmental chamber using nitrogen gas at 1.0 MPa gas pressure and a deposition distance of 350 mm. The preforms were hot pressed at 350 ^{0}C for 2 h under a vacuum of the order of 10^{-6} Torr. The maximum length of needle-like Si was up to 25 μm, and the average grain size of α-Al was over 40 μm with segregated β-Sn phase.

Yu et al. [8] produced Al-Si-Pb alloys by liquid phase co-spray forming. Some deposit was extruded and then microstructure and mechanical properties were studied. An equi-axed microstructure was observed and the Pb particles were distributed uniformly in the Al-matrix. The average Al grain size was about 35 μm. The strength and ductility of the extruded Al-Si-Pb alloys were depended mainly on the Pb concentration: the greater the Pb content, the lower the strength and the higher the ductility. Rudrakshi et al. [6] also produced spray deposited Al-Si-Pb alloys. They observed that the primary α-phase exhibited an equiaxed grain morphology with grain size of 10-25 μm. The sizes of Si and Pb particles were 0.5-5 μm and 0.1-25 μm, respectively.

Characterization parameters values of spray deposited and mechanically worked spray deposited Al- alloys of various investigators are reported in **table 2.1**. The processes parameters include the alloy composition, spray deposited or mechanically worked spray deposited alloy and percentage reduction. The alloy characterization parameters include the microstructure of the alloy, its porosity, applied wear load, sliding speed during wear, wear rate, coefficient of friction, its hardness and corrosion potential.

2.2 Porosity of spray deposited alloys

Payne et al. [37] studied the relating porosity and mechanical properties in spray deposited tubulars. The experimental data showed that more porous materials tend to be weaker and softer than the less porous materials. The yield strength and UTS were almost have an inverse relationship with porosity.

The effects of processing parameters on porosity in spray deposited materials was investigated by Lavernia et al. [101]. They conclude that the level of porosity was influenced by melt superheat, deposition distance, atomization pressure and melt flow rate. Also, the variations in porosity with all these processing parameters were followed V-shaped curves.

Tripathy et al. [87] prepared the steel backed Al-10 wt% Sn strip by spray deposition. The strips were rolled to various thickness deformation in the range 20-75%. Porosity was

found to decrease and hardness was found to increase with percentage thickness deformation. A curious observation found during tension test was that the specimens, subjected to 60 and 75 % thickness deformation did not show any cracking in the deposit layer. Though, the specimens rolled to 40 % thickness deformation showed cracks.

Gui et al. [41] have examined the effect of porosity on dry sliding wear behaviour in spray deposited Al-6Cu-Mn/13 vol.%SiC_p composite in both as-sprayed and forged states. It was found that at lower loads, the pores beneath the worn surface of the as-sprayed composite were stable and could not propagate significantly. Thus, porosity displayed a very small influence on wear behaviour of the composite. At higher loads, the pores beneath the worn surface became unstable and the crack originated from these pores could propagate during wear process, which resulted in a higher wear rate.

The deformation behaviours of porous 4032 Al alloy preform prepared by spray deposition were studied by Zhan et al. [88]. They select the rolling processing to produce fully dense sheet from porous preform. It was seen that the variation in porosity after deformation was in good agreement with the strain distribution. Deshmukh et al. [86] have also analysed the cold densification rolling of a sintered porous metal strip. They demonstrate that there was exist a global minimum value for the rolling power that corresponds to proper densification and metal flow rate.

Tomar et al. [102] spray deposit a disk shape Al-Si-Pb alloy preform. Porosity of this disc was investigated as a function of Pb content. The porosity of the spray deposited alloy was increased with the increase in Pb content. Candan [103] has deliberate the effect of alloying additions on the porosity of SiC_p preforms infiltrated by aluminium. He also observed that the addition of Pb, increased the porosity while Cu, and Si addition did not effect it appreciably.

Table 2.1 Characterization parameters values of spray deposited and mechanically worked spray deposited Al-alloys of various investigators.

Reference	*Process Parameters*			*Micro structural features (μm)*			*porosity (%)*	*Wear*				*Hardness (VHN)*	*Corrosion*	
	Composition (wt%)	*Spray deposit / mechanical working of spray deposit*	*Reduction (%)*	*Al*	*Si*	*Pb*		*Load (N)*	*Sliding speed (m/s)*	*Rate ($m^3/mx10^{-13}$)*	*Friction coeff.*		*Medium*	*Corrosion potential (mV)*
87.	Al-Sn	Rolling of spray deposit	75				8					90		
41.	Al-Cu-Mn/Si Cp	Forging of spray deposit					Spray-4.6 Forged-0.8	5-400	1.2	Spray-57 at 250N Forged-50 at 400N				
6.	Al-Si-Pb	Spray deposit		10-25	0.5-5	0.1-25		10-90	1	7-45	0.22 - 0.57			

36.	Al-Pb Cu-Pb	Spray deposit		10-15		0.1-1		10-40		40				
27.	Al-Si	Spray deposit		5-25	2-5			10-60		18				
99.	Al-12Si, 20Si, 25Si	Spray deposit						8.9 17.8 26.7 35.6	0.48	3-18				
61.	Al-20Si	Spray deposit and as cast						8.9-35.6		10-ascast 8.5-spray deposit				
28.	Al-10Si-20Pb-3.5Cu	Spray deposit			<5	0.5-25			0.5-2	7.5-38.7	0.25 - 0.57			
98.	Al-Si-Sn	Spray deposit and hot pressed		40	1-2			10-80	1.15	2-7.5	0.2-0.5			
100.	Al-Li-Mg	Spray deposit											3.5 % NaCl	43

The microstructure and mechanical properties of a spray deposited and extruded AA7050 recycled alloy were studied by Godinho et al. [81]. They found that the hot extrusion at 425 ^{o}C reduced the porosity of the deposit from about 5.5 to less than 1 % promoting partial recrystallization.

The influence of both particle content and porosity on the tribological behaviour of Al (Mn)-Al_2O_3(MnO_2) composite were evaluated by Hamid et al. [104]. The wear rate of composites found to increased gradually with increasing porosity content due to its combined effect on real area of contact and subsurface crack propagation. However, the wear rate of composites with relatively lower porosity decreased with increasing particle content. No substantial effect of reinforcing particle or porosity content on the coefficient of friction could be identified.

Lin et al. [105] investigate the effect of porosity on the wear behaviour of the composite. The wear rate was increased with increasing porosity. It was observed that pores may even exert beneficial effect on wear resistance through trapping wear debris on the surface pores, which can decrease the contact pressure and reduce the possibility of particle agglomeration during sliding and formation of large abrasive agglomerates. Therefore, the composite containing low porosity showed excellent wear resistance. In addition, porosity has more important influence on wear rate at high load than at low load.

2.3 Wear behaviour of spray deposited Al samples

Wang et al. [61] compared the wear behaviour of a hypereutectic Al-Si alloy prepared by spray-deposition and conventional casting methods. The wear resistance of spray deposited alloy was better than the conventional cast one. The dominant wear mechanism was oxidative and delamination for the spray-deposited and conventional cast one alloy, respectively. Also, the effect of spray deposition process on the tribological performance of hyper-eutectic Al-Si alloys was reported by Raghukiran et al. [52]. They found that the spray deposited hyper-eutectic Al-Si alloys have shown superior wear performance in contrast to similar alloys produced through other processing routes.

Ojha et al. [27] worked on the shape, microstructure and wear of spray deposited hypoeutectic Al-Si alloys. They conclude that the shape of the spray deposit could be controlled by rotation and inclination of the substrate with respect to the spray axis. The wear rate of the alloys increased with the applied load. However, the wear rate initially decreased with speed of the rotation disc up to 0.75 m/s and beyond this speed it increases. Rudrakshi et

al. [6] have studied the wear characteristics of spray deposited Al-Si-Pb alloys. It was found that the wear properties of the spray deposited alloys were affected by the microstructural features.

Wear characteristics of spray deposited liquid immiscible alloys were studied by Gouthama et al. [36]. They observed that the microstructure of spray deposited hypo-monotectic Cu-20Pb alloy exhibited an equiaxed grain morphology of the primary phase with a uniform dispersion of lead particles in the matrix. Also, Cu-Pb alloy showed a low wear rate than Al-based alloys.

Anil et al. [98] have seen the influence of tin content on tribological characteristics of spray deposited Al-Si alloys. It was found that Al-12.5Si-25Sn alloy showed the higher wear resistance compared to that of Al-6.5Si and Al-12.5Si alloys. The SEM of worn surfaces and the debris particles of the alloys revealed that Al-Si alloys were prone to wear than the Al-Si-Sn alloy. The wear behaviour of cast and mushy state rolled Al-4.5Cu alloy and in-situ Al-4.5Cu-5TiB_2 composite were studied by Herbert et al. [106]. Both the mushy state rolled alloy and the composite have shown lower wear rates compared to that observed when those were in as cast condition. Also, wear rates of the mushy state rolled alloy and composite showed strong correlation with hardness and the wear rates of the composite decreased with increasing thickness reduction. Mondal and Das [107] also observed that hardness of the materials played a significant role in controlling their wear resistance. The wear rate decreased linearly with increase in hardness.

Rudrakshi et al. [28] observed the microstructural development in spray deposited Al-3.5Cu-10Si-20Pb alloy and its comparative wear behaviour in different environmental conditions. It was observed that the thickness and the coverage of the lead film controlled the wear behaviour of the alloys in two different conditions. The ultrafine thickness and maximum spreading of the lead film in vacuum resulted in higher resistance to wear and large reduction in coefficient of friction. Bauri et al. [108] have studied the sliding wear behaviour of Al-Li-SiC_p composites in ass-extruded and peak-aged conditions using a pin-on-disk machine. At lower loads, wear debris was finer and at higher load coarser plate-like debris was generated. In peak-aged condition, proportion of plate like coarse debris was higher compared to extruded condition.

2.4 Corrosion behaviour of Al samples

Moore et al. [100] have studied the pitting corrosion of spray deposited Al-Li-Mg alloys. They conclude that the overall refinement of the microstructural scale provided by the spray deposition process did not have either a beneficial or detrimental effect on corrosion behaviour.

The electrochemical and corrosion behaviour of cold rolled AISI 301 in 1 M H_2SO_4 were studied by Barbucci et al. [109]. The intergranular corrosion was observed as the main phenomenon that was occurred. It was also reported that the important changes in the microstructure was promoted by cold working. Ramachandra et al. [110] have seen the effect of reinforcement of flyash on sliding wear, slurry erosive wear and corrosion behaviour of Al-matrix composite. They observed that the resistance to corrosion was good in unreinforced composite specimens. Formation of oxide layer was also visible within 24 h of commencement of test.

Ahlatci [111] has worked on the wear and corrosion behaviour of extruded Al-12Si-XMg alloys. They investigate that the microstructure of the alloy was consisted of the Si needles and Mg_2Si precipitates in the Al matrix, while in the microstructure of the Mg free alloy the Mg_2Si type intermetallic precipitation was not detected. The Mg addition increased the size and amount of Mg_2Si precipitates, which was accompanied by an increase in hardness and wear resistance but a decrease in corrosion resistance.

The corrosion performance of Al-Si-Cu hypereutectic alloys in a synthetic condensed automotive solution were studied by Santos et al. [112]. It was found that the alloy with higher copper content and prepared by spray processing was more susceptible to pitting compared to the other alloys.

CHAPTER -3

Problem Formulation

After going through the literature critically, the scope of the problem and objectives of the present study have been formulated which are as follows:-

1. To cold roll the spray deposited preform to increase its density.
2. To study the microstructure of Al-Si-Pb preform of different compositions for different thickness reductions.
3. To study the porosity variation in Al-Si-Pb preform of different compositions for different thickness reductions.
4. To study the hardness of the Al-Si-Pb preform of different compositions for different thickness reductions.
5. To study the tribological properties like wear rate, coefficient of friction of the Al-Si-Pb preform of different compositions for different thickness reductions.
6. To study the corrosion behavior of the Al-Si-Pb preform of different compositions for different thickness reductions.

In present study, the composition and the process used to develop the alloy is significantly different from that of the literature.

CHAPTER -4

EXPERIMENTAL SET-UP and PROCEDURE

This chapter consists of three main parts viz. (1) spray deposition of Al-Si-Pb alloys (2) cold rolling of spray deposited Al-Si-Pb alloys and (3) characterization of the spray deposited cold rolled samples. **Fig. 4.1** revealed the schematic flow diagram of experimental work.

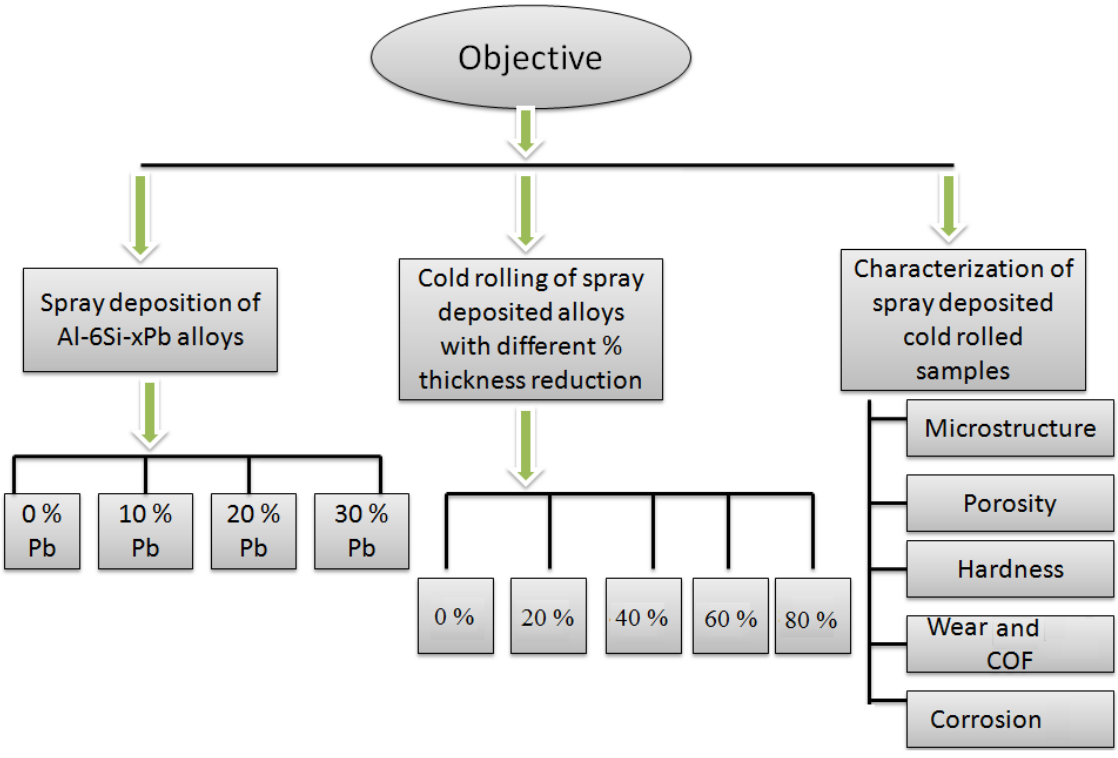

Fig.4.1 Schematic flow diagram of experimental work.

4.1 SPRAY DEPOSITION OF Al-Si-Pb ALLOYS

A spray deposition set-up is schematically shown in **fig.4.2**. The whole set-up consisted of a graphite crucible, an induction furnace, a graphite melt delivery tube, a stopper rod, an atomizer, a N_2 gas cylinder and a spray chamber. The alloy was permitted to melt into a graphite crucible placed inside an induction furnace as shown in the figure. A graphite melt delivery tube was fitted at the centre of the bottom of crucible to produce melt flow stream in down word direction. A stopper rod was used to either open or close the entrance of the delivery tube to restrict the melt. Other end of this delivery tube was fitted into the atomizer which was placed above the cooling chamber. Design of atomizer is described in section 4.1.1. Height of cooling chamber was 1500 mm. The stopper rod was raised up after starting the gas flow in atomizer to start the atomization of melt and thereby spray deposition. The high energy gas jet interacts with vertically falling liquid metal stream at the tip of melt delivery tube which induces the atomization of melt into small size droplets. The atomization takes place inside the cooling or spray chamber and atomized droplets were deposited over a copper substrate which can be placed at a different distances from the atomizer. Copper substrate can be inclined at desired angle from the horizontal axis and also can be rotated at varying rpm to get a uniform shape of preform. Overspray powder was collected over a tray placed at the bottom of cooling chamber.

The base alloy used in the present work consisted of Al-Si alloy having 6% Si. The alloy was super-heated to 200^0 C above its melting temperature in graphite crucible using an induction furnace. Different amount of Pb and Al were added in this Al-Si alloy to make Al-6Si-xPb (where, x= 0, 10, 20 and 30) alloys. In each run 800 gm of Al-Si-Pb alloy was taken in the crucible. For avoiding the oxide formation nitrogen gas was used for atomization prior to melt flow. The atomization was carried out at a N_2 gas pressure of 1 MPa. The details of the process variables are given in **table 4.1**. The spray droplets were deposited over a rotating (240 rpm) copper substrate which was inclined to 30^o to achieve a disc shape preform. This preforms was taken out of the substrate after deposition.

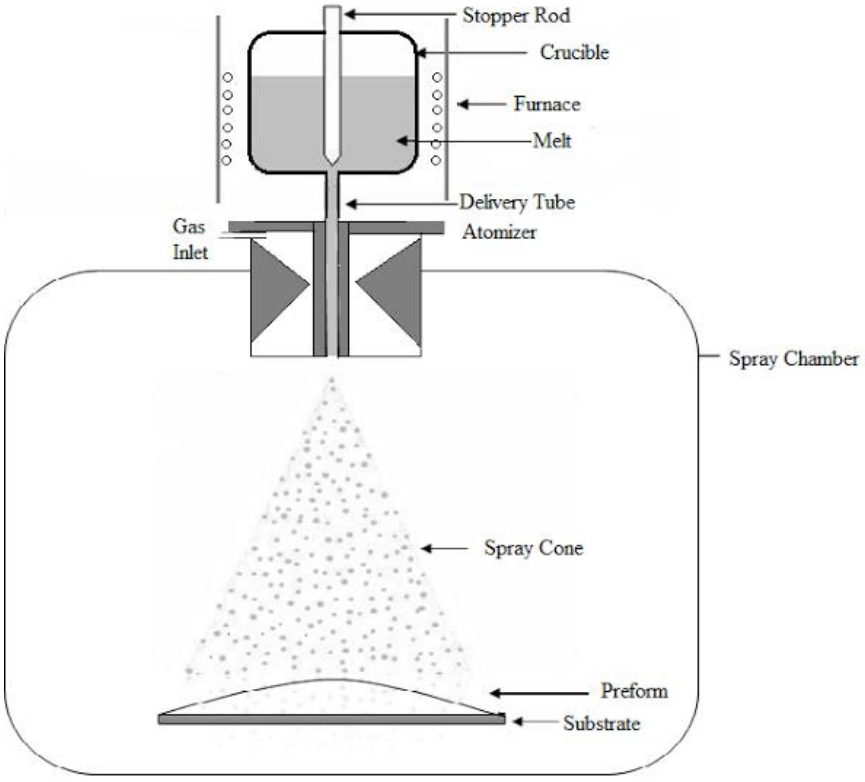

Fig.4.2 Schematic of spray deposition.

4.1.1 Atomizer design

The design of an atomizer used in present study is shown in **fig.4.3** and its photograph is shown in **fig.4.4**. This atomizer falls in the category of confined type atomizer in which gas interact with the melt as it leaves the melt delivery tube. But, the design is slightly different from that of the conventional confined type atomizer. In conventional atomizer opposite axes of annular slit or discrete nozzles intersect at a common point, whereas in the present nozzle axes are parallel i.e. they do not intersect. Therefore, in convectional design gas compress the melt stream towards its central line or axis of atomizer. Whereas, in present case the gas stream will be parallel to the melt stream or it will not compress the melt stream. The outer and inner diameters at the throat are 16 and 18 mm, respectively and hence the throat width is 1.0 mm which is required to calculate the maximum mass flow rate through the atomizer.

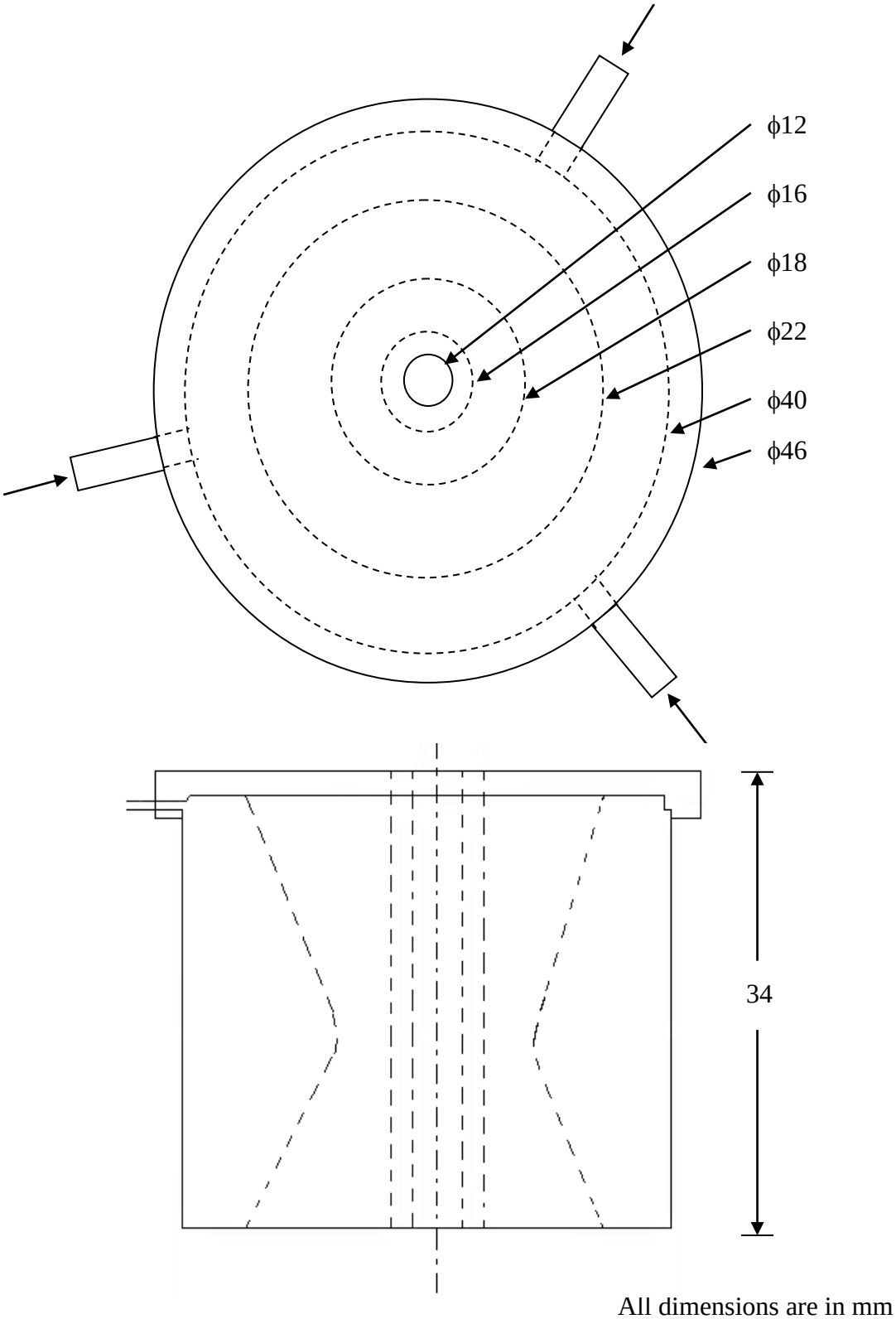

Fig. 4.3 Design of the atomizer.

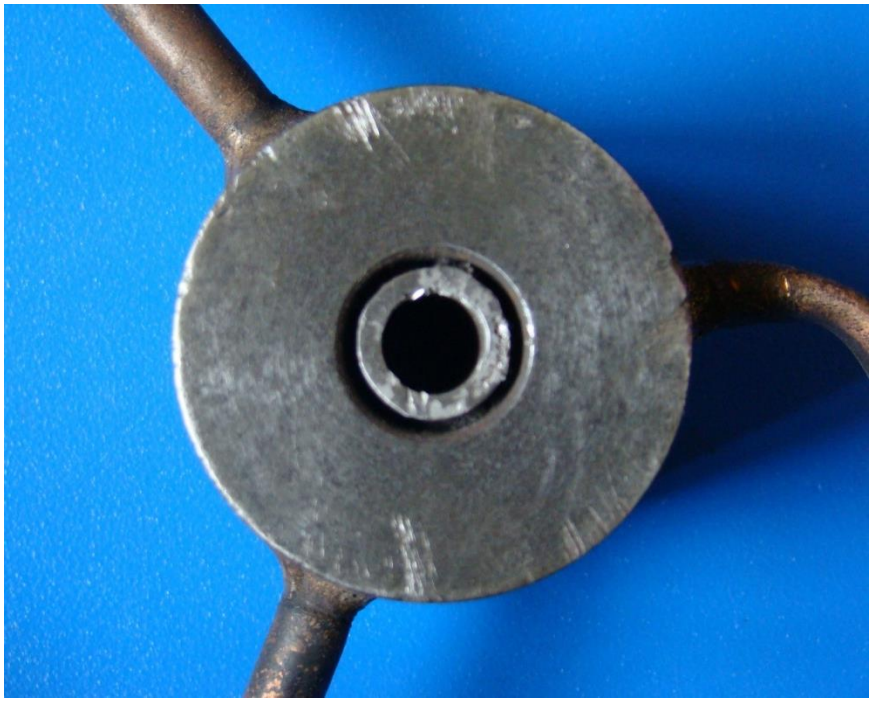

Fig. 4.4 Photograph of atomizer used in spray deposition technique.

Table 4.1 Values of various variables used in present study.

Variables Used	**Values of the Variables**
Weight of alloy taken for each run	800 gm
Melt delivery tube diameter	5 mm
Substrate thickness	8 mm
Substrate diameter	200 mm
Substrate rotational speed	240 rpm
Nitrogen gas plenum pressure	1 MPa
Melt temp	860 ^{0}C
Angle of the substrate	30 deg
Distance from substrate to atomizer	400 mm

The objective of the work is to characterize the spray deposited cold rolled Al-Si-Pb alloys and hence different compositions of Pb in Al-6Si alloy were added to study the characteristics of the spray deposit.

4.2 Cold rolling of spray deposited Al-Si-Pb alloys

The spray deposited Al-Si-Pb alloys were further processed via cold rolling process. The schematic of two high rolling mill is shown in **fig 4.5**. The arrangement consists of two rolls rotating in the one direction having diameter of 110 mm with maintained speed of 8 rpm. However, the number of passes through the rolls itself induces the thickness reduction of spray deposit. Therefore, thickness reduction was performed with number of repeated passes through rolls. The experimental thickness reductions at various passes are tabulated in **table 4.2** and conducted studies of different alloy composition with different thickness reductions are given in **table 4.3**.

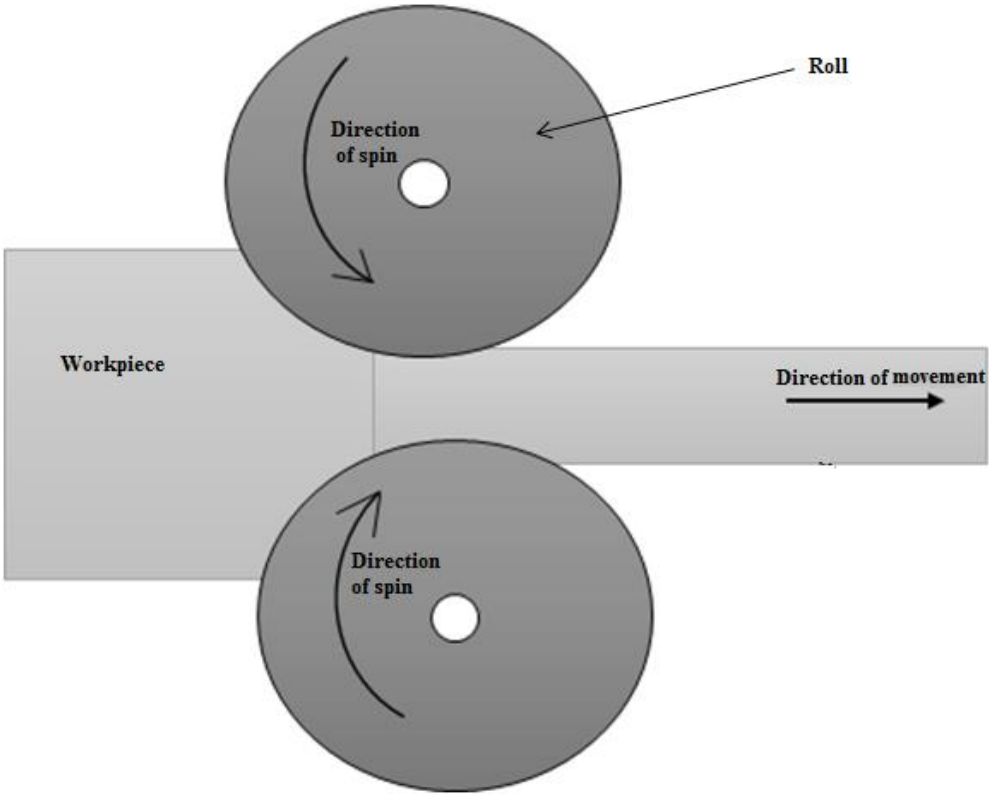

Fig.4.5 Schematic of Two high rolling mill.

Table 4.2 Values of experimental thickness before and after cold rolling.

Initial thickness (mm)	No. of passes	Final thickness (mm)	Final reduction (%)
7.75	4	6.16	20
7.83	9	4.71	40
7.25	15	2.88	60
7.42	20	1.49	80

Table 4.3 Conducted studies of different alloy composition with different thickness reductions.

Conducted study (Spray deposit)	Alloy compositions (wt %)	Thickness reduction (%)
Porosity	Al-6Si-(0-30)Pb	0,20,40,60 & 80
Microstructure	Al-6Si-(0-30)Pb	0,20,40,60 & 80
Hardness	Al-6Si-(0-30)Pb	0,20,40,60 & 80
Corrosion rate	Al-6Si-(0-30)Pb	0,20,40,60 & 80
Wear rate	Al-6Si-(0-30)Pb	0,20,40,60 & 80
SEM	Al-6Si-0Pb	0,40 & 80
	Al-6Si-20Pb	0, 60 & 80
EDX	Al-6Si-20Pb	0 & 80
XRD	Al-6Si-(0-30)Pb	0
	Al-6Si-20Pb	0,20,40,60 & 80

4.3 Spray Deposit Cold Rolled Characterization

Cold rolled preform (spray deposit) was characterized by microstructure, porosity, elemental analysis (EDX), phase analysis (XRD), hardness, tribological properties like wear rate & coefficient of friction, and corrosion rate.

4.3.1 Microstructure

Samples from the central and peripheral regions of the preform (as shown in **fig.4.6**) were cut down and then cold rolled to different thickness reductions for its microstructural study. These samples were polished using standard metallographic technique of polishing with an emery paper of 1/0, 2/0, 3/0 and 4/0 specification and then followed by wheel cloth polishing using an emulsion of alumina powder particles suspended in water. Afterwards these samples were polished by kerosene oil and brasso. Then samples were etched with Keller's reagent and examined with Letiz optical microscope and scanning electron microscope. Scanning electron microscope was operated at an accelerating voltage of 20-25 kV and a working distance of 9-11 mm in secondary electron mode. Phases present in spray deposited Al-6Si-20Pb alloy preform were examined by (EDX) energy dispersive x-ray analysis technique.

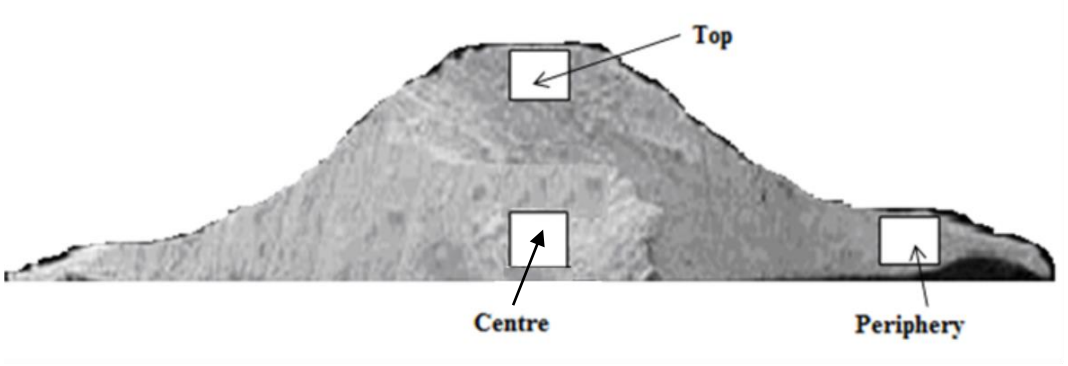

Fig 4.6. Sample locations for microstructural study of the preform.

4.3.2 Porosity

To measure the total porosity, samples were cut from different locations of spray deposit as shown in **fig.4.7** having 0, 10, 20 and 30% Pb and cold rolled to 0, 20, 40, 60 and 80% thickness reduction. These samples were examined for surface porosity by image analysis using the optical microscope 'Olympus model PM-3-311U' in conjunction with a computer having image analysis software from 'Dewinter material plus'. The total porosity was calculated [102] from the following equation.

$$Total\ Porosity = 1 - \frac{Measured\ density\ of\ sample}{Theoretical\ density\ of\ sample} \qquad (4.1)$$

The measured density was determined by Archimedes principle (explained in appendix A) and followed the ASTM B 328-96 practice. Mean values of three measurements were taken and hence the observed values are equal to mean ± δ. The value of δ was found to vary between 0.004 to 0.01 gm/cc. Procedure to determine theoretical density is also reported in appendix A.

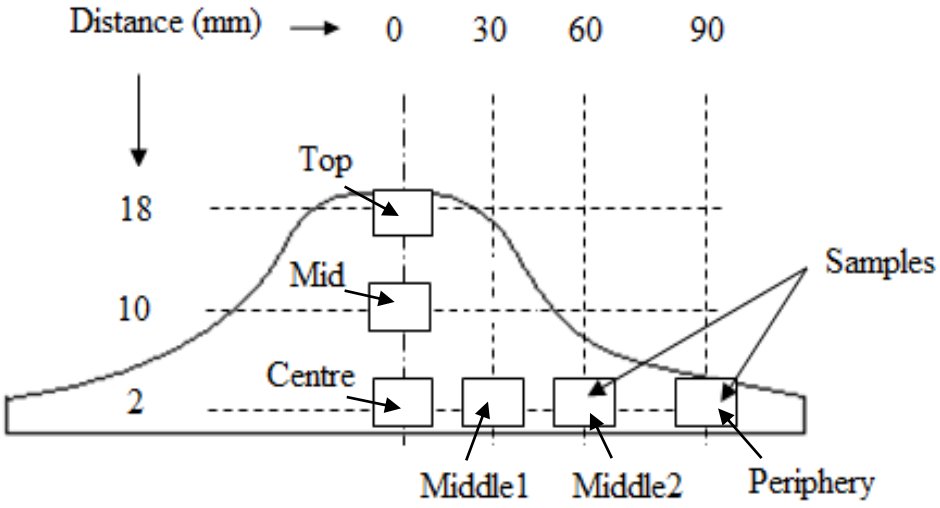

Fig.4.7 Locations of samples cut from spray deposit for porosity measurements.

4.3.3 XRD analysis

XRD analysis of spray deposit for different composition of Pb viz. 0, 10, 20 and 30% in Al-6Si alloy for 0 % thickness reduction and in Al-6Si-20Pb alloy for different thickness reduction viz. 0, 20, 40, 60 and 80 % was carried out by Bruker D8 Advanced X-Ray diffractometer, using Cu target and Ni filter. Diffraction angle (2θ) was varied from 20 to 100^0 in step of 0.05 deg. The Goniometer speed was 2^0/min.

4.3.4 Hardness

Samples for hardness investigation were cut down from central and peripheral regions of preform of different lead contents i.e. 0, 10, 20 & 30 as shown in **fig.4.8** and then cold rolled to different thickness reductions viz. 0, 20, 40, 60, 80%. Before commencement of test, samples were ground and polished using standard metallographic technique. A Brinell-cum- Vicker's

hardness tester of model HPO 250 was used to measure the Vicker hardness at 5 kg load. Indentations were taken at different points of central and peripheral regions of each sample as shown in **fig.4.9**.

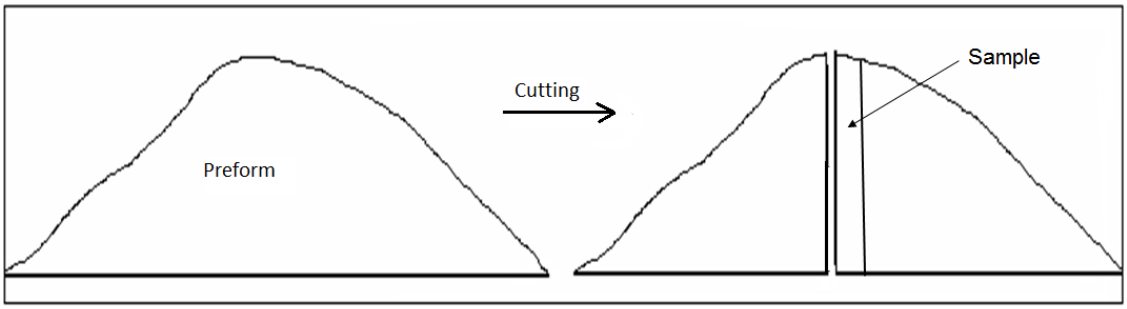

Fig.4.8 Cutting of sample in strip form from preform for hardness study.

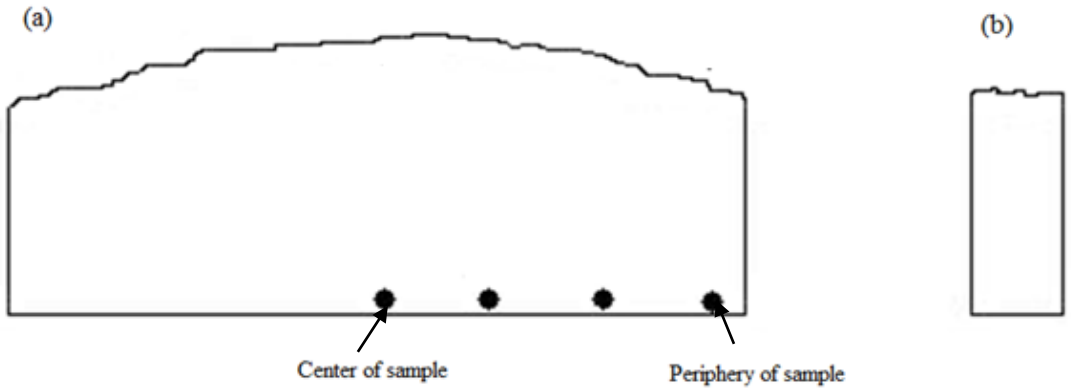

Fig.4.9 (a) Front and (b) Side view of sample cut from the preform for hardness study.

4.3.5 Wear testing

The spray deposited cold rolled samples with different lead contents were machined into cylindrical pins having 5 mm diameter and 3 or 2.5 or 2 mm height. In order to ensure that all the specimens had similar surface topography, all specimens were mechanically polished with

SiC papers and then thoroughly degreased by acetone and dried before the commencement of each wear test.

A pin-on-disc wear apparatus was used for wear and friction testing of spray deposited cold rolled samples. It consisted of a hardened EN-24 steel disc and a specimen holder. The diameter, surface roughness and Rockwell hardness of this steel disc were 12 cm, 0.4-0.5 μm and 57 HRC, respectively. Wear test specimen was mounted in the specimen holder. The load on the specimen was applied by placing a load on the opposite side of a fulcrum of the lever attached to the specimen holder. The samples were run for a period of 25 minutes before determining their weight loss which was used to find the resultant wear volume. Rotation speed of the disk and the radius of rotation were kept constant at 2 m/s and at 36.5 mm, respectively throughout the investigation. Sliding distance for one run comes out to be around 3000 m for this radius. The standard wear test procedure was followed for evaluating the wear rate for different load ranging from 10 to 50 N. All the tests were carried out in dry sliding conditions and at room temperature. The disc surface was cleaned with acetone before each experiment. Pin specimens were weighed both before and after testing on a single pan electrical balance that gave reading to 0.01 mg. The worn surfaces of the wear pins and the debris generated during wear experiments were examined by using JEOL JXA840A scanning electron microscope (SEM) after the test.

4.3.6 Corrosion testing

Before the test, all the samples were ground progressively upto 800 grit SiC paper followed by cloth polishing with 10 μm alumina paste. Finally, the samples were ultrasonically cleaned in acetone for 5 min to remove any grease and rinsed with distilled water. All the tests were performed in a 3.5% NaCl solution (analytical grade, 99.5% purity) at room temperature. The solution was naturally aerated and unstirred.

A conventional electrochemical flat bottom cell was used for electrochemical investigations and all the polarization tests were performed on a potentiostat (Model 2263, Princeton Applied Research, USA) at a scan rate of 0.166 mV/s. Platinum gauze was used as a counter electrode. The electrode potential was measured with respect to a standard saturated calomel electrode (SCE), whose standard reduction potential is E_{SCE} = +241 mV at 25 ºC. All the data were plotted with reference to SCE. The sample to the cell of 1 cm^2 area was exposed to the test solution. The open circuit potential (OCP) was determined before polarizing the test samples in freely aerated 3.5% NaCl solution after stabilizing the same for 1 h. The samples were

polarized in the scan range of ±250 mV with respect to the open circuit potential (OCP) in freely aerated 3.5 % NaCl solution. OCP values were determined before polarizing the test electrode. All the experiments were repeated three times in order to ensure reproducibility.The corroded surfaces were examined using optical microscopy and JEOL JXA840A scanning electron microscopy (SEM).

CHAPTER -5

RESULTS

This chapter consists of results on microstructure, porosity, hardness, wear rate and corrosion rate of spray deposited cold rolled Al-6Si-(0-30)Pb alloys. These results were taken for different parameters viz. sample locations on the preform, Pb variation in the preform and percentage thickness reduction of the samples.

5.1 Microstructure

Optical micrographs of Al-Si-Pb spray deposited cold rolled samples are shown in **figs. 5.1** to **5.12** having different sample locations, i.e. either top, centre or peripheral and different Pb content, i.e. either 0, 10, 20 or 30 % at five different thickness reductions viz. (a) 0, (b) 20, (c) 40, (d) 60 and (e) 80 percent.

Fig. 5.1 shows the microstructure of spray deposited Al-6Si (i.e. without Pb) alloy for different thickness reductions of the samples taken from the top region. The microstructure for 0 % thickness reduction (**fig. 5.1(a)**) shows fine equiaxed grain morphology with a uniform distribution of Si phase in an Al-matrix. The gray contrast region in the microstructure corresponds to Si phase whereas the bright region is that of Al phase (as revealed by EDS in **fig. 5.13**). The Si phase is present within the grains and along the grain boundaries. The sizes of Al grains and Si particles are 15-25 and submicron to 5 μm, respectively. Some irregular pores of 10-20 μm can also be seen in the matrix. After rolling grains are elongated in the rolling direction with the thickness reduction as can be seen in **fig. 5.1(b, c, d & e)**. Therefore, it's better to express the grain size in terms of aspect ratio. The aspect ratio of Al-grains increases with the increase in thickness reduction as shown in **fig 5.1(b)** to **5.1(d)**. This ratio is 1.2-1.4 (**fig. 5.1(b & c)**) and 1.6-2.2 (**fig. 5.1(d & e)**) for 20, 40 and 60, 80 % thickness reduction, respectively.

Microstructure at centre and peripheral regions of spray deposited Al-6Si alloy for different thickness reductions is shown in **figs. 5.2** and **5.3**, respectively. It can be seen that the size of the aluminum grains at the centre region (**fig. 5.2**) is almost same as that of the top (**fig. 5.1**)

whereas it is lower at the peripheral (**fig. 5.3**). Pore size is also lower at peripheral region. In **fig. 5.3(a)**, the size of Al grains and pores is 10-20 and 10-15 µm, respectively. In **fig. 5.3(b & c)** and **(d & e)**, the aspect ratio of Al-grains is 1.2-1.8 and 1.8-2.6, respectively.

Similarly, the effect of thickness reductions on the microstructure of spray deposited Al-6Si-10Pb alloy at top, centre and peripheral regions is shown in **figs. 5.4** to **5.6**, respectively. In these figs., the dark black color represents the Pb phase (as depicted by EDS in **fig. 5.13**). It can be seen that the Pb distribution is almost uniform throughout the aluminum phase. In **fig. 5.4(a)** which is for 0 % thickness reduction, the size of Pb particles is submicron to 5 µm. The aspect ratio of Al-grains at both, top and centre (**figs. 5.4** and **5.5**) regions is 1.6-2.2 and 2.0-2.5 for 20, 40 and 60, 80 % thickness reduction, respectively. At peripheral region (**fig. 5.6**), the size of Pb particles is submicron to 4 µm (**fig. 5.6(a)**) and the aspect ratio of Al-grains is 1.2-1.5 (**fig. 5.6(b & c)**) and 1.5-2.5 (**fig. 5.6(d & e)**) for 20, 40 and 60, 80 % thickness reduction, respectively. It can be observed that the aspect ratio is lower for peripheral region as compared to that of the other regions.

The change in microstructure of spray deposited Al-6Si-20Pb alloy for different thickness reductions at top, centre and peripheral regions is shown in **figs. 5.7** to **5.9**, respectively. In **fig. 5.7(a)**, the size of Pb particles is submicron to 10 µm. It can be seen that the size of Pb particles increases with the increase in Pb content of the alloy. The aspect ratio of Al-grains at both, top and centre (**figs. 5.7** and **5.8**) regions is 1.2-1.7 and 1.5-2.5 for 20, 40 and 60, 80 % thickness reduction, respectively. In bottom region (**fig. 5.8**), the size of Pb particles remains the same as that of top (**fig. 5.7**), whereas it is lower at the periphery (**fig. 5.9**). At peripheral region, the size of Pb particles is submicron to 8 µm (**fig. 5.9(a)**) and the aspect ratio of Al-grains is 1.2-1.5 (**fig. 5.9(b & c)**) and 1.5-2.5 (**fig. 5.9(d & e)**) for 20, 40 and 60, 80 % thickness reduction, respectively.

Microstructure of spray deposited Al-6Si-30Pb alloy for different thickness reductions at top, centre and peripheral regions is shown in **figs 5.10** to **5.12**, respectively. In **fig. 5.10(a)**, the size of Pb particles is submicron to 15 µm. The aspect ratio of Al-grains at both, top and bottom (**figs. 5.10** and **5.11**) regions is 1.2-1.7 and 2.0-2.7 for 20, 40 and 60, 80 % thickness reduction, respectively. The aspect ratio of Al-grains and the size of Pb particles in centre region (**fig. 5.11**) remains the same as that of the top.

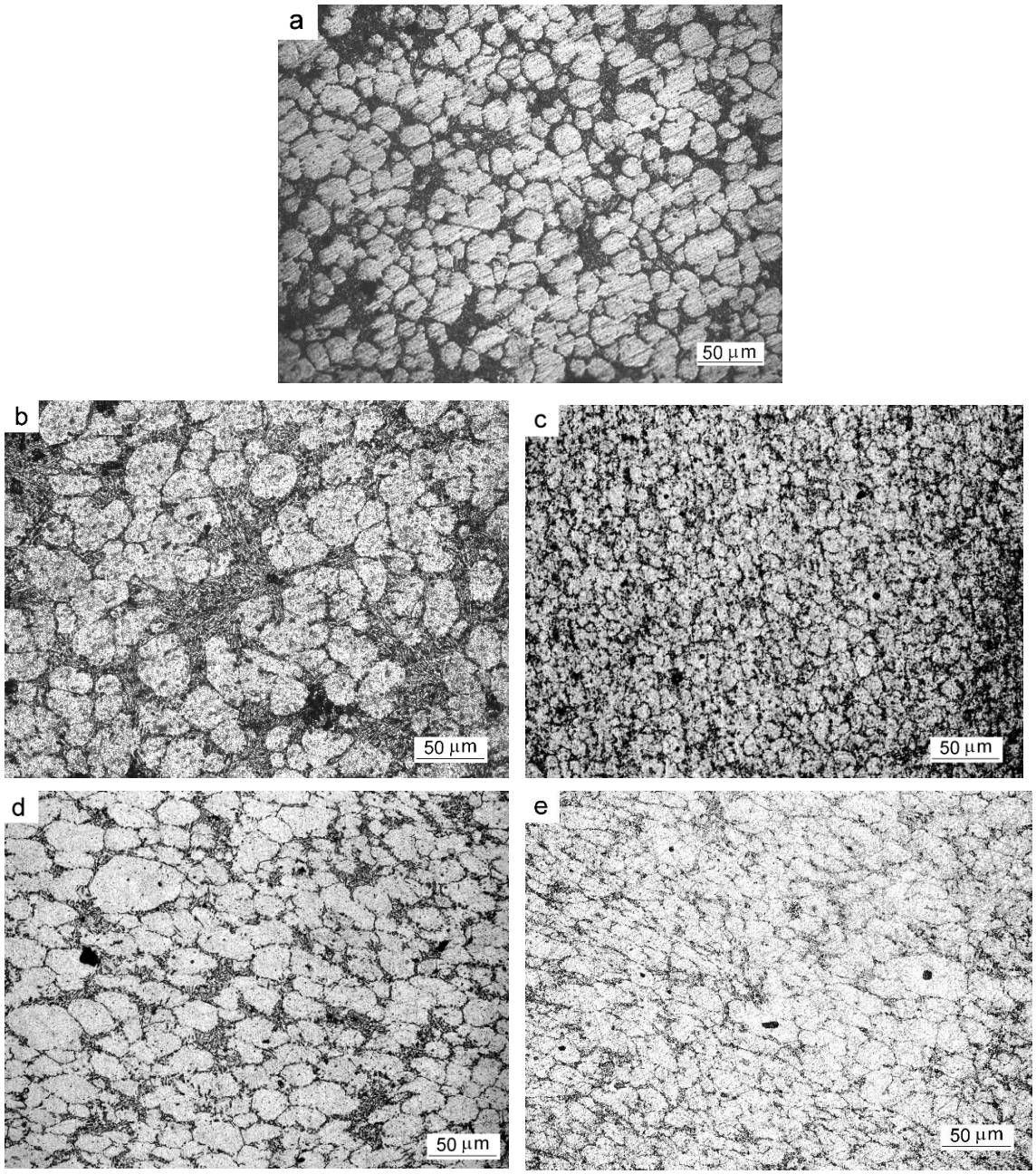

Fig. 5.1 Microstructure at top region of spray deposited Al-6Si alloy for (a) 0; (b) 20; (c) 40; (d) 60 and (e) 80 % thickness reduction.

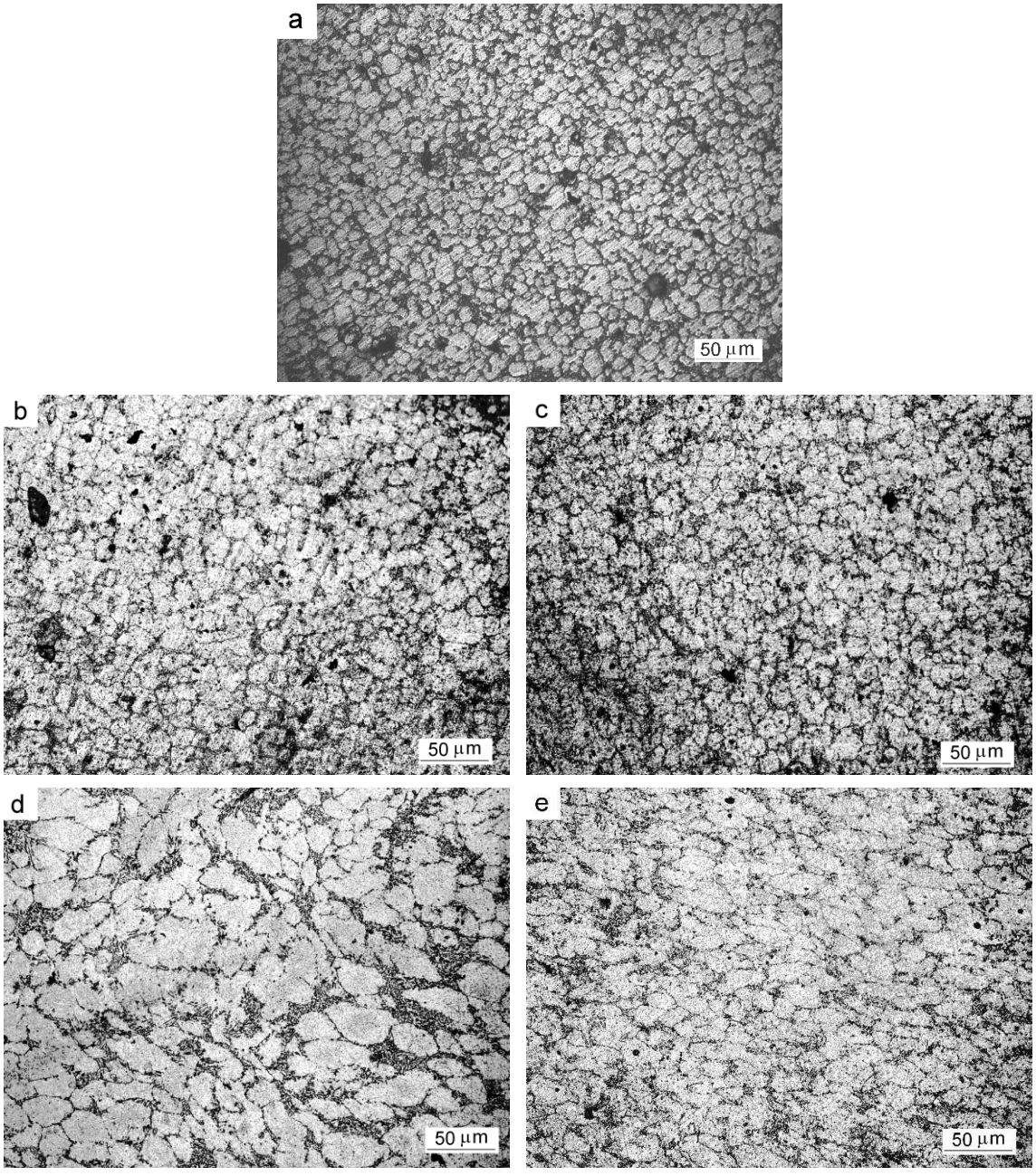

Fig. 5.2 Microstructure at centre region of spray deposited Al-6Si alloy for (a) 0; (b) 20; (c) 40; (d) 60 and (e) 80 % thickness reduction.

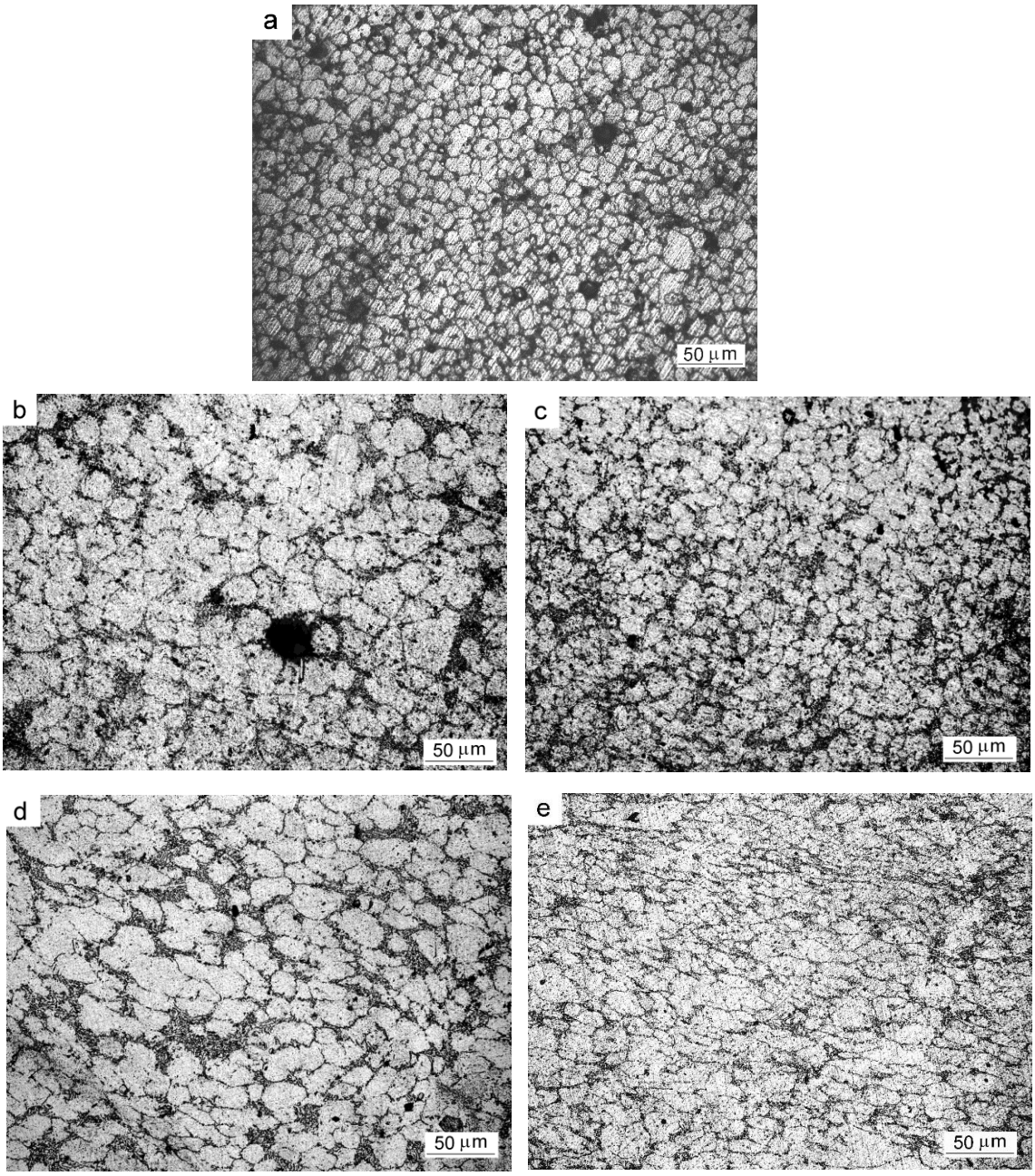

Fig. 5.3 Microstructure at peripheral region of spray deposited Al-6Si alloy for (a) 0; (b) 20; (c) 40; (d) 60 and (e) 80 % thickness reduction.

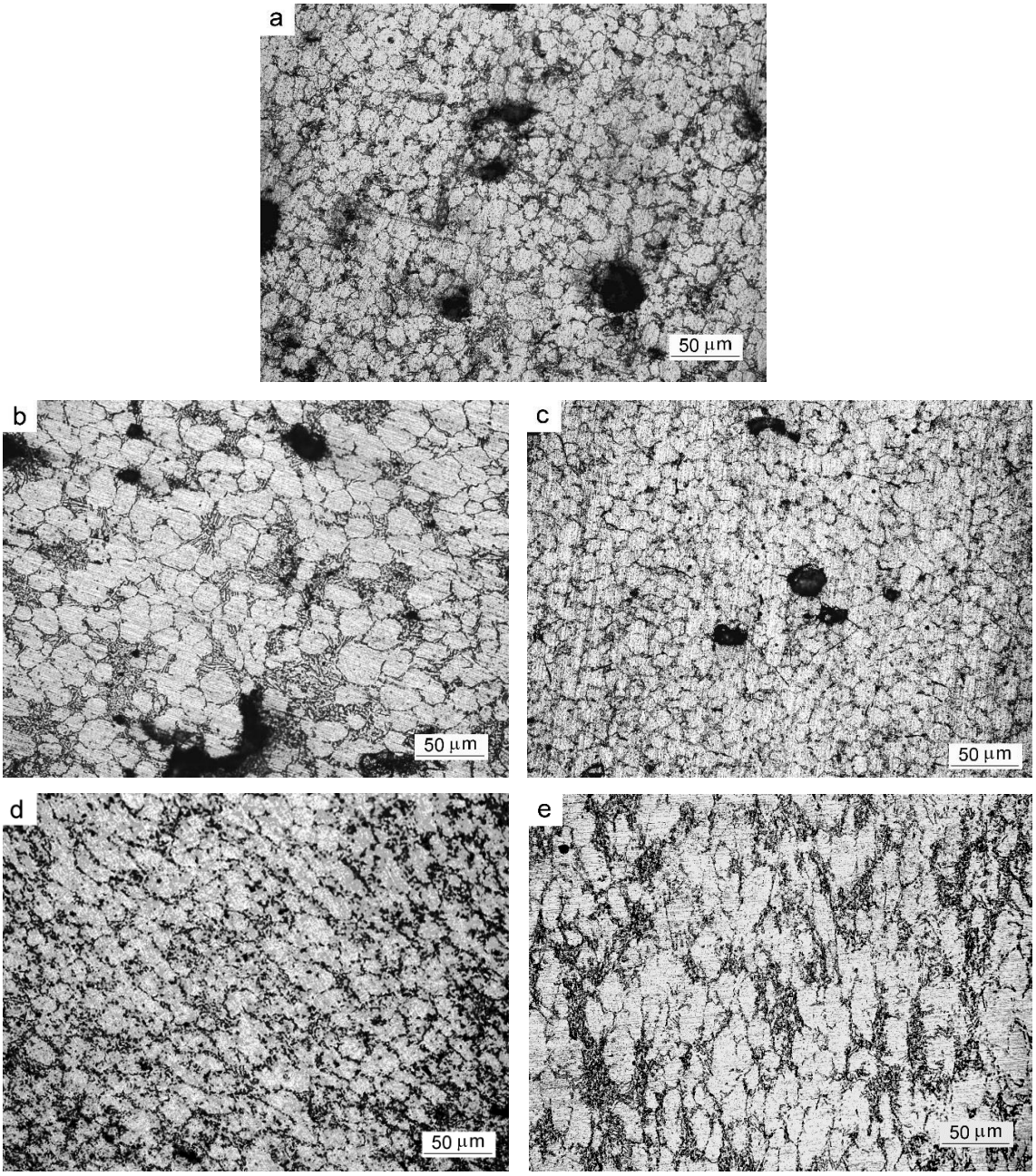

Fig. 5.4 Microstructure at top region of spray deposited Al-6Si-10Pb alloy for (a) 0; (b) 20; (c) 40; (d) 60 and (e) 80 % thickness reduction.

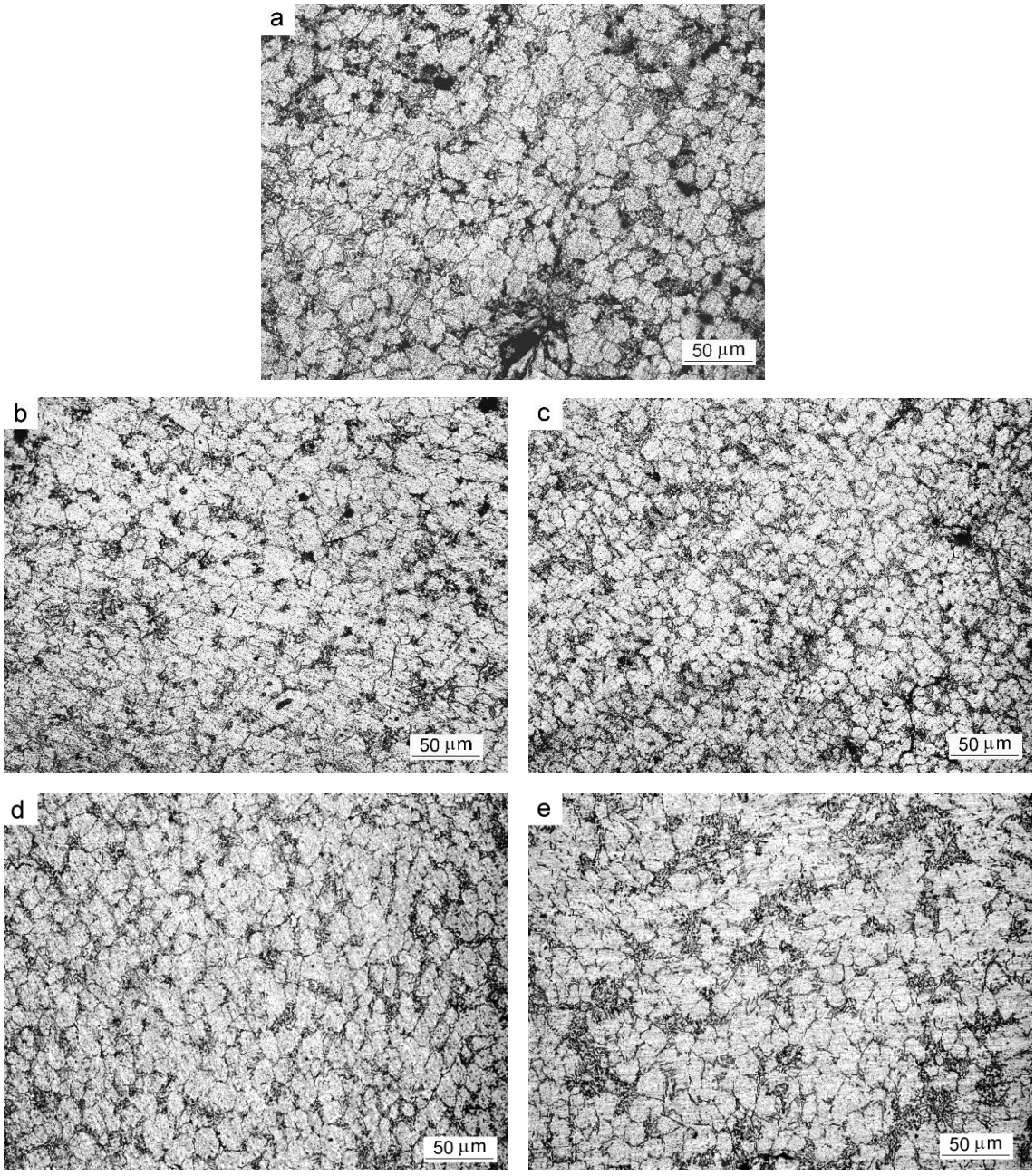

Fig. 5.5 Microstructure at centre region of spray deposited Al-6Si-10Pb alloy for (a) 0; (b) 20; (c) 40; (d) 60 and (e) 80 % thickness reduction.

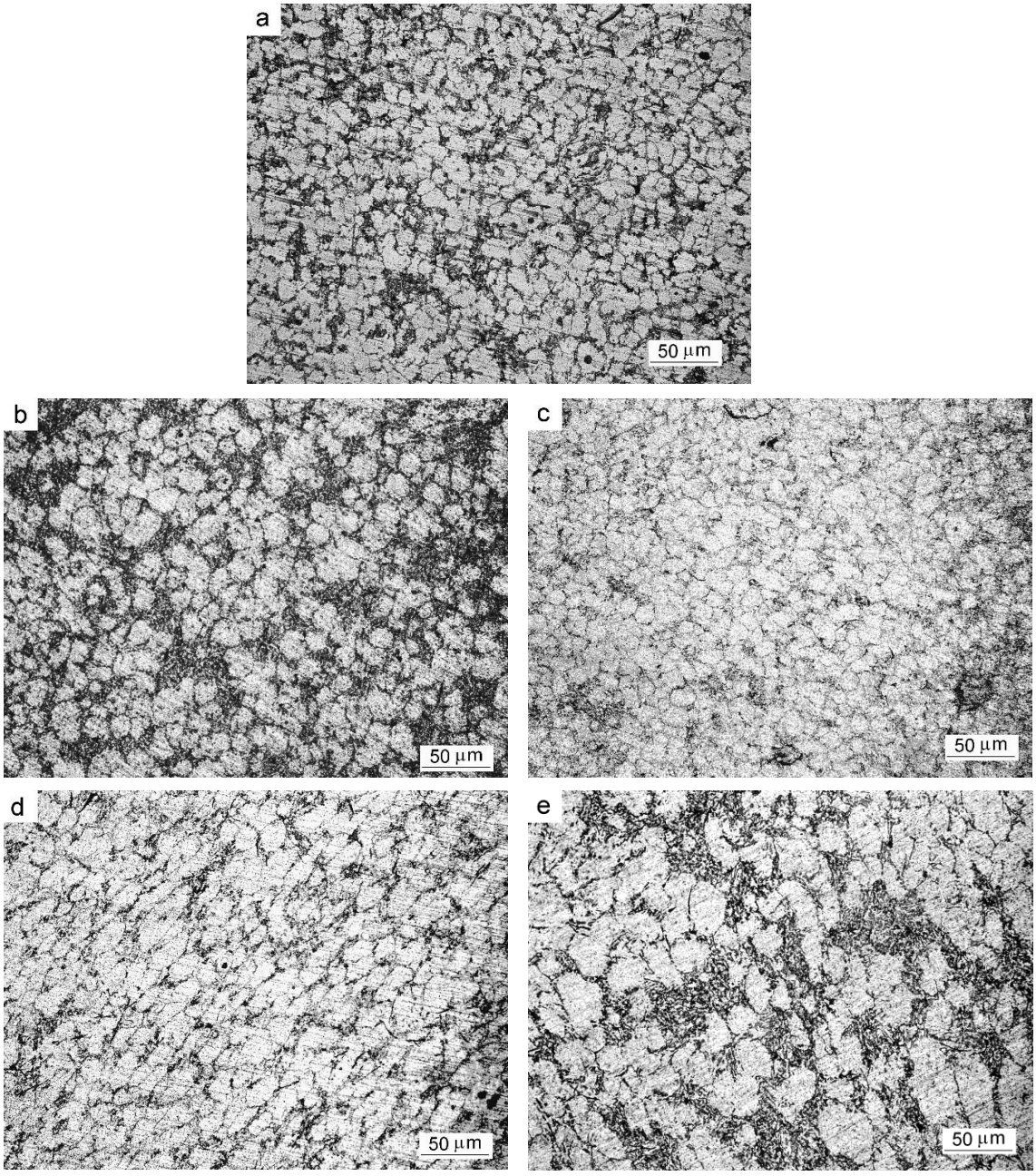

Fig. 5.6 Microstructure at peripheral region of spray deposited Al-6Si-10Pb alloy for (a) 0; (b) 20; (c) 40; (d) 60 and (e) 80 % thickness reduction.

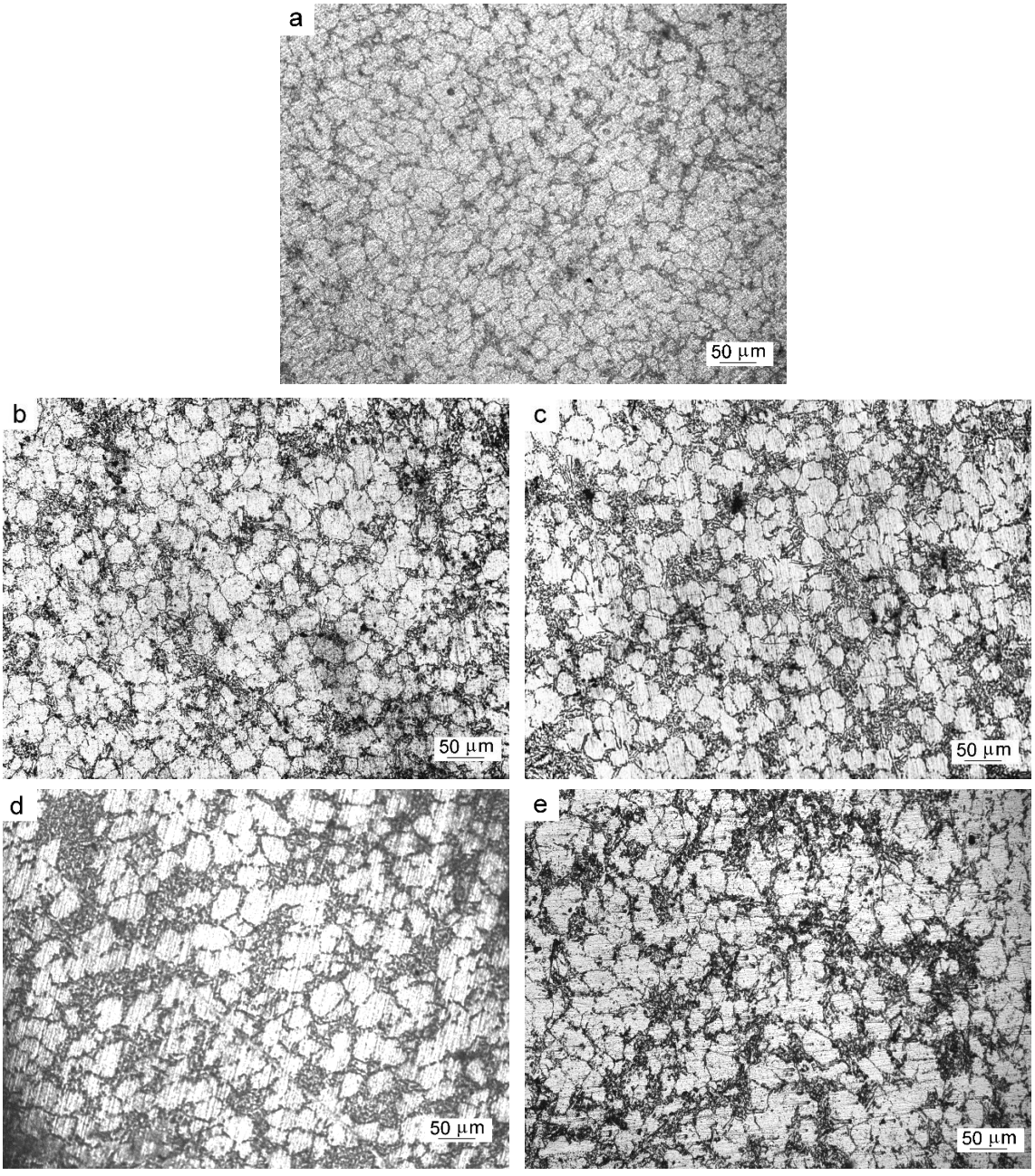

Fig. 5.7 Microstructure at top region of spray deposited Al-6Si-20Pb alloy for (a) 0; (b) 20; (c) 40; (d) 60 and (e) 80 % thickness reduction.

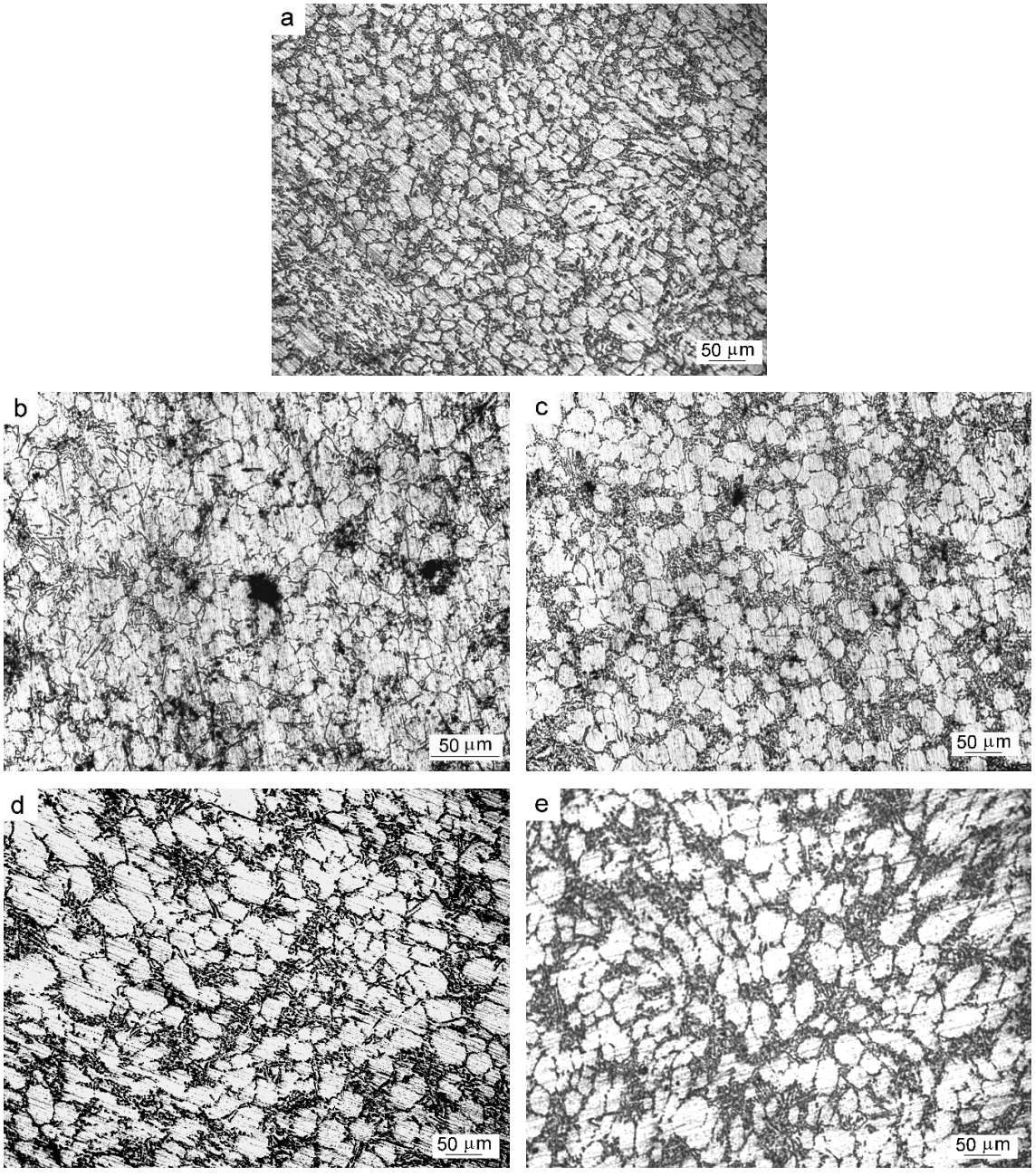

Fig. 5.8 Microstructure at centre region of spray deposited Al-6Si-20Pb alloy for (a) 0; (b) 20; (c) 40; (d) 60 and (e) 80 % thickness reduction.

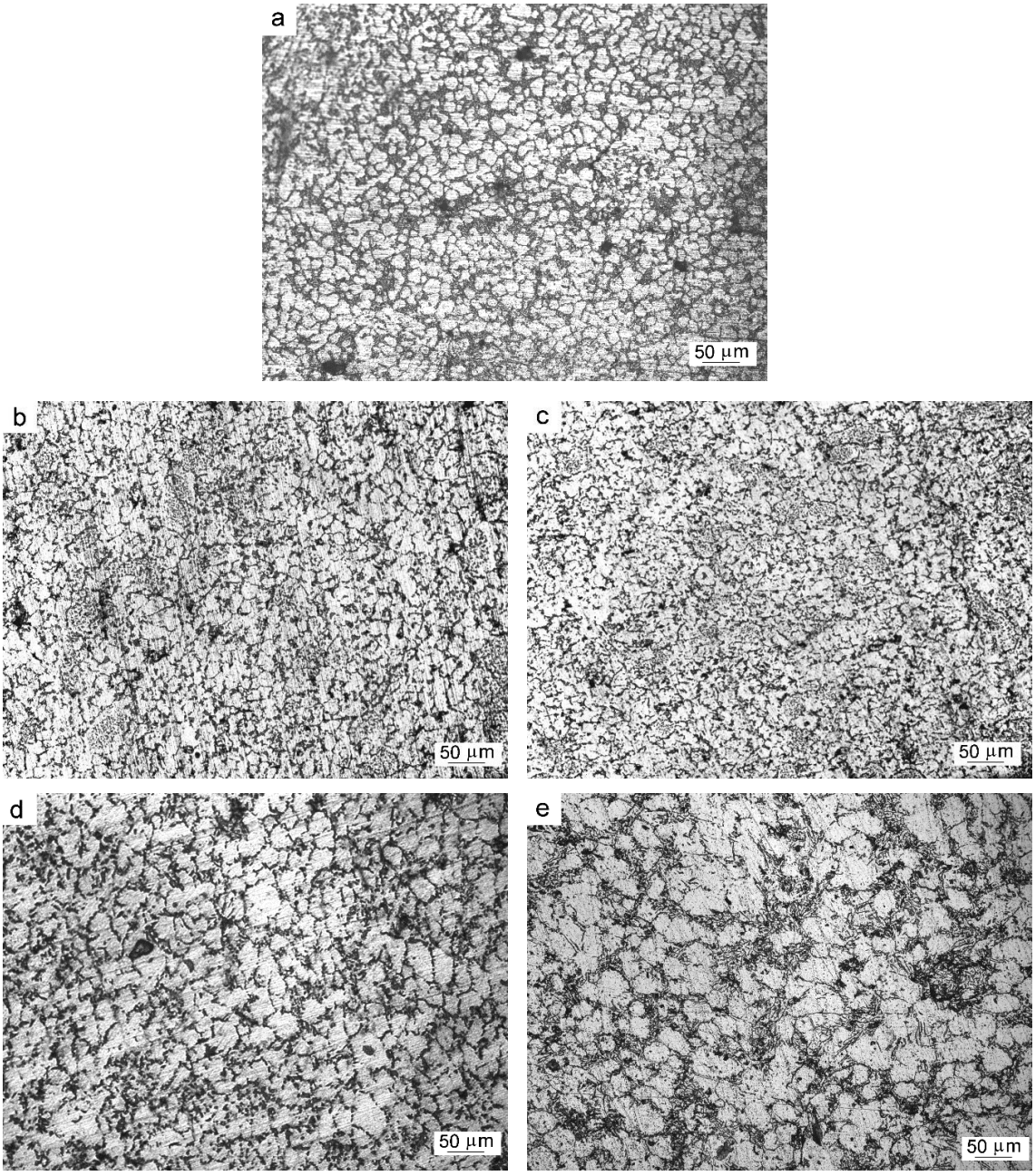

Fig. 5.9 Microstructure at peripheral region of spray deposited Al-6Si-20Pb alloy for (a) 0; (b) 20; (c) 40; (d) 60 and (e) 80 % thickness reduction.

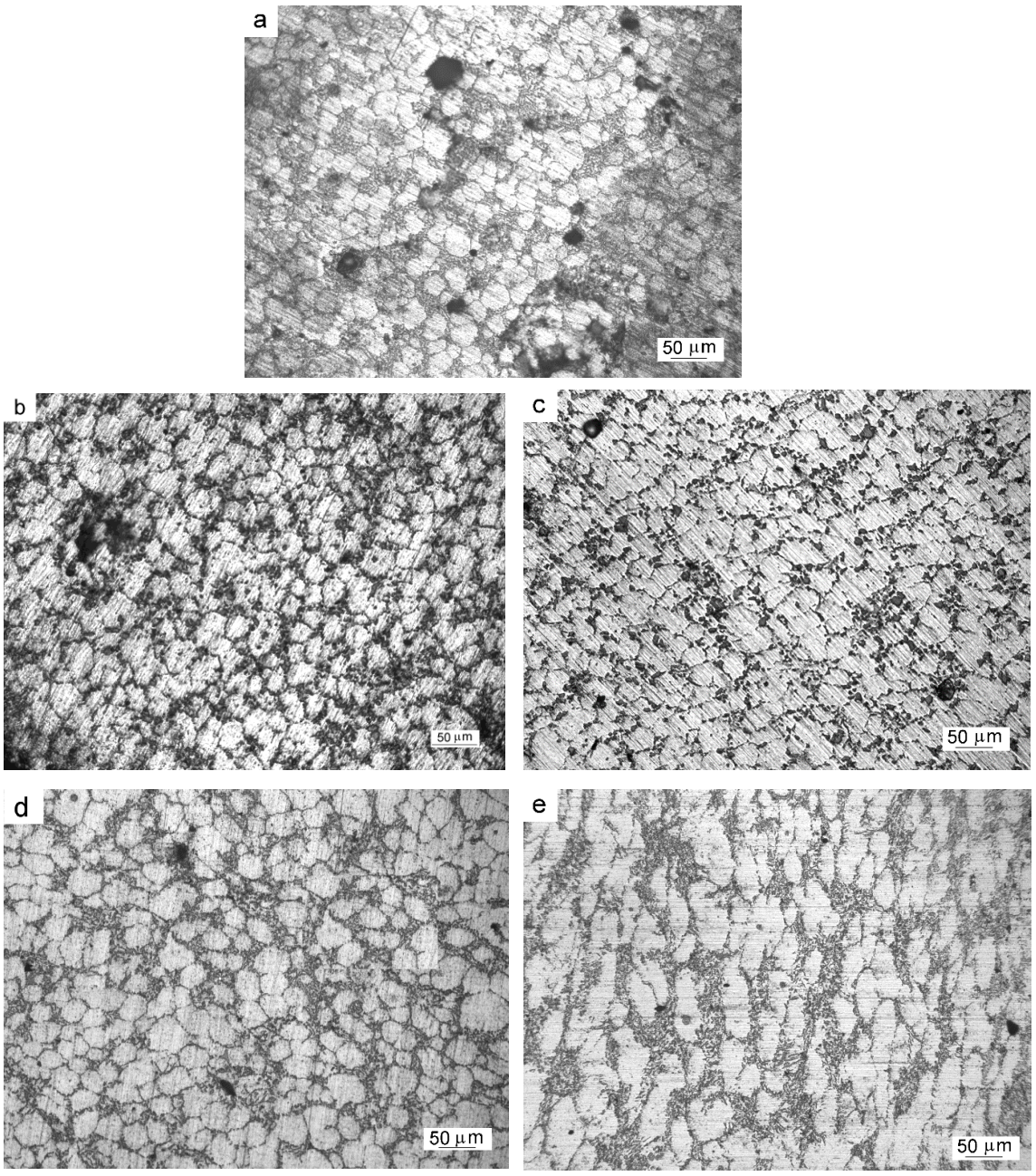

Fig. 5.10 Microstructure at top region of spray deposited Al-6Si-30Pb alloy for (a) 0; (b) 20; (c) 40; (d) 60 and (e) 80 % thickness reduction.

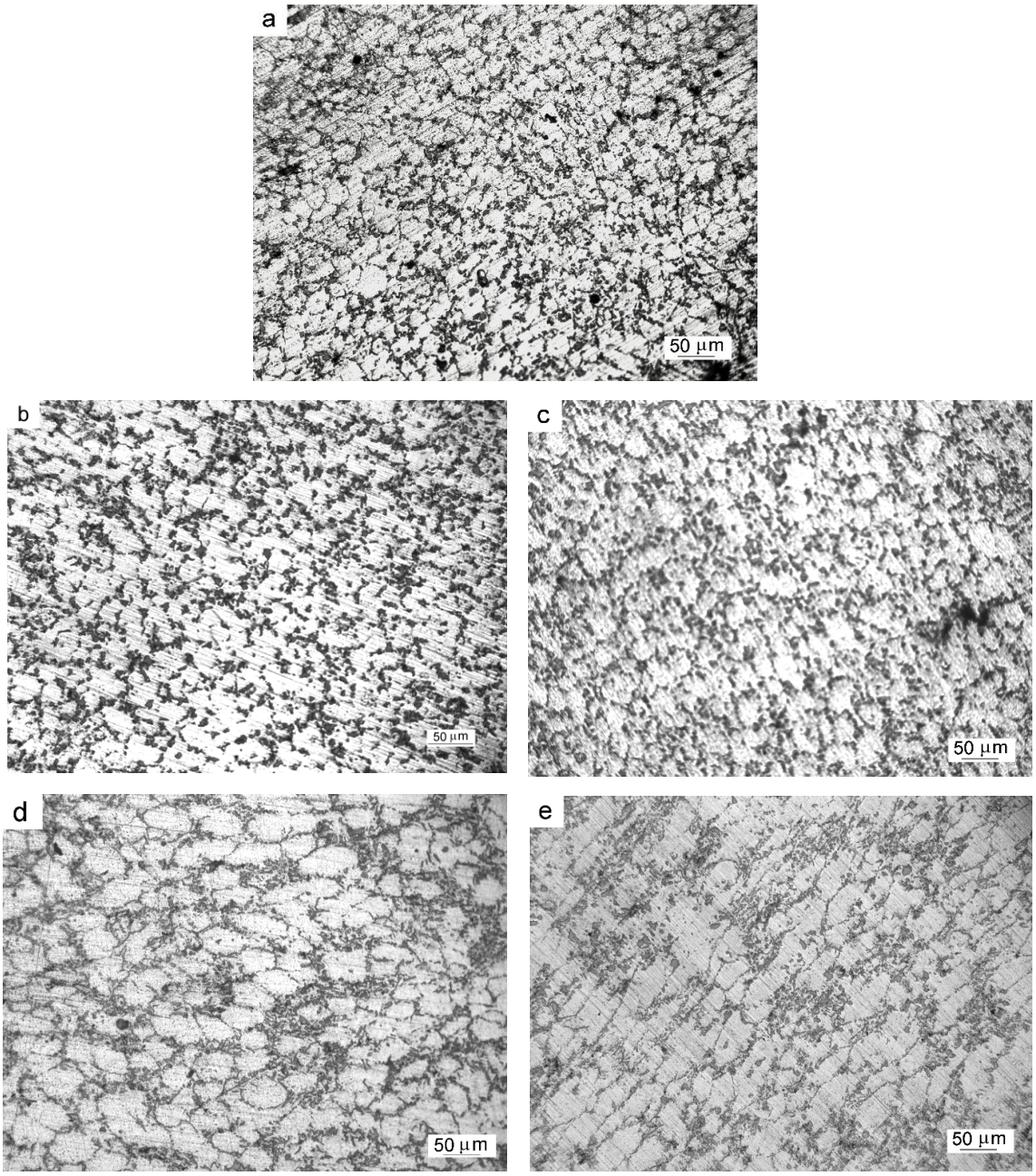

Fig. 5.11 Microstructure at centre region of spray deposited Al-6Si-30Pb alloy for (a) 0; (b) 20; (c) 40; (d) 60 and (e) 80 % thickness reduction.

In **fig. 5.12** which is for peripheral region, the size of Pb particles is submicron to 12 μm (**fig. 5.12(a)**) and the aspect ratio of Al-grains is 1.2-1.7 and 1.6-2.0 for 20, 40 (**fig. 5.12(b & c)**) and 60, 80 % (**fig. 5.12(d & e)**) thickness reduction, respectively.

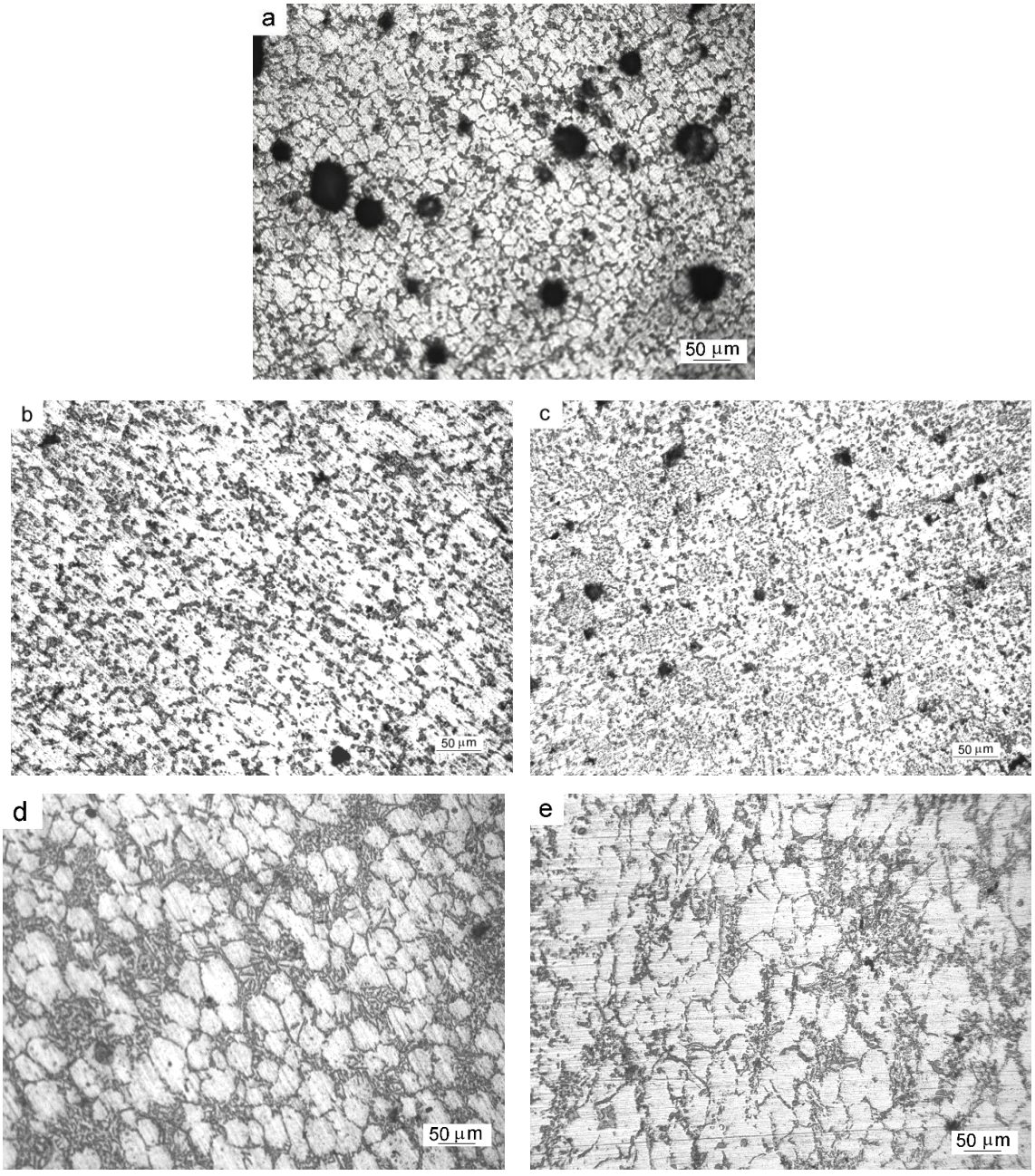

Fig. 5.12 Microstructure at peripheral region of spray deposited Al-6Si-30Pb alloy for (a) 0; (b) 20; (c) 40; (d) 60 and (e) 80 % thickness reduction.

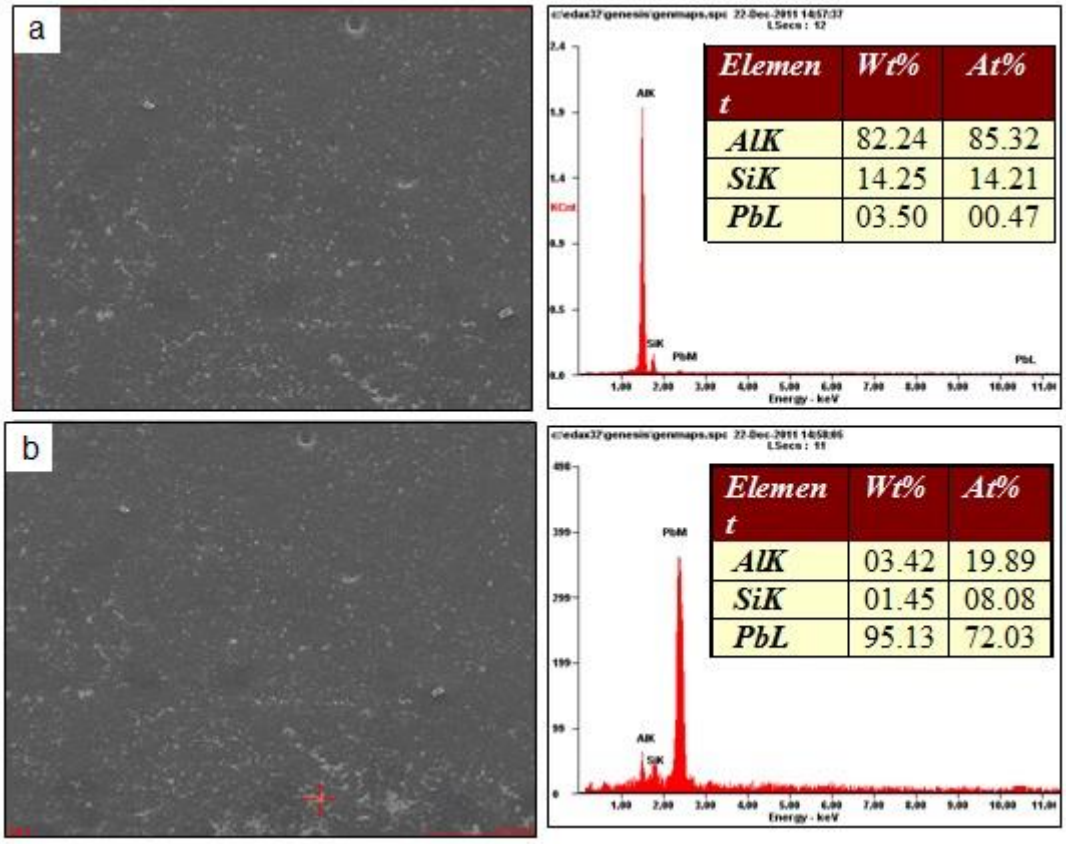

Fig. 5.13 EDS spectrum with analyzed (a) whole region and (b) bright region, indicating Al, Pb and Si phases in spray deposited Al-6Si-20Pb alloy.

It can also be observed from the microstructures that the porosity increases with the increase in Pb content but decreases with the thickness reduction and it is almost eliminated at 80 % thickness reduction for all the values of Pb content. The distance between the Al-grains also increases with the increase in thickness reduction which may be due to the spreading of Pb. Values of distinct input and output parameters of spray deposited cold rolled Al-Si-Pb alloy is reported in **table-5.1**.

Table 5.1: Values of input and output parameters of spray deposited cold rolled Al-Si-Pb alloy.

Input parameters				Output parameters		
S.No	Location of the samples	Pb (%) in Al-Si-Pb alloy	Thickness reduction (%)	Aspect ratio of Al grains	Pb particle size (μm)	Pore size (μm)
1.	Top and centre	0	0	1		10-15
			20 & 40	1.2-1.4		5-10
			60 & 80	1.6-2.2		< 3
		10	0	1	< 5	15-20
			20 & 40	1.6-2.2		10-15
			60 & 80	2.0-2.5		< 5
		20	0	1	< 10	15-25
			20 & 40	1.2-1.7		10-15
			60 & 80	1.5-2.5		< 5
		30	0	1	< 15	15-25
			20 & 40	1.2-1.7		10-20
			60 & 80	2.0-2.7		< 5
2.	Peripheral	0	0	1		5-15
			20 & 40	1.2-1.8		2-10
			60 & 80	1.8-2.6		< 2
			0	1	< 4	10-15

		10	20 & 40	1.2-1.7		5-10
			60 & 80	1.5-2.0		< 5
		20	0	1	< 8	10-20
			20 & 40	1.2-1.5		5-15
			60 & 80	1.5-2.5		< 5
		30	0	1	< 12	15-25
			20 & 40	1.2-1.7		5-15
			60 & 80	1.6-2.0		< 5

5.2 X-ray diffraction pattern

The XRD patterns of spray deposited Al-6Si-xPb (where x=0, 10, 20, 30) alloy are shown in **Fig. 5.14**. The patterns were taken for the samples obtained from the centre location of the spray deposit preform. These diffraction patterns shows similarity in which all the possible Al and Si phase reflections are expectedly present and none of the other possible oxide formation (Al_2O_3 reflections) are present. In Al-6Si alloy, the reflections [(220), (311) and (422)] for Si have lower relative intensities, indicated that the amount of Si in Al matrix is nearer to 5-6 wt%.

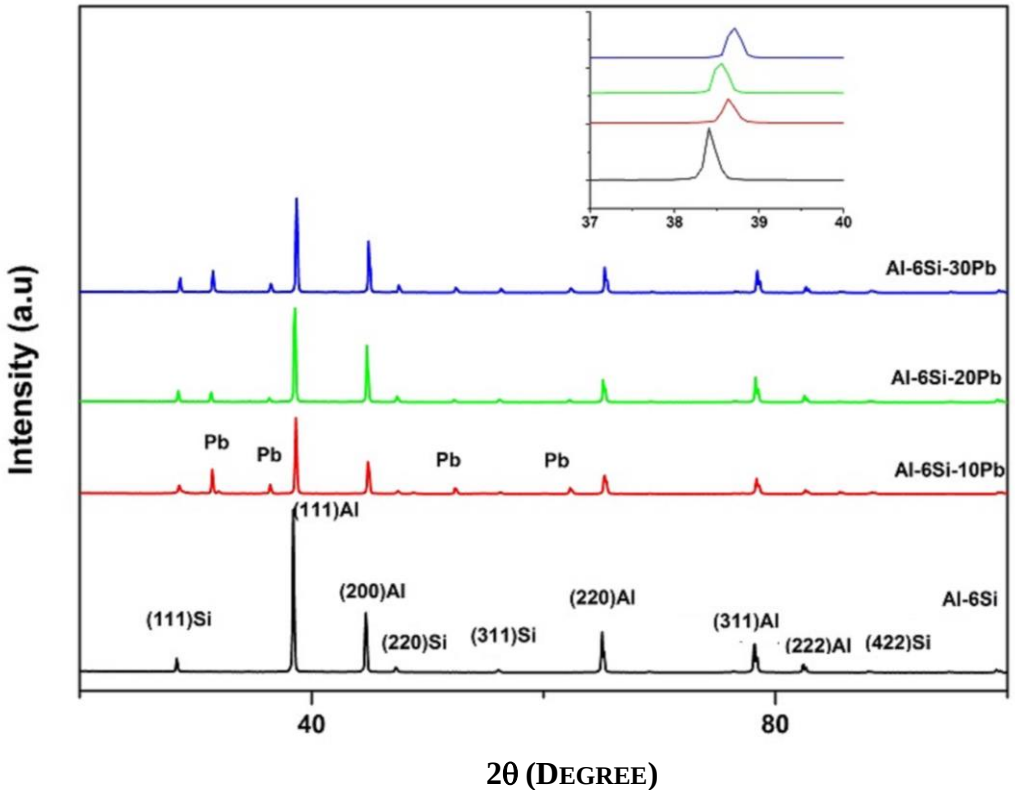

Fig. 5.14 XRD patterns for Al-6Si, Al-6Si-10Pb, Al-6Si-20Pb and Al-6Si-30Pb alloy.

From the above fig., a shift in peak position is observed by increasing the Pb content. An aluminum peak shifts towards the left, right & left side by adding 10, 20 & 30 % Pb content, respectively.

Fig. 5.15 shows the XRD patterns of Al-6Si-20Pb alloy for (a) 0, (b) 20, (c) 40, (d) 60 & (e) 80 % thickness reduction. The peak intensity decreases with the increase in thickness reduction as shown in **fig. 5.16.**

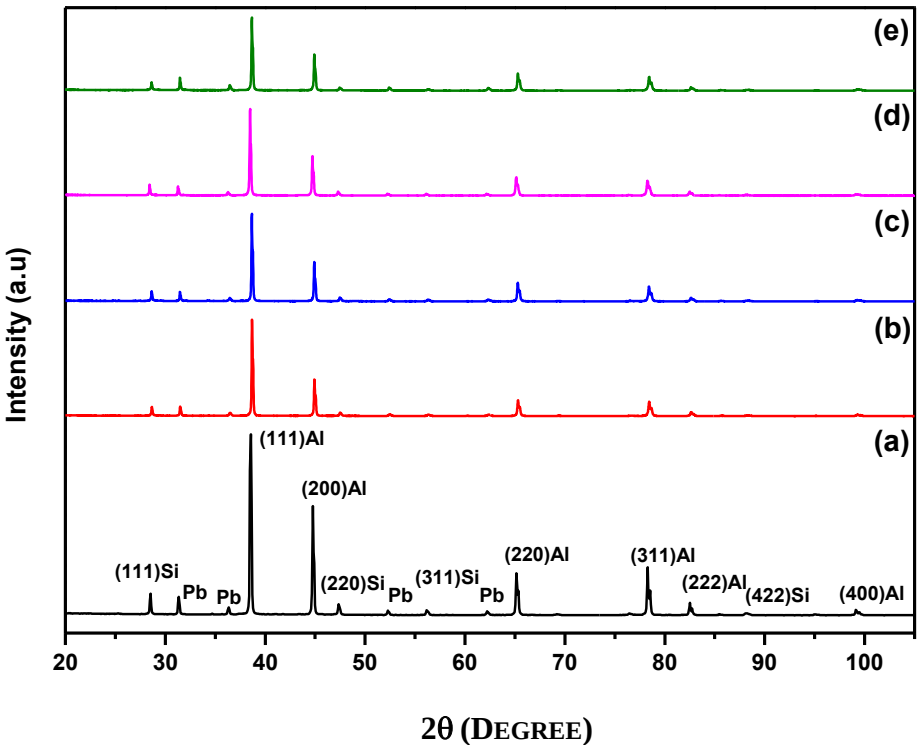

Fig. 5.15 XRD pattern of Al-6Si-20Pb alloy for (a) 0, (b) 20, (c) 40, (d) 60 & (e) 80 % thickness reduction.

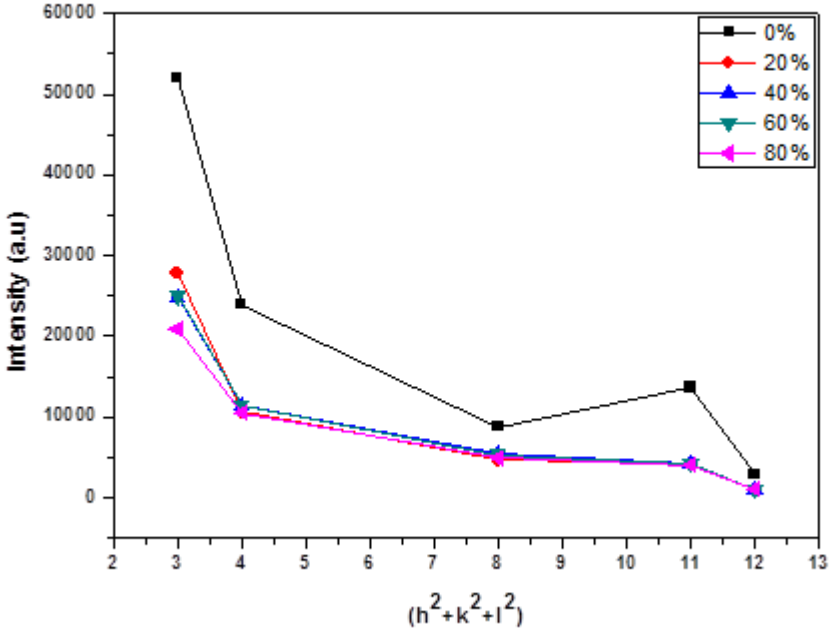

Fig. 5.16. Peak intensity of crystallographic planes for different thickness reductions.

5.3 Porosity

Theoretical densities calculated for the Al-6Si-xPb alloys used in present study are given in **table 5.2**.

Table 5.2 Theoretical density of Al-6Si-xPb alloys.

X =	0	10	20	30
Density (g/cc)	2.62	2.89	3.15	3.46

Fig. 5.17 shows that there is no change in the density and hence porosity in the thickness direction of the deposit for all the percentage of Pb content. Variation in the porosity of spray deposited Al-6Si-(0-30)Pb alloy as a function of samples from centre to periphery is shown in **fig. 5.18**. The change in porosity is observed from centre to periphery of the deposit. It decreases from centre to periphery. Therefore, porosities are calculated for the samples from

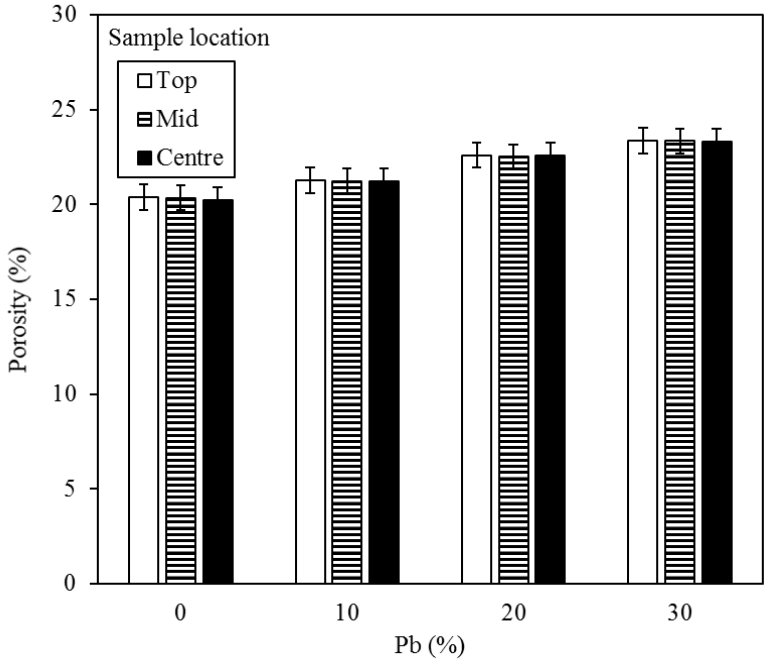

Fig. 5.17 Variation in the porosity of spray deposited Al-6Si-(0-30)Pb alloy as a function of Pb content along the thickness of the spray deposit.

centre to periphery after different percentage of thickness reductions. **Fig. 5.19** shows the samples of spray deposit Al-6Si alloy for porosity measurements after different percentage of thickness reductions.

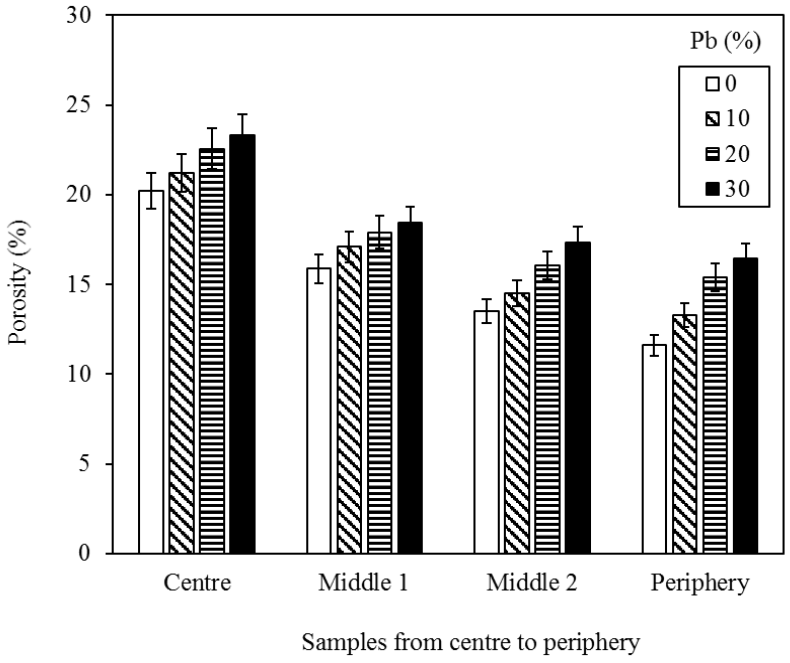

Fig. 5.18 Variation in the porosity of spray deposited Al-6Si-(0-30)Pb alloy as a function of samples from centre to periphery.

Variation in the porosity of spray deposited Al-6Si-(0-30)Pb alloy as a function of thickness reduction at different locations of the preform viz. centre, middle 1, middle 2 & periphery are shown in **figs. 5.20** to **5.23**.

Fig. 5.20 shows the variation in porosity of spray deposited Al-6Si-0Pb alloy for aforementioned parameters. It can be seen that the porosity decreases up to a thickness reduction of 20 % and then it increases up to that of 40 %. Afterwards the porosity decreases at a faster rate up to a thickness reduction of 60 % than that of 20 % and again a small decrement in the porosity occurs up to that of 80 % for all the samples.

Results on the porosity variation of Al-6Si-10Pb alloy are presented in **fig. 5.21**. It can be observed that the porosity decreases continuously up to a thickness reduction of 60 % and then a small increment in the porosity occurs up to that of 80 % for all the samples.

The change in porosity of spray deposited Al-6Si-20Pb alloy with thickness reduction at different locations of the preform is shown in **fig. 5.22**. In this case, the porosity decreases up to a thickness reduction of 40 % and then it increases up to that of 60 % and again it decreases up to that of 80 %.

Results of Al-6Si-30Pb alloy are illustrated in fig. **5.23**. It can be seen that the porosity decreases up to a thickness reduction of 40 % and then it increases up to that of 60 %. Beyond a thickness reduction of 60 %, it again decreases up to that of 80 %. In this fig. the porosity variation pattern is same as that of the alloy having 20 %Pb.

Also, in all the figs. porosity decreases from centre to periphery of the preform for all the samples.

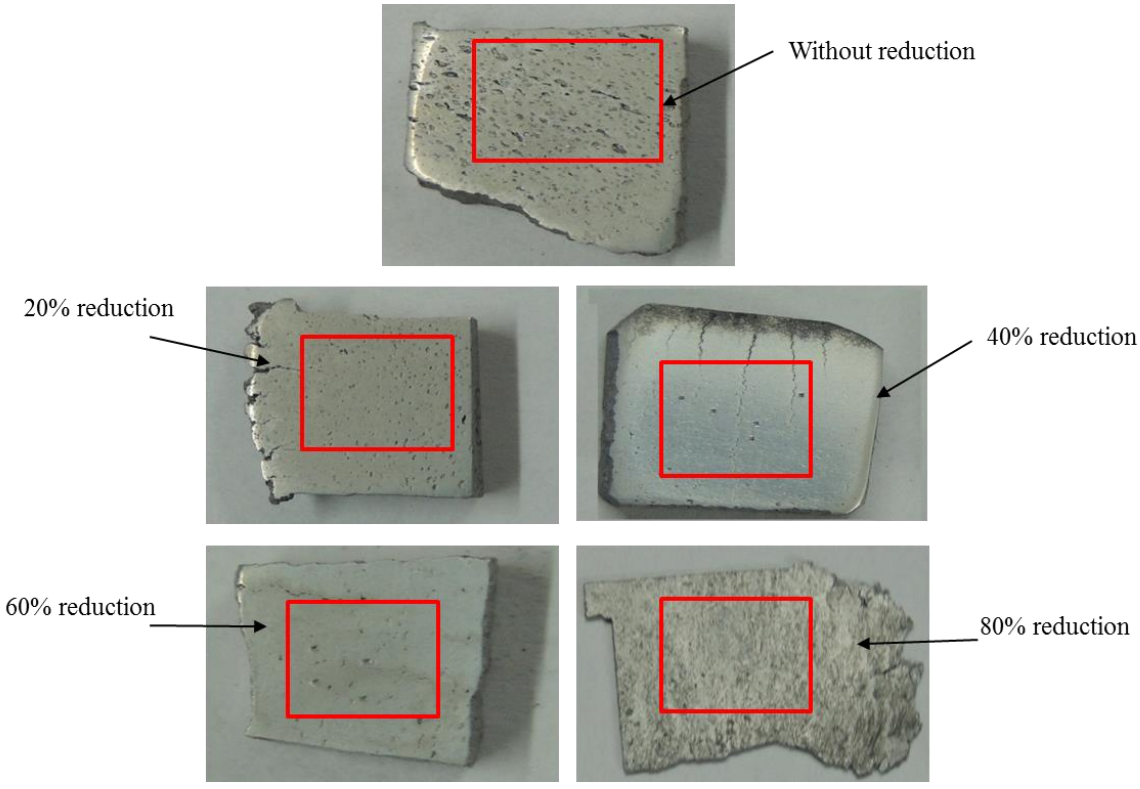

Fig. 5.19 Samples of spray deposit Al-6Si alloy for porosity measurements after different percentage of thickness reductions.

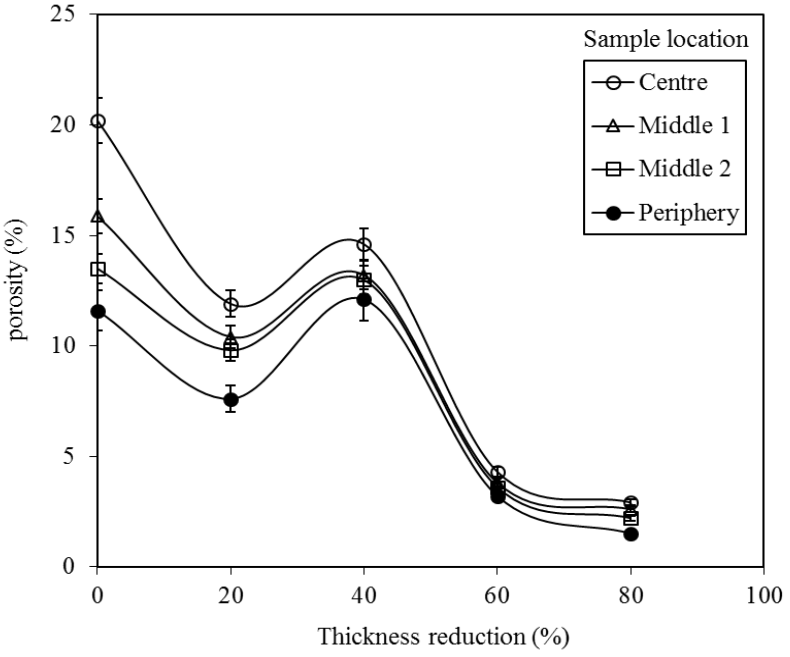

Fig. 5.20 Variation in the porosity of spray deposited Al-6Si-0Pb alloy as a function of thickness reduction at different locations of the preform viz. centre, middle 1, middle 2 & periphery.

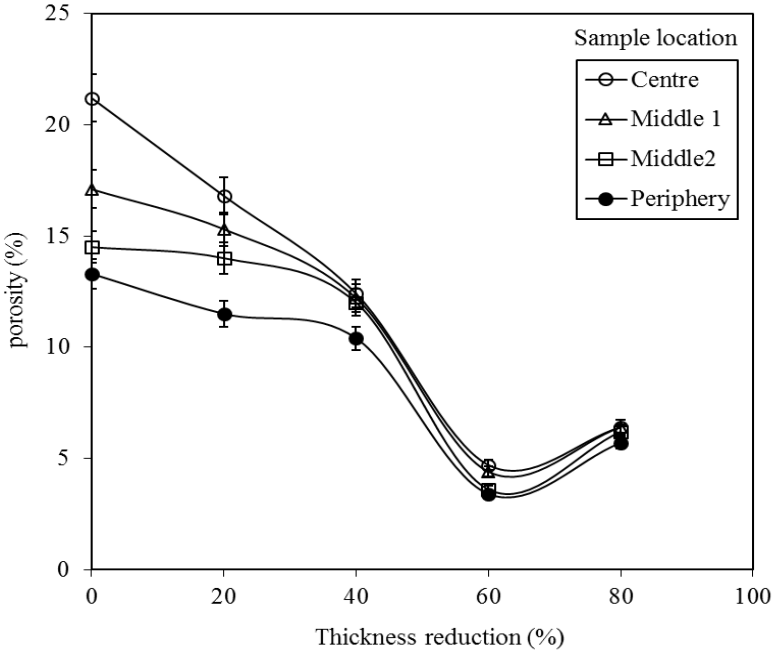

Fig. 5.21 Porosity variation of spray deposited Al-6Si-10Pb alloy as a function of thickness reduction at different locations of the preform viz. centre, middle 1, middle 2 & periphery.

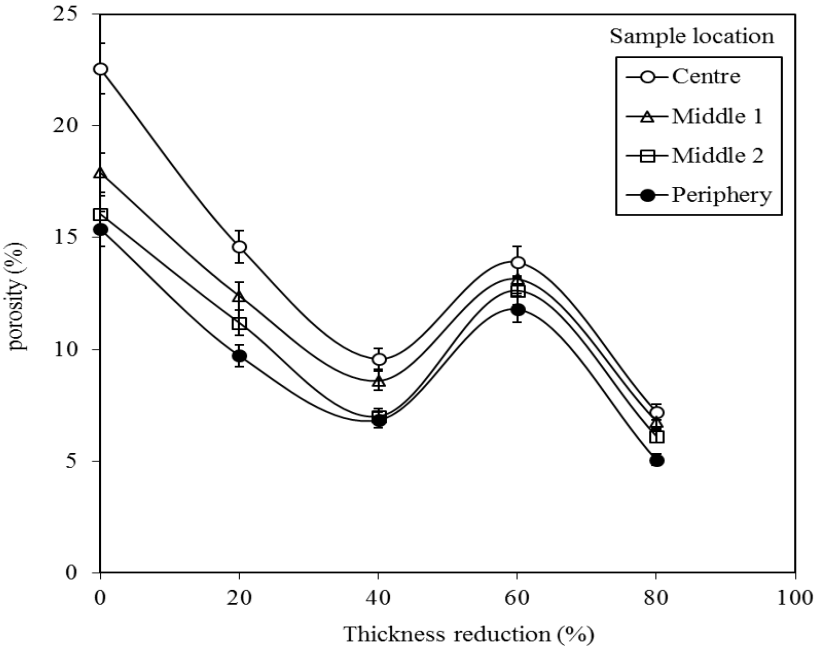

Fig. 5.22 Porosity variation of spray deposited Al-6Si-20Pb alloy with thickness reduction at different locations of the preform viz. centre, middle 1, middle 2 & periphery.

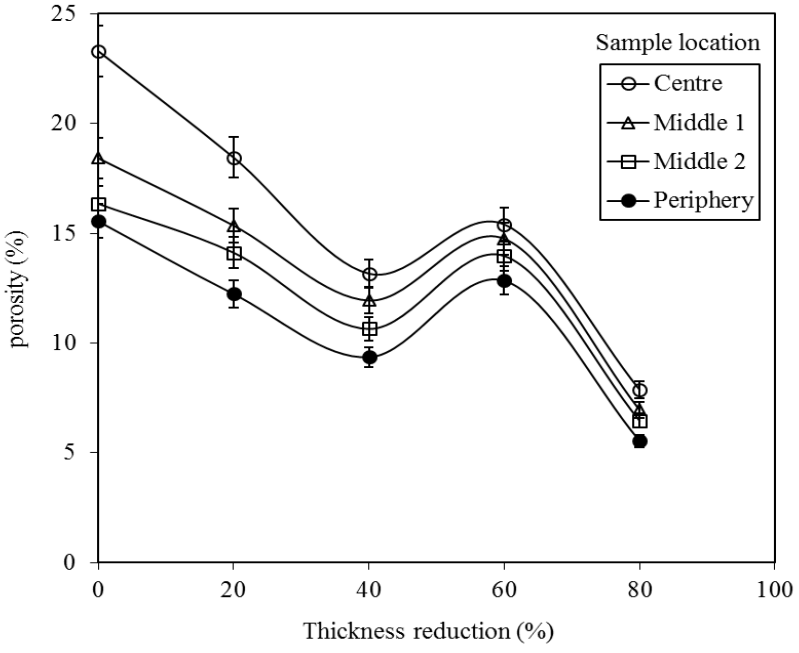

Fig. 5.23 Variation in the porosity of spray deposited Al-6Si-30Pb alloy as a function of thickness reduction at different locations of the preform viz. centre, middle 1, middle 2 & periphery.

Fig. 5.24 shows the variation in the porosity of spray deposited Al-6Si alloy as a function of Pb content for different samples. It can be seen that porosity increases with increase in Pb content. Also, porosity is highest for centre region and lowest for peripheral region.

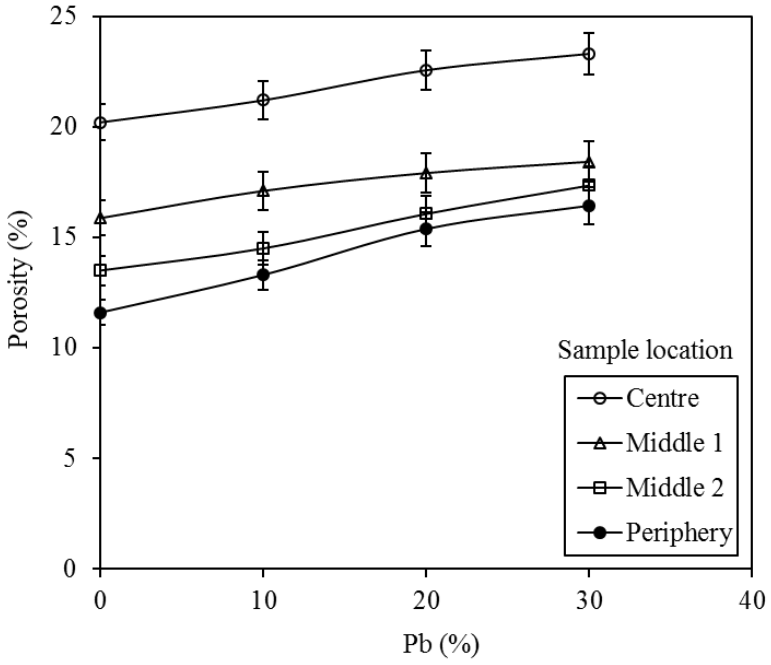

Fig. 5.24 Variation in the porosity of spray deposited Al-6Si alloy as a function of Pb content.

To observe porosity and its distribution with the Pb content and thickness reductions the recorded micrographs are shown in **figs.5.25** and **5.26**, respectively. **Fig.5.25** shows porosity for 0, 10, 20 and 30 % Pb content at centre of the deposit and **fig.5.26** shows porosity distribution with thickness reduction of 0, 20, 40, 60 and (e) 80 % at centre of the deposit.

The effect of Pb content on porosity is shown in **fig.5.25**. Red spots in micrographs represent porosity. It can be seen that the porosity increases with the increase in Pb content. Every micrograph is having two types of areas viz. first type area is having large amount of porosity and the second type area is having small amount of porosity. The large and small amount porosity areas belong to the Pb and Al rich areas, respectively. The effect of thickness reduction on porosity is shown in **fig.5.26.** It can be seen that the porosity decreases with the increase in thickness reduction.

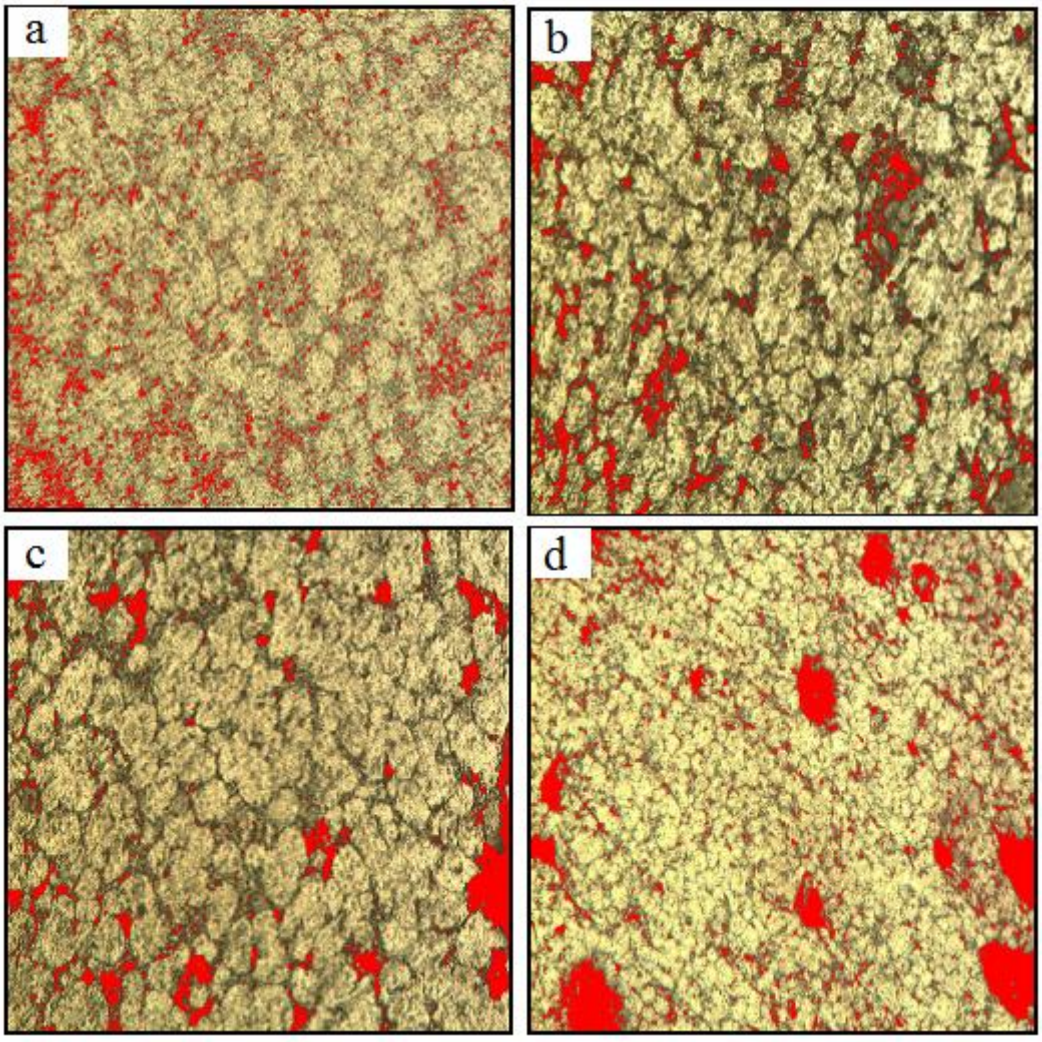

Fig. 5.25 Micrograph showing the porosity distribution with Pb content of (a) 0; (b) 10; (c) 20 and (d) 30% at centre of the deposit.

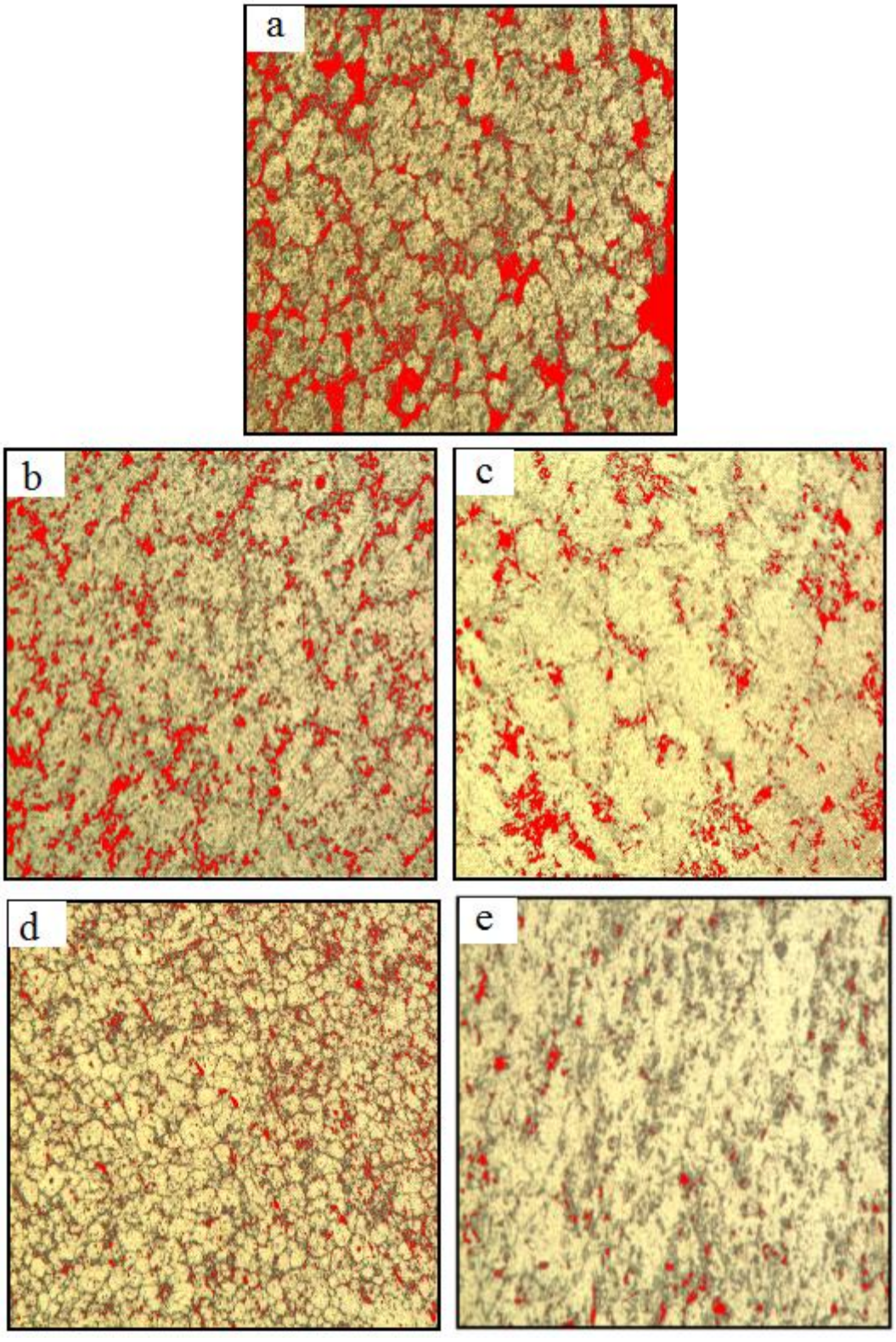

Fig. 5.26 Micrograph showing the porosity distribution with thickness reduction of (a) 0; (b) 20; (c) 40; (d) 60 and (e) 80% at centre of the deposit.

5.4 Hardness

Hardness variation of spray deposited Al-6Si-(0-30)Pb alloy as a function of thickness reduction at different locations of the preform viz. centre, middle 1, middle 2 & periphery are shown in **figs. 5.27** to **5.30**.

Results of Al-6Si-0Pb alloy for aforesaid parameters are shown in **fig. 5.27**. It can be seen that the hardness increases up to a thickness reduction of 60 % with same rate and after this, it is almost constant up to 80 % thickness reduction although in some cases marginal increment occurs.

The effect of thickness reduction on hardness of spray deposited Al-6Si-10Pb, Al-6Si-20Pb and Al-6Si-30Pb alloy at different locations of the preform is depicted in **fig. 5.28**, **5.29** and **5.30**, respectively. In all these cases, hardness increases continuously up to a thickness reduction of 80 %.

Also, in all these figs. hardness increases from centre to periphery of the preform for all samples.

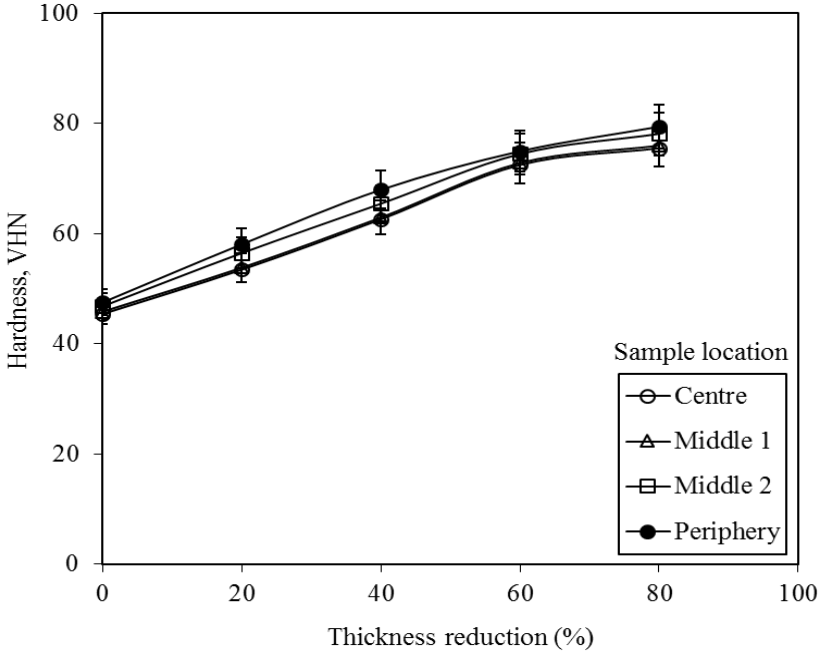

Fig. 5.27 Hardness variation of spray deposited Al-6Si-0Pb alloy as a function of thickness reduction at different locations of the preform viz. centre, middle 1, middle 2 & periphery.

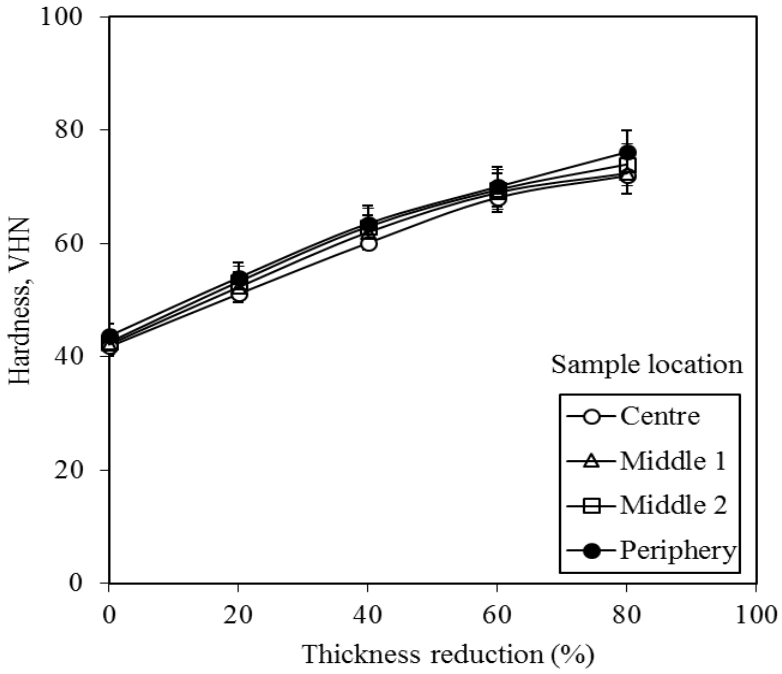

Fig. 5.28 Hardness variation of spray deposited Al-6Si-10Pb alloy as a function of thickness reduction at different locations of the preform viz. centre, middle 1, middle 2 & periphery.

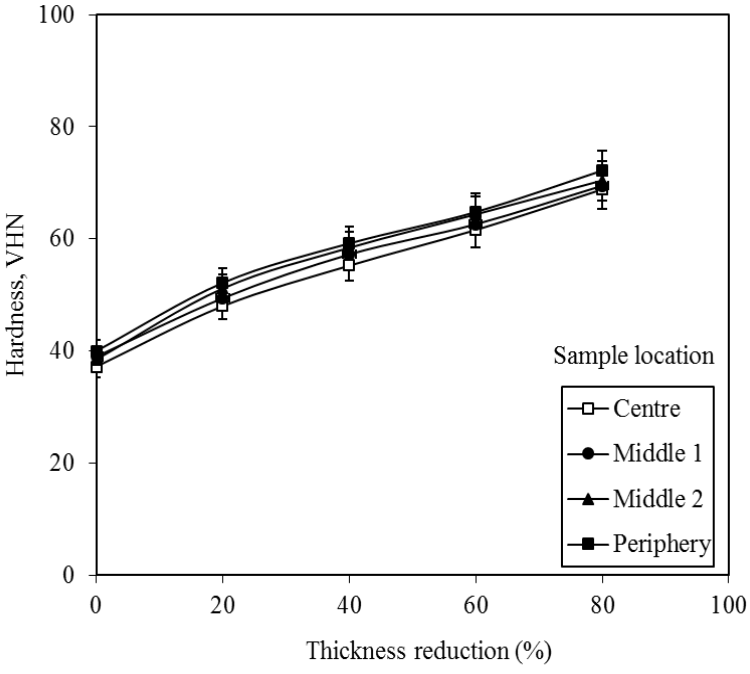

Fig. 5.29 Hardness variation of spray deposited Al-6Si-20Pb alloy as a function of thickness reduction at different locations of the preform viz. centre, middle 1, middle 2 & periphery.

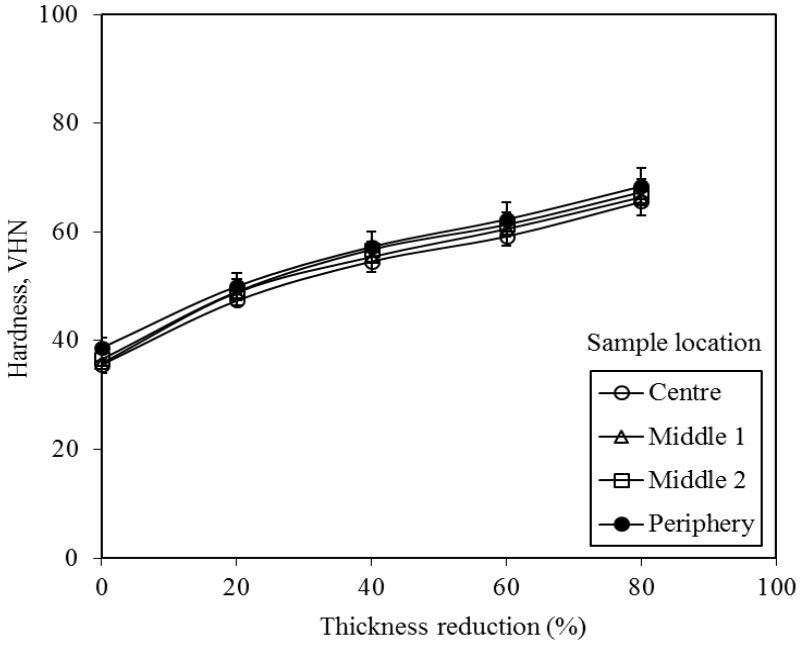

Fig. 5.30 Hardness variation of spray deposited Al-6Si-30Pb alloy as a function of thickness reduction at different locations of the preform viz. centre, middle 1, middle 2 & periphery.

Fig. 5.31 shows the variation in hardness of spray deposited Al-6Si alloy as a function of Pb content for different samples. It can be seen that hardness decreases with increase in Pb content. Also, hardness is highest for peripheral region and lowest for centre region. **Fig. 5.32** shows the variation in hardness of spray deposited Al-6Si-(0-30)Pb alloy as a function of samples from centre to periphery. Hardness increases from centre to periphery of the deposit. Also, it is highest for 0% Pb content and lowest for 30 % Pb content.

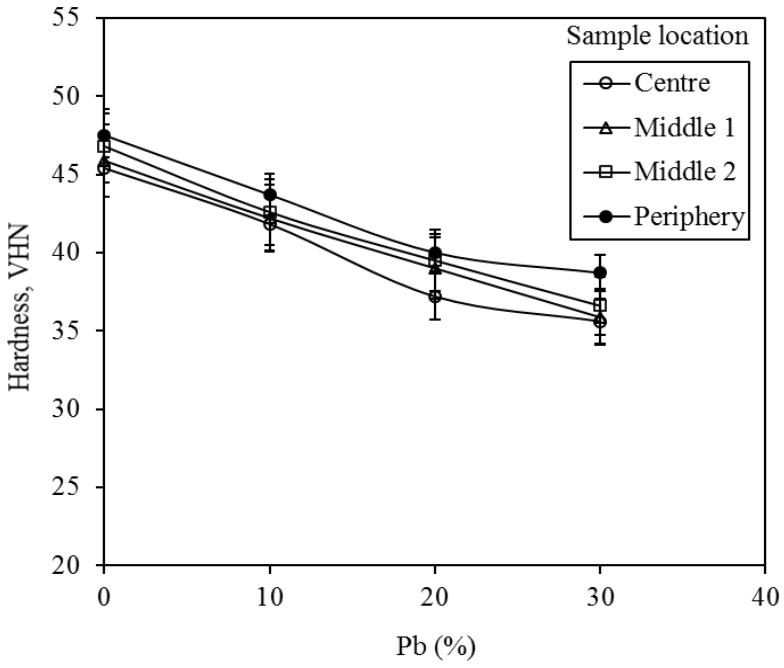

Fig. 5.31 Hardness variation of spray deposited Al-6Si alloy with Pb content for different samples.

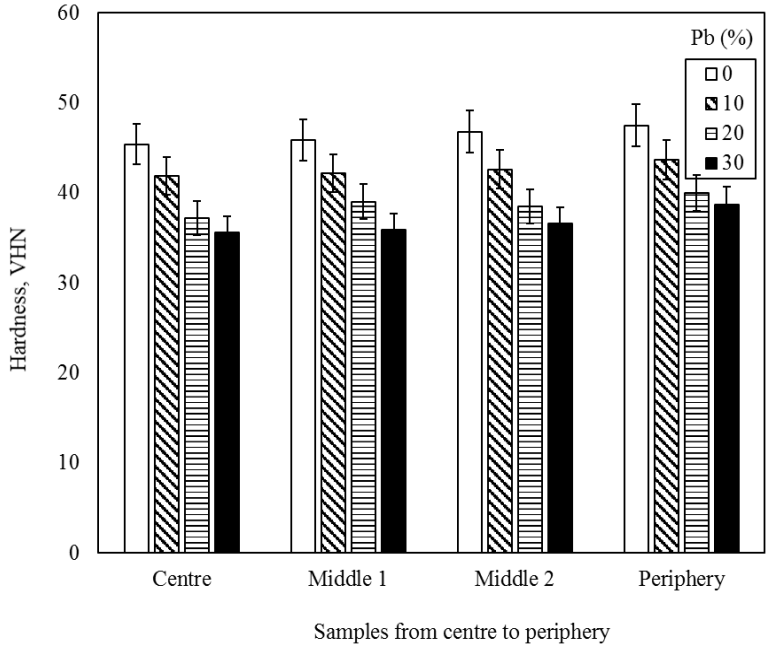

Fig. 5.32 Hardness variation of spray deposited Al-6Si-xPb alloy with the samples from centre to periphery for different Pb content.

5.5 Wear rate

The dependence of wear rate of spray deposited Al-6Si-(0-30)Pb alloy on applied load at different thickness reduction is shown in **figs. 5.33** to **5.36**.

Variation in wear rate of spray deposited Al-6Si-0Pb alloy is plotted against the applied load in **fig. 5.33**. As usual the wear rate increases with the applied load for all the thickness reduction, although the rate of increase is not the same at all the applied loads. It can be seen that these plots can be divided into three regions having three different rate of increase in wear rate with the increase in applied load. In first region i.e. up to a load of 30 N, wear rate increases at a moderate rate. In second region i.e. up to a load of 40 N, it is almost constant. Beyond a load of 40 N i.e. in third region, the wear rate again increases at a higher rate as compared to that of up to a load of 30 N i.e. region first. Also, the wear rate is lowest for a thickness reduction of 80 % and it is highest for that of 0 %.

Fig. 5.34 illustrates the wear rate variation of spray deposited Al-6Si-10Pb alloy as a function of applied load at different thickness reduction. It can be seen that the wear rate increases with the increase in applied load in three regions same as above. Also, the wear rate is highest for a thickness reduction of 0 % and lowest for that of 60 % at all the applied loads.

The change in wear rate of spray deposited Al-6Si-20Pb and Al-6Si-30Pb alloy as a function of applied load at different thickness reduction is depicted in **fig. 5.35** and **5.36**, respectively. It can be observed that the wear rate is lowest for 80 % thickness reduction and it is highest as that of 0 % in both these cases.

The variation in wear rate of spray deposited Al-6Si-(0-30)Pb alloy as a function of thickness reduction at different applied loads are shown in **figs. 5.37** to **5.40.**

Fig. 5.37 shows the plots depicting the variation in wear rate of spray deposited Al-6Si-0Pb alloy as a function of thickness reduction at different applied loads. Wear rate decreases up to a thickness reduction of 20% and then it increases up to that of 40% for all the applied loads. Wear rate again decreases up to a thickness reduction of 60% and then it is almost constant up to that of 80 %. Obviously, wear rate is higher at higher applied load.

Wear rate variation of spray deposited Al-6Si-10Pb alloy with thickness reduction at various applied loads is shown in **fig. 5.38**. It can be seen that wear rate decreases continuously up to a thickness reduction of 80 % for all the applied loads.

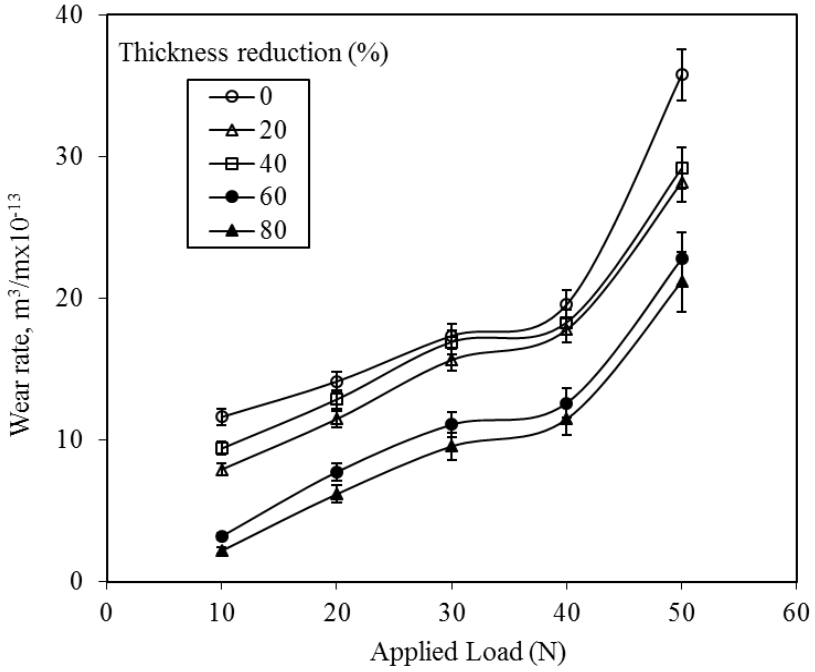

Fig. 5.33 Wear rate variation of spray deposited Al-6Si-0Pb alloy with applied load at different thickness reduction.

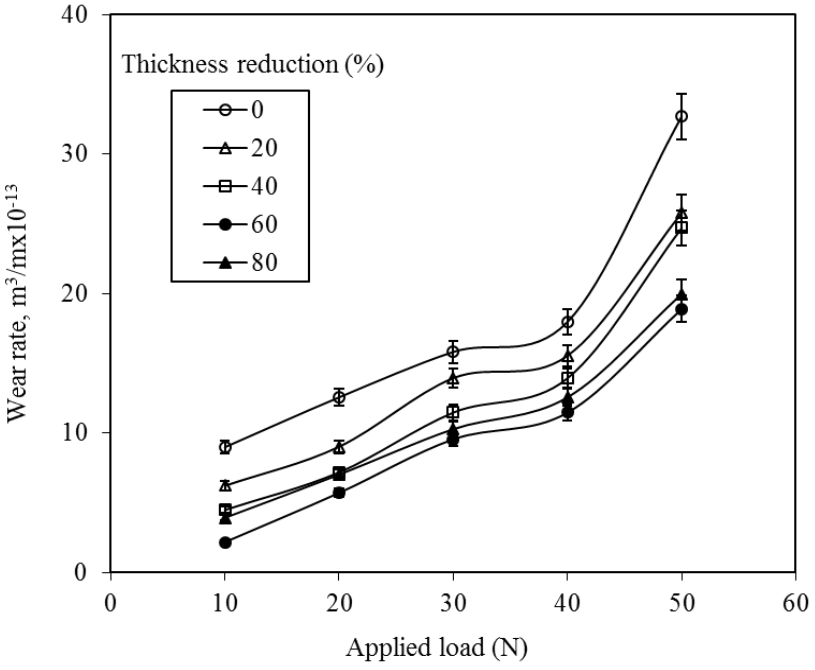

Fig. 5.34 Wear rate variation of spray deposited Al-6Si-10Pb alloy with applied load at different thickness reduction.

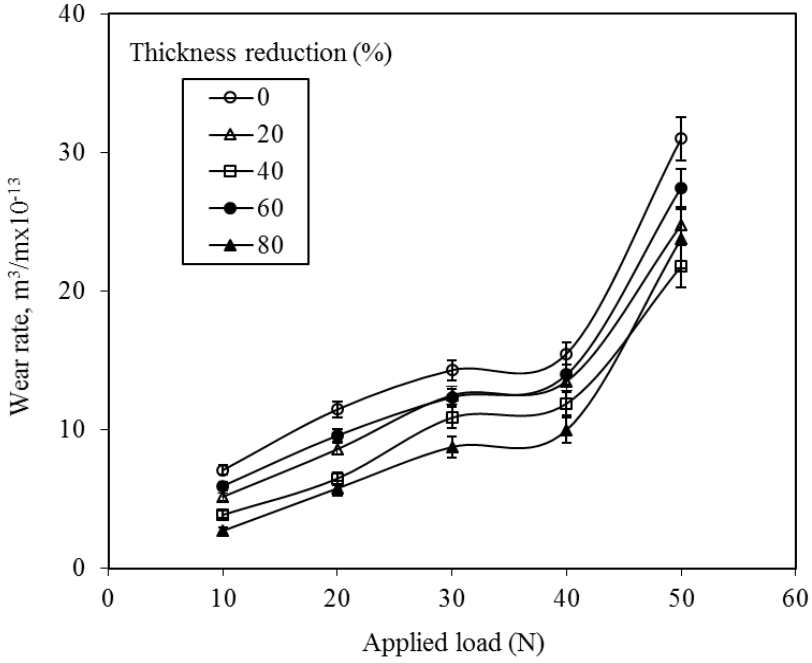

Fig. 5.35 Wear rate variation of spray deposited Al-6Si-20Pb alloy with applied load at different thickness reduction.

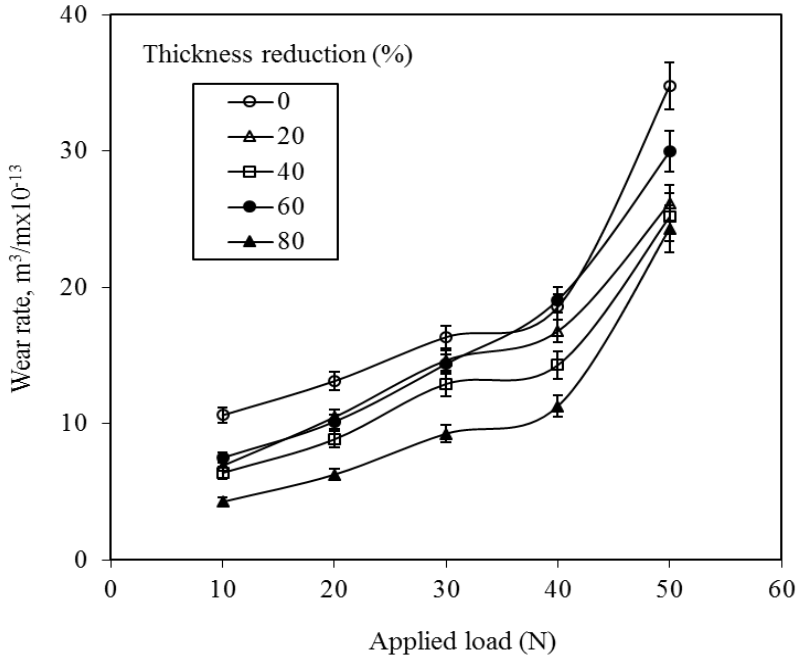

Fig. 5.36 Wear rate variation of spray deposited Al-6Si-30Pb alloy with applied load at different thickness reduction.

Fig. 5.39 illustrates the results of Al-6Si-20Pb alloy. It can be observed that the wear rate decreases up to a thickness reduction of 40 % and then it increases up to that of 60 %. Beyond a thickness reduction of 60 %, it again decreases continuously up to that of 80 %.

The change in wear rate of spray deposited Al-6Si-30Pb alloy as a function of thickness reduction at various applied loads is presented in **fig. 5.40**. It can be seen that the wear rate decreases continuously up to a thickness reduction of 40 % and then it increases up to that of 60 % and afterwards it again decreases up to that of 80 % for all the samples.

Fig. 5.41 shows the wear rate variation with Pb content at various applied loads. Wear rate decreases with Pb content up to 20 % after this it increases. Also, wear rate is lowest for 10 N load and highest for 50 N load. **Fig. 5.42** represents the wear rate variation with the samples from centre to periphery at various applied loads. It can be observed that wear rate decreases from centre to periphery of the deposit.

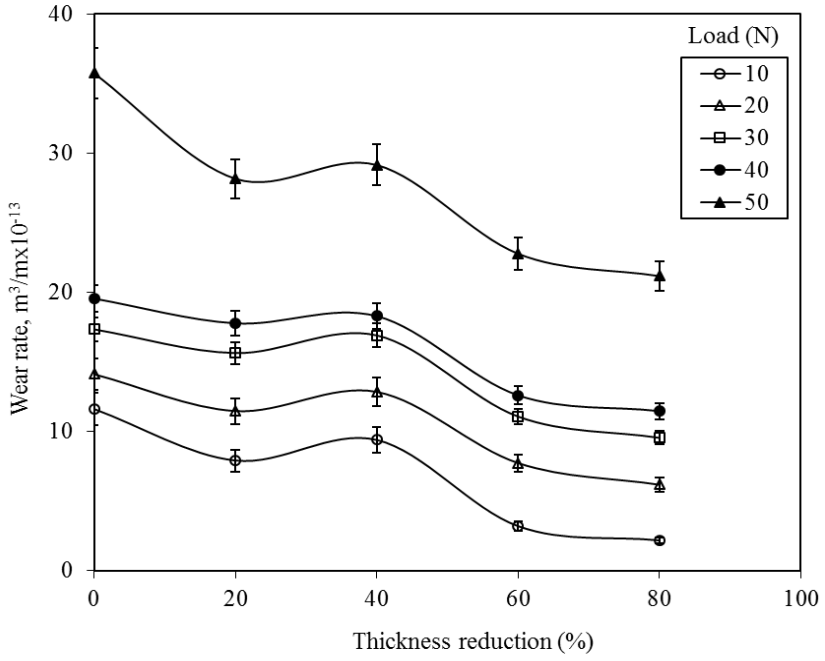

Fig. 5.37 Wear rate variation of spray deposited Al-6Si-0Pb alloy as a function of thickness reduction at different applied loads.

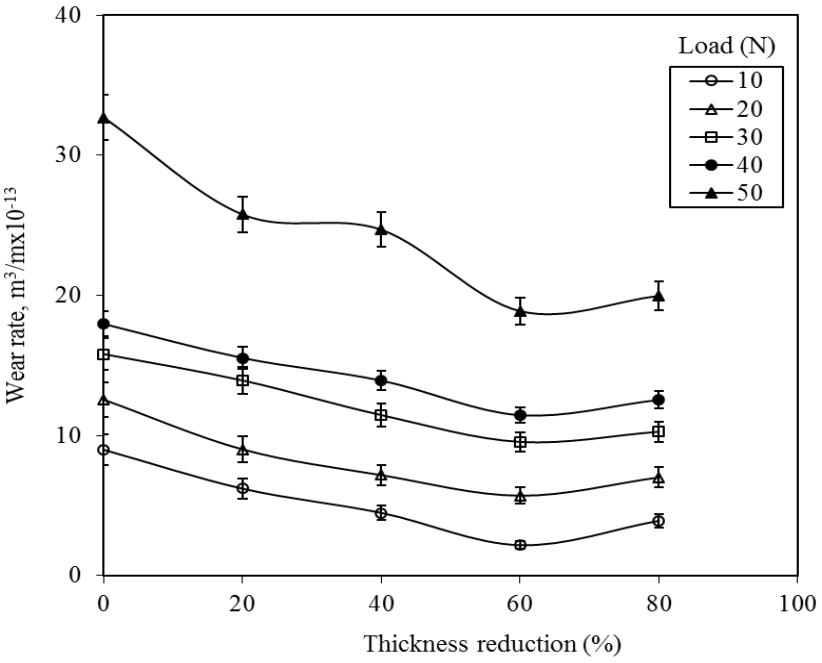

Fig. 5.38 Wear rate variation of spray deposited Al-6Si-10Pb alloy with thickness reduction at various applied loads.

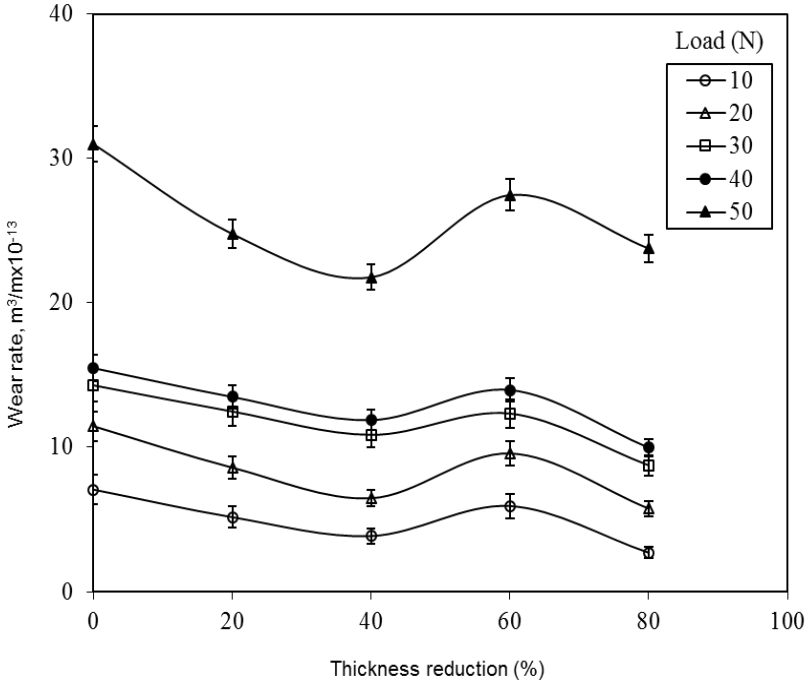

Fig. 5.39 Wear rate variation of spray deposited Al-6Si-20Pb alloy with thickness reduction at various applied loads.

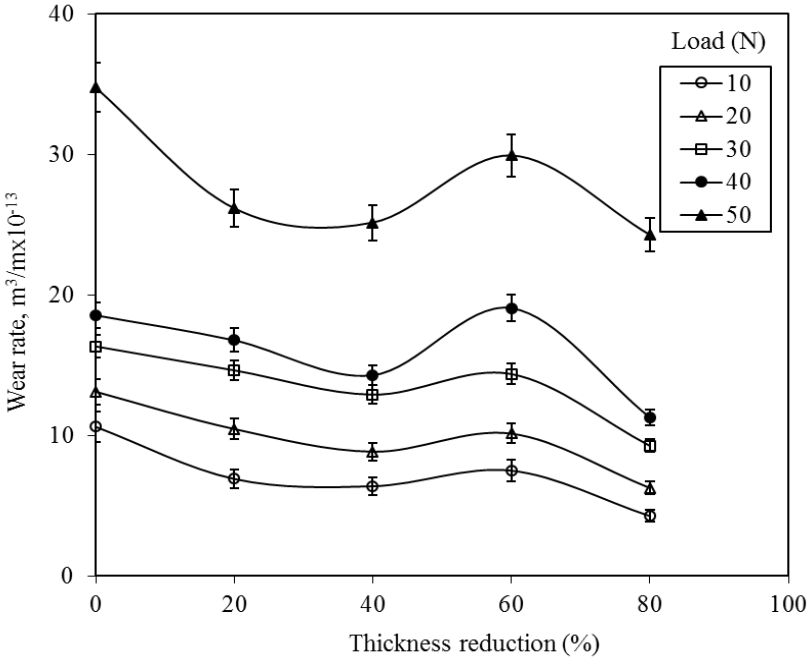

Fig. 5.40 Wear rate variation of spray deposited Al-6Si-30Pb alloy with thickness reduction at various applied loads.

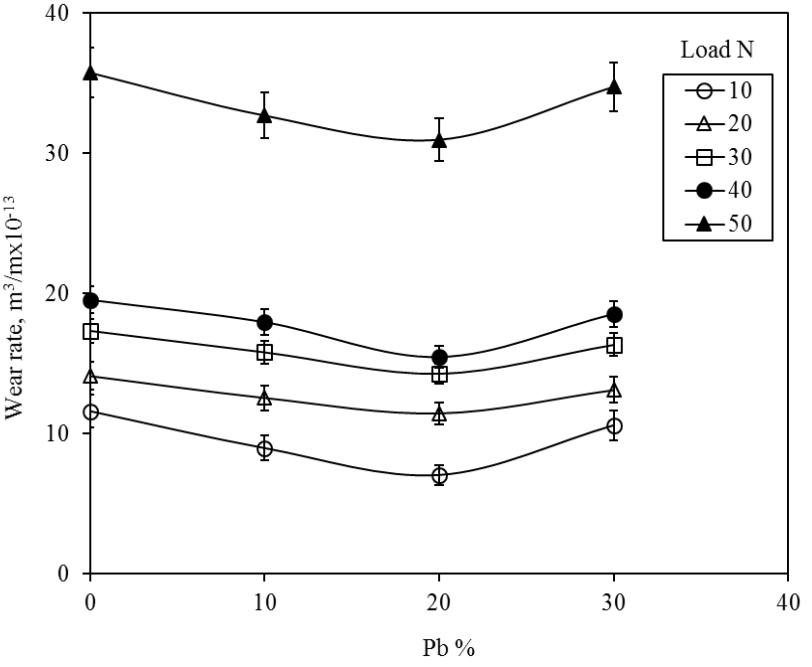

Fig. 5.41 Wear rate variation with Pb content at various applied loads.

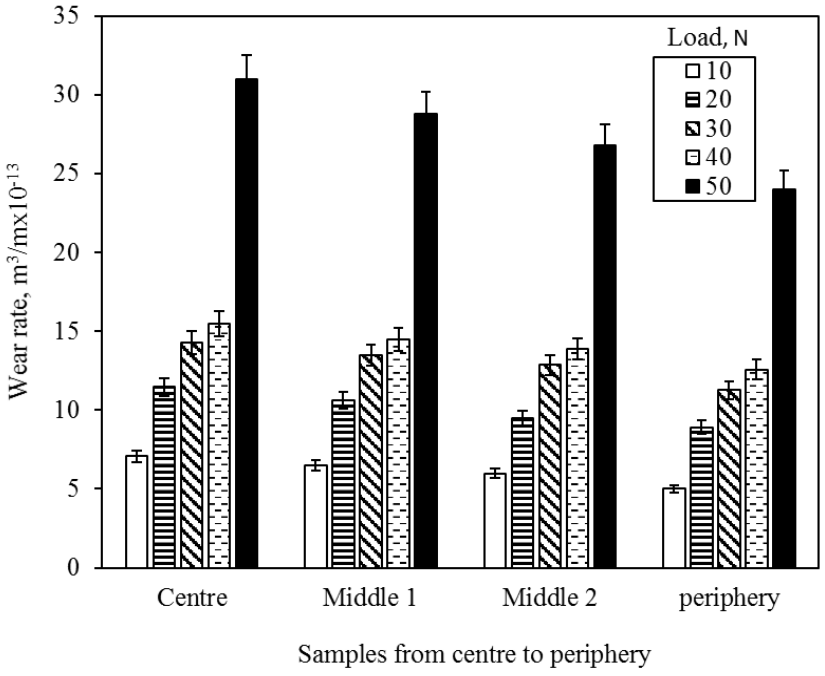

Fig. 5.42 Wear rate variation with the samples from centre to periphery at various applied loads.

5.5.1 Worn-out surface analysis

The SEM micrographs of worn surface of spray deposited Al-6Si-0Pb and Al-6Si-20Pb alloys for 0, 40 & 80 and 0, 60 & 80 % thickness reduction at three different (one load from each region) applied loads is shown in **figs. 5.43** and **5.44,** respectively. Micrographs arranged in the vertical and horizontal direction were taken at different % thickness reduction and at different applied load during wear test, respectively. In **figs. 5.43** and **5.44**, micrographs **(a), (b)** and **(c)** worn at 30 N load, micrographs **(d), (e)** and **(f)** worn at 40 N load and micrographs **(g), (h)** and **(i)** worn at 50 N load.

Micrographs **(a)** and **(c)** worn at the load of 30 N correspond to 0 and 80 % thickness reduction, respectively. Clearly, the topography of the worn surfaces was identical. It was characterized by a smooth surface with fine abrasion grooves while in micrograph **(b)** the grooves on the worn surface became wider. A white film of oxides (as depicted by EDS) was formed at the load of 30 N. At the load of 40 N (micrograph **(d)**) the development of shallow grooves can be seen on the pin surface. In micrograph **(e)**, the worn surface appears to be totally devoid of any wear track. With increasing load, the craters were formed as shown in

micrographs **(h)** and **(i)**. In **fig. 5.43(g)**, the worn surface was characterized by a series of stripe like river wave.

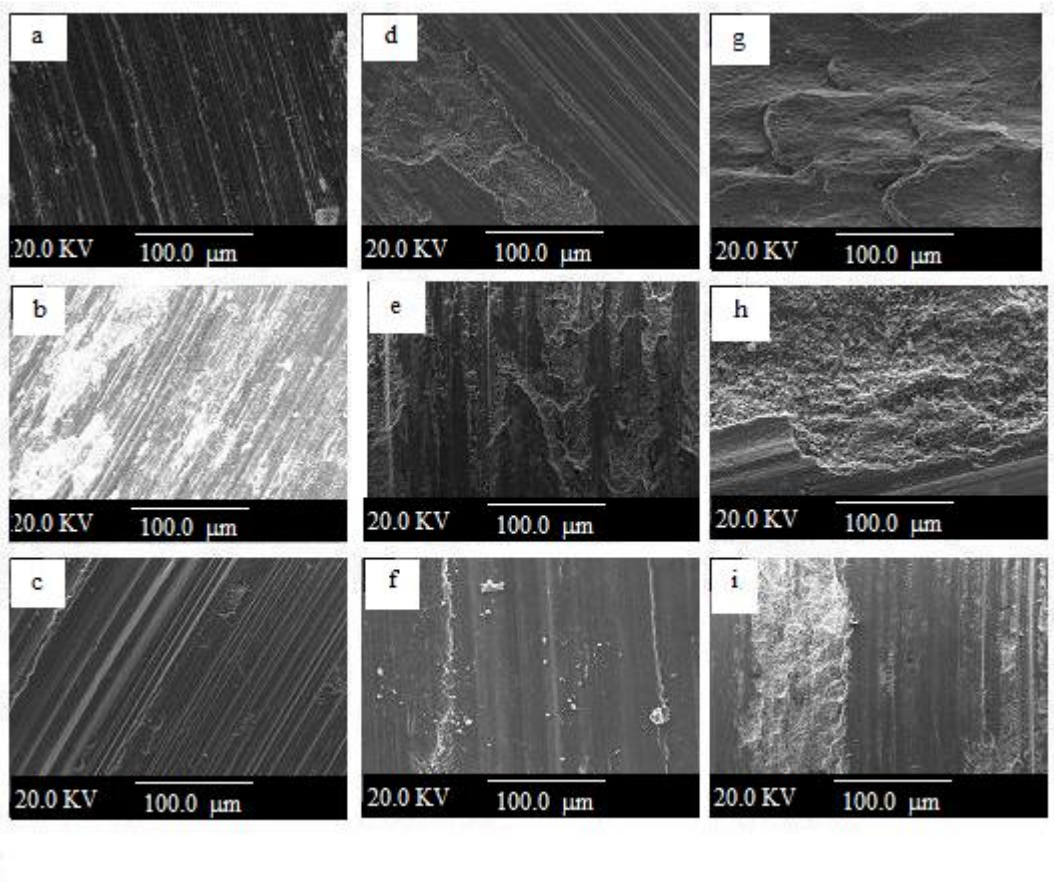

Fig. 5.43. SEM micrographs of the worn surface of spray deposited Al-6Si alloy at a thickness reduction of 0 ((a), (d) and (g)), 40 ((b), (e) and (h)) and 80 % ((c), (f) and (i)) for different applied loads viz. 30 N ((a), (b) and (c)), 40 N ((d), (e) and (f)) and 50 N ((g), (h) and (i)).

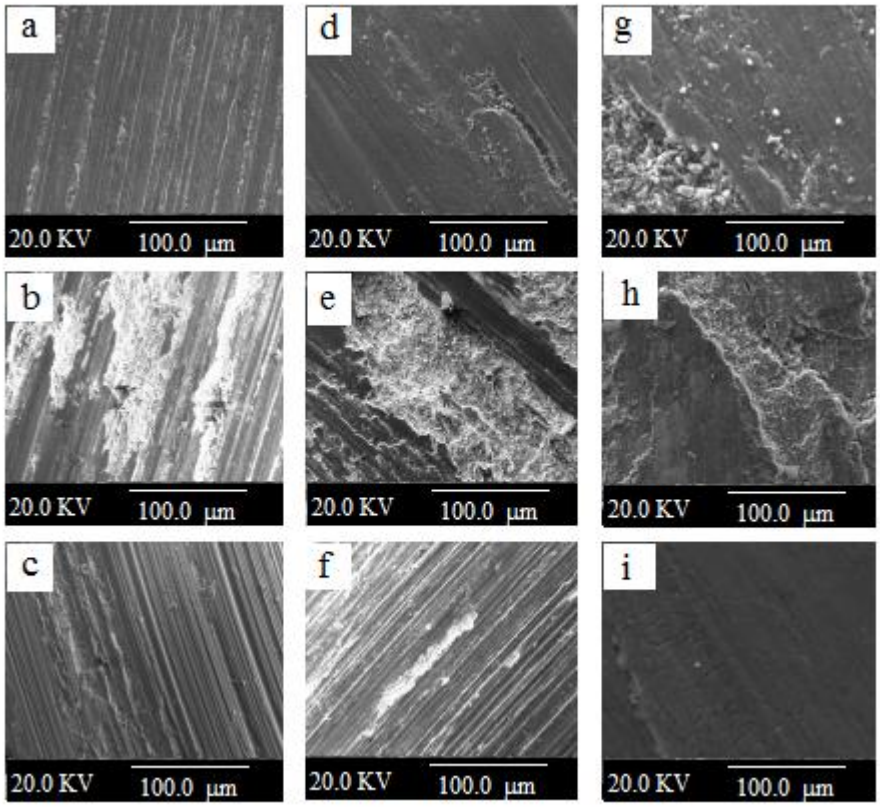

Fig. 5.44. SEM micrographs of the worn surface of spray deposited Al-6Si-20Pb alloy at a thickness reduction of 0 ((a), (d) and (g)), 60 ((b), (e) and (h)) and 80 % ((c), (f) and (i)) for different applied loads viz. 30 N ((a), (b) and (c)), 40 N ((d), (e) and (f)) and 50 N ((g), (h) and (i)).

5.5.2 Worn-out debris analysis

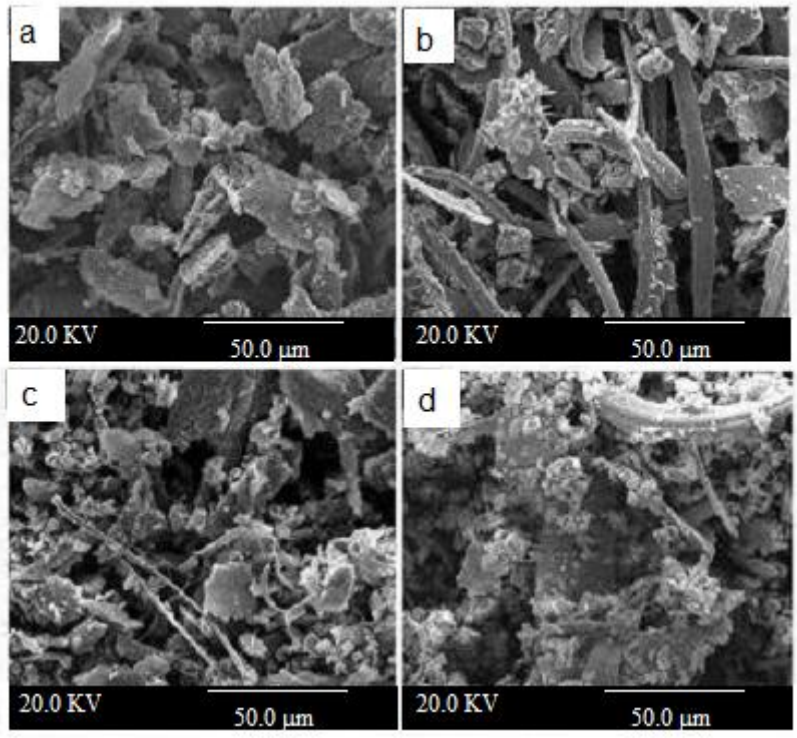

Fig. 5.45. SEM micrographs showing wear debris of spray deposited Al-6Si-20Pb alloy for without ((a), (b)) and with 80 % ((c), (d)) thickness reduction at different loads; 30 N ((a), (c)) and 50 N ((b), (d)).

The debris generated during wear was collected from disc after wear test and observed using SEM. The debris was in the form of fine grey particles. **Fig. 5.45** shows SEM micrographs of the wear debris generated at 0 and 80 % thickness reductions and at 30 and 50 N load. At low load, (**Fig. 5.45 (a)** and **(c)**) the debris consists primarily of oxide particles, consistent with a primary oxidative wear mechanism (as depicted by EDS and XRD in **figs. 5.46** and **5.47,** respectively). The shape of debris particles is irregular and the average size of the particles is less than 20 µm. With increasing load (**Fig. 5.45 (b)**), the average size of debris particles increased and platelet debris was formed. In **Fig. 5.45 (d)**, the debris was in the form of a mixture of particles and platelets.

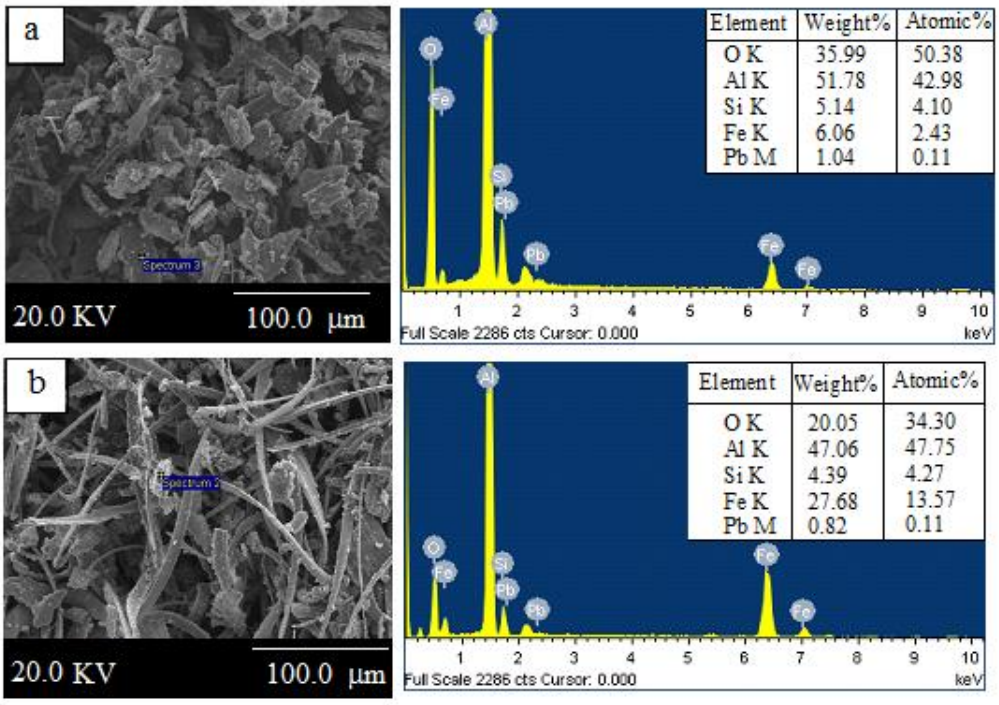

Fig. 5.46. EDS spectrum of the worn-out debris of spray deposited Al-6Si-20Pb alloy at the load of (a) 30 N and (b) 50 N.

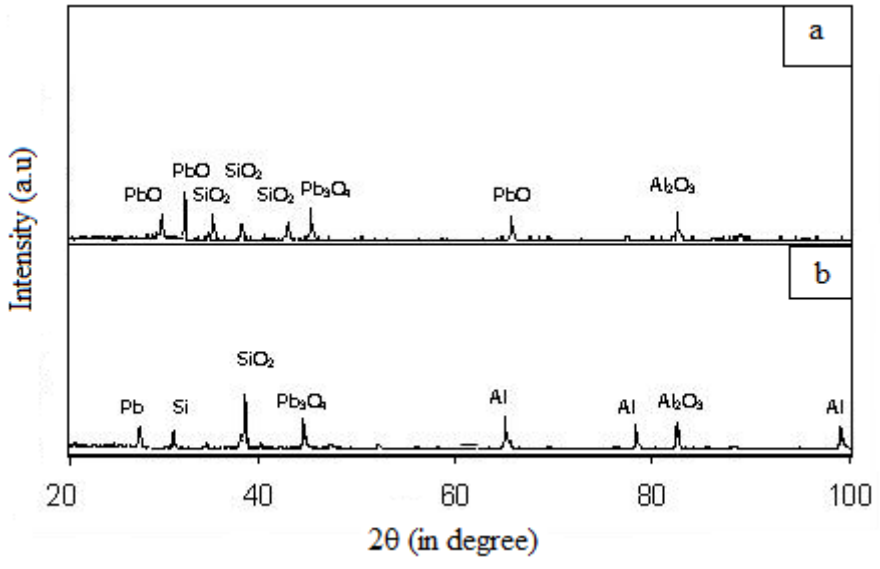

Fig. 5.47. XRD of the worn-out debris of spray deposited Al-6Si-20Pb alloy at the load of (a) 30 N and (b) 50 N.

5.6 Coefficient of friction

Variation in coefficient of friction of spray deposited Al-6Si-(0-30)Pb alloy with the thickness reduction at different applied loads are presented in **figs. 5.48** to **5.51**.

The change in coefficient of friction of spray deposited Al-6Si-0Pb alloy with the thickness reduction is shown in **fig. 5.48** at different applied loads. It can be observed that the coefficient of friction decreases up to a thickness reduction of 80 % continuously for all the applied loads also, it is highest for 10 N load and lowest for 30 N load.

The coefficient of friction of spray deposited Al-6Si-10Pb, Al-6Si-20Pb and Al-6Si-30Pb alloy is plotted against the thickness reduction in **fig. 5.49, 5.50** and **5.51**, respectively. Coefficient of friction decreases continuously with almost same rate up to a thickness reduction of 80 %.

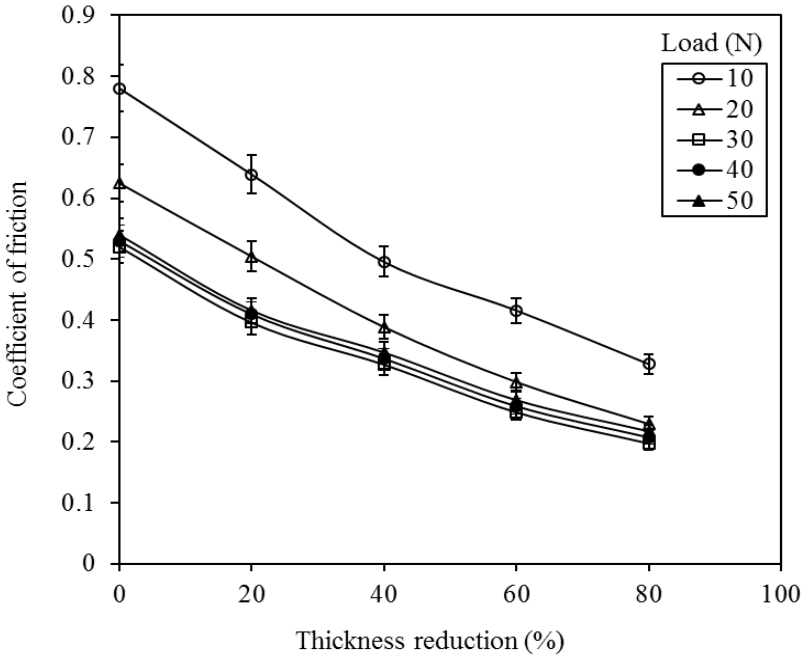

Fig. 5.48 Variation in coefficient of friction of spray deposited Al-6Si-0Pb alloy as a function of thickness reduction at different applied loads.

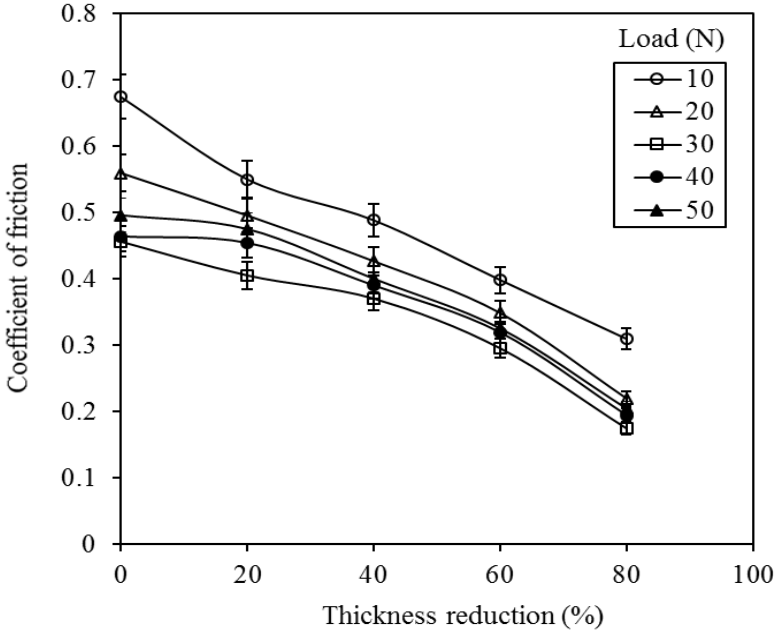

Fig. 5.49 Variation in coefficient of friction of spray deposited Al-6Si-10Pb alloy as a function of thickness reduction at different applied loads.

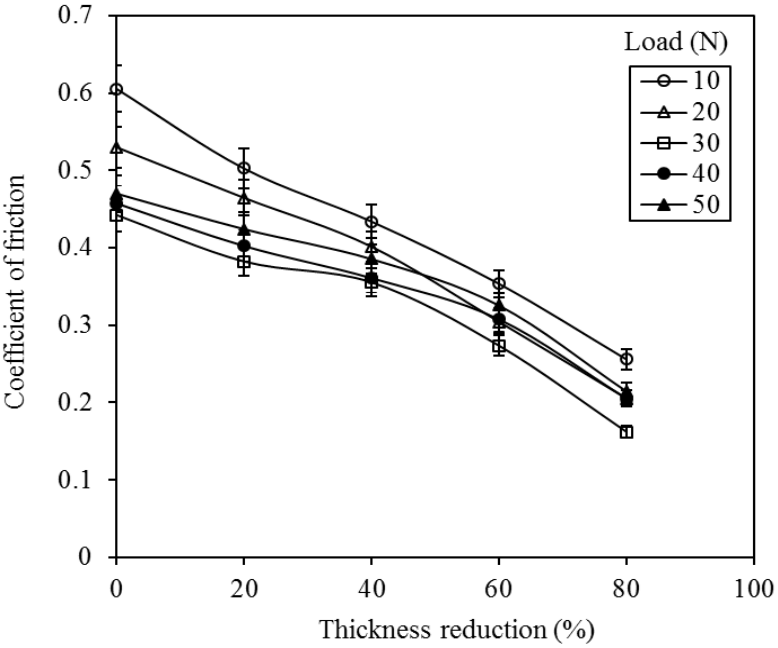

Fig. 5.50 Variation in coefficient of friction with thickness reduction for spray deposited Al-6Si-20Pb alloy.

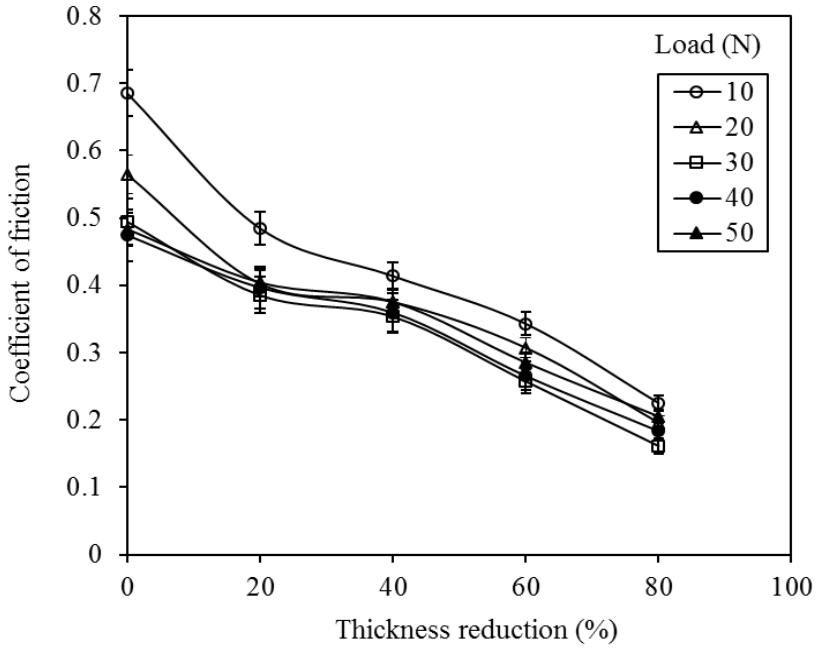

Fig. 5.51 Variation in coefficient of friction with thickness reduction for spray deposited Al-6Si-30Pb alloy.

Fig. 5.52 shows the **v**ariation in coefficient of friction with Pb content for spray deposited Al-6Si-xPb alloy for different applied loads. It can be seen that coefficient of friction decreases with increases Pb content up to 20 % and after this, it starts increasing. **Fig. 5.53** shows the variation in coefficient of friction with applied load for spray deposited Al-6Si-xPb alloy for different Pb content. Coefficient of friction decreases up to 30 N load and after this, it is almost constant.

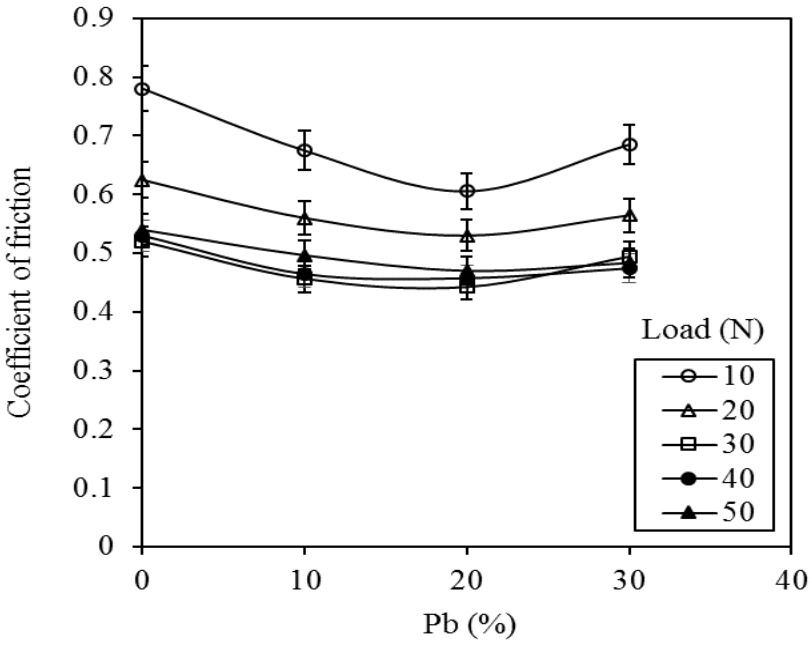

Fig. 5.52 Variation in coefficient of friction with Pb content for spray deposited Al-6Si-xPb alloy for different applied loads.

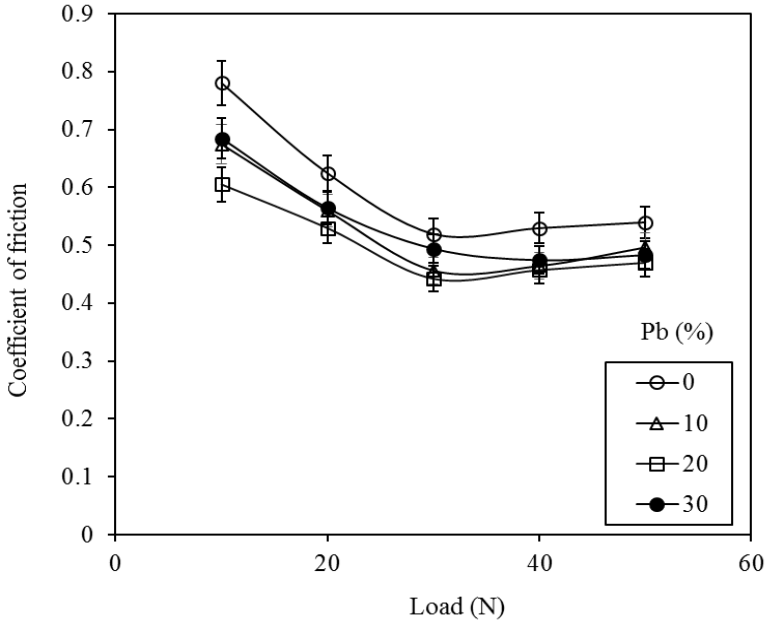

Fig. 5.53 Variation in coefficient of friction with applied load for spray deposited Al-6Si-xPb alloy for different Pb content.

5.7 Corrosion rate

Fig. 5.54 shows the Tafel extrapolation plots of spray deposited Al-6Si alloy for (a) 0, (b) 10, (c) 20 and (d) 30 % Pb contents.

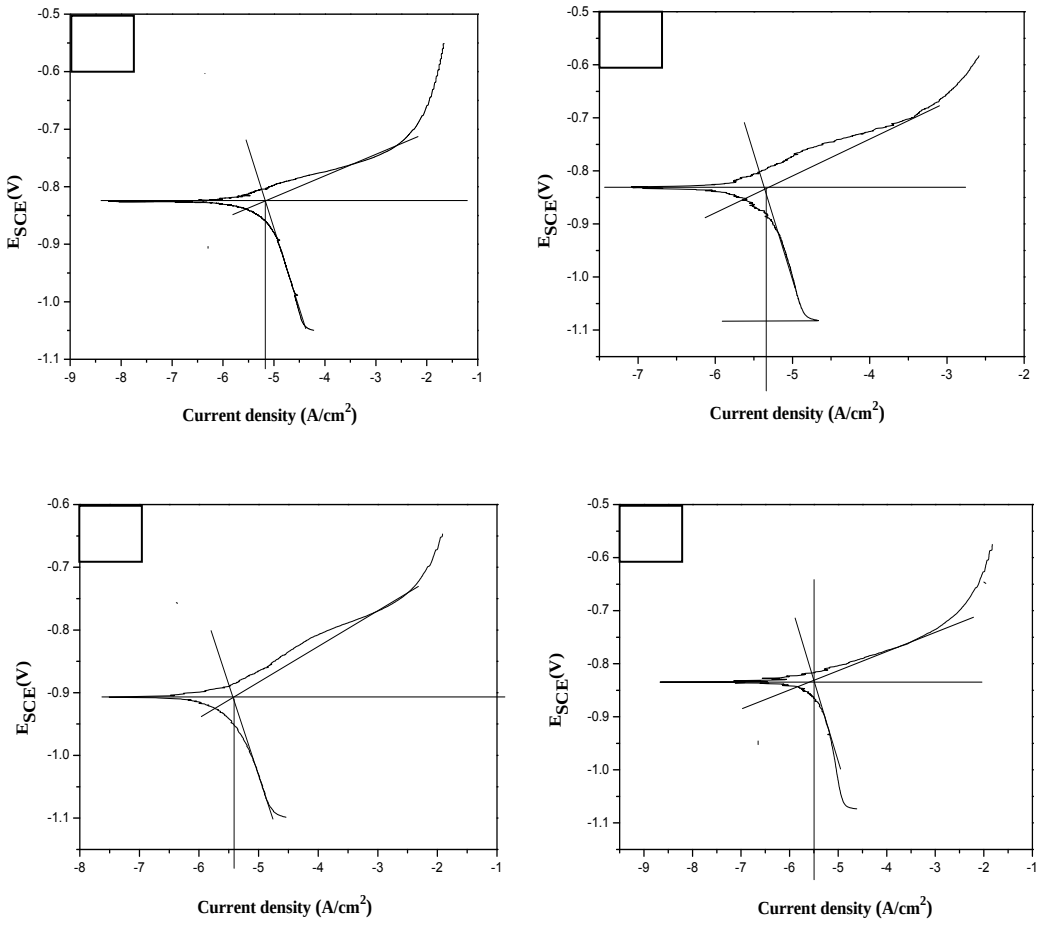

Fig. 5.54 Tafel extrapolation plots of spray deposited Al-6Si alloy for (a) 0, (b) 10, (c) 20 and (d) 30 % Pb contents.

Corrosion rate variation of spray deposited Al-6Si-(0-30)Pb alloy with the thickness reduction is shown in **fig. 5.55**. For the alloy having 0 % Pb, it can be seen that corrosion rate decreases up to a thickness reduction of 20 % and then it increases up to that of 40 % and beyond 40 % thickness reduction, it remains almost constant. For the alloy having 10 % Pb, Corrosion rate increases up to a thickness reduction of 20 % and then it decreases up to that of 40 %. It again increases up to a thickness reduction of 60 % and then decreases up to that of 80 %.

For the alloy having 20 % Pb, Corrosion rate increases up to a thickness reduction of 20 % and then it decreases up to that of 40 % and afterwards it again increases up to that of 80 %. For the alloy having 30 % Pb, It can be observed that the corrosion rate increases up to a thickness reduction of 20 % and then it decreases up to that of 40 %. Beyond 40 % thickness reduction, it again starts increasing. The graph shows the same behavior as that of the alloy having 20 % Pb.

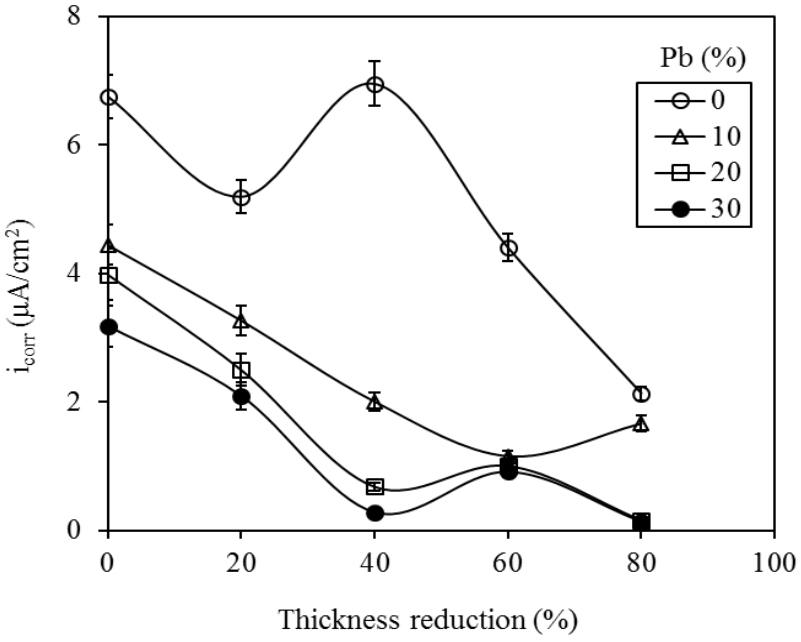

Fig. 5.55. Variation in corrosion current of spray deposited Al-6Si-(0-30)Pb alloy as a function of thickness reduction.

Fig. 5.56 shows the variation in corrosion current of spray deposited Al-6Si-(0-30)Pb alloy as a function of Pb content for different samples. It can be observed that corrosion current decreases with increasing the Pb content. Also, for every percentage of Pb content, value of corrosion current decreases from centre to periphery. **Fig. 5.57** represent the SEM micrographs showing corrode surface of spray deposited Al-6Si-20Pb alloy for (a) 0, and (b) 80 % thickness reduction. It can be seen that the surface is more corroded at 0 % thickness reduction as compare to that of 80 %.

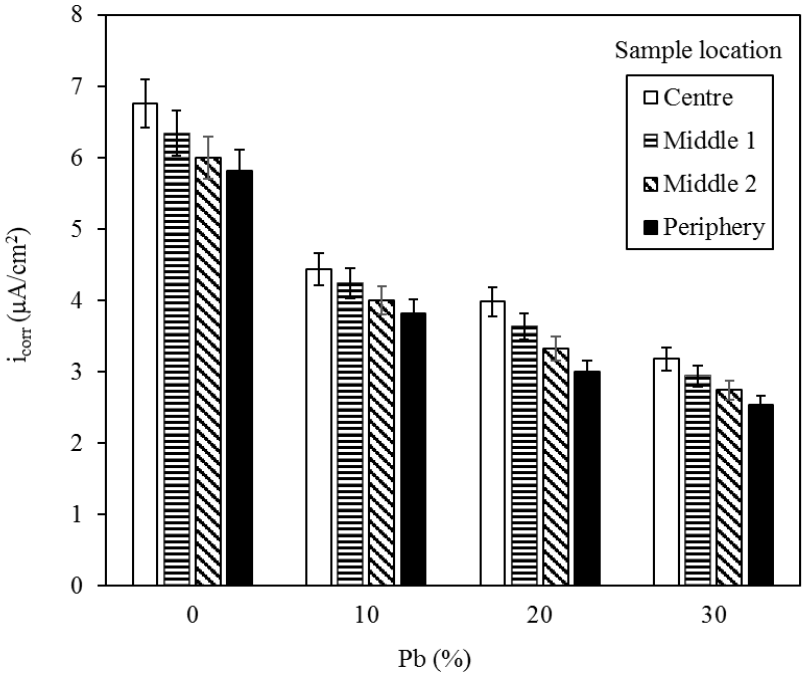

Fig. 5.56. Variation in corrosion current of spray deposited Al-6Si-(0-30)Pb alloy as a function of Pb content for different samples.

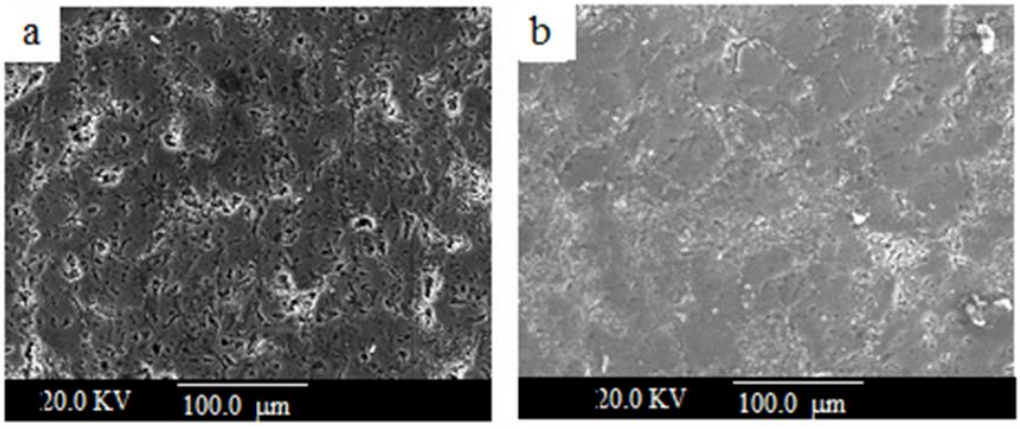

Fig. 5.57. SEM micrographs showing corrode surface of spray deposited Al-6Si-20Pb alloy for (a) 0, and (b) 80 % thickness reduction.

CHAPTER -6

DISCUSSION

6.1 Solidification and microstructural evolution in spray deposit preform

The turbulent fluid flow conditions and the high impact velocity of the droplets on the growing deposit give rise to fragmentation of dendritic arms. These fine fragments act as nuclei for the solidification of melt on the surface [27]. On the other hand, a continuously depositing and solidifying semi-liquid or semi- solid mass will release heat rapidly to the surroundings having high gas velocity. This high gas velocity leads to high rate of heat transfer by convection and previously deposited mass leads to heat transfer by conduction from the depositing mass. Therefore, the formation of nuclei and high rate of heat transfer leads to very high solidification rate of the spray deposit and thus formation of equiaxed structure [29] (**fig. 5.1(a)**). In **fig. 5.1(a)**, silicon is in particulate form, contrary to that of the convectional cast structure [38, 113, 114]. It also indicates rapid solidification of the deposit [38].

There was almost same grain size at the top and centre of the preform (**figs. 5.1** and **5.2**). It indicates almost same solidification rate at these locations. It can be understood as follows. Under a steady state condition i.e. when there is no change in substrate temperature with time and metal is depositing continuously on it, the solidification rate cannot vary along the thickness of the deposit. It can be understood as follows. A constant mass flow rate of droplets/ particles varying in radial direction in the spray cone moves towards the substrate. The deposit grows in thickness direction with a constant rate. This deposition rate varies only in radial direction of the deposit which results in a non-uniform thickness of the deposit. It implies that the solidification rate should be constant in thickness direction and vary in radial direction. If solidification rate is not constant in thickness direction i.e. it is decreasing or increasing with the thickness, in that case one condition will arrive at which nothing or everything will solidify on top surface of the deposit. Both of these events are not occurring. Therefore, under steady state condition, solidification rate will not vary along the thickness of the deposit. So, it can give rise to same solidification rate at top and centre regions of the deposit and hence same grain size.

The grain size is lower at peripheral region (**fig. 5.3**). The small thickness of the deposit at peripheral region leads to an increase in the heat transfer rate by conduction as compared to that of central region. High heat transfer rate means more cooling rate at peripheral region which induces the formation of more fine grains structure. Although, the velocity of the gas is higher at centre as compared to that of the periphery of the deposit. Therefore, the grain size should be finer at centre as compare to that of periphery but the reverse is true in the present study. Hence, the former reason explained above dominates over this factor.

Lead will solidify after the solidification of aluminum therefore molten lead will diffuse towards the liquid present in the deposit during solidification of the Al-rich deposit. Hence, molten lead diffuses towards the grain boundary of aluminum and accumulates over there in small droplets (**fig. 5.4**). More quantity of lead in aluminum rich melt means more accumulation of lead at the grain boundaries (**figs. 5.4** to **5.12)**. The spherodization time and the solidification time of Al-rich melt are responsible for the shape of these lead droplets. The lead droplet will be spherical if Al-rich melt solidify after the spherodization time of lead, otherwise non-spherical. The large size lead droplets will take more time to spherodize and hence these will remain non spherical. Silicon will also diffuse to the grain boundary and solidify before solidification of the lead. Therefore, some silicon particles at grain boundaries were observed to be surrounded by lead.

6.1.1 Effect of thickness reduction on microstructure

The reduction in thickness is accompanied by an elongation of the Al-grains in the rolling direction [69] as shown in **fig. 1(b), (c), (d)** and **(e)**. In the preliminary stage of rolling i.e. about 40 % reduction, movement of porous mass resulting in the removal of porosity. As a result the pores are removed by a process involving pore elongation in the direction of rolling followed by fragmentation into several smaller size pores. This process of elongation and fragmentation of pores continues with rolling. When the width of the pores becomes very small, the opposite faces of the pores collapse and the porosity is almost eliminated [87]. If there is an oxide layer in the pores that can also rapture by the deviatoric stresses but it would be difficult to have a proper bonding between the surfaces of the pores. Beyond this deformation, plastic deformation becomes the major mechanism of densification during rolling. The change in the shape of the Al-grains from globular to elongated confirm the plastic deformation of the grains [115]. The probable causes of cracks during cold rolling may be the porosity and internal voids existing in the spray cast structure. Normally, the free surfaces of cavities and porosities are coated with an

oxide film, disallowing the closure of those upon application of compressive pressure, as a result of which cracking may be initiated.

6.2 Study of the influence of Pb content on structural parameters of Al-Si alloy via X-ray diffraction.

To determine the effect of Pb (**fig. 5.14**), the lattice parameter of Al reflections and lattice strain are determined by using equation 1 (Bragg's law), 2 and 3 respectively.

According to Bragg's law,

$$n\lambda = 2d.Sin\theta \tag{6.1}$$

For lattice parameter,

$$a = d.(h^2 + k^2 + l^2)^{1/2} \tag{6.2}$$

For lattice strain,

$$\varepsilon = \beta/tan\theta \tag{6.3}$$

Where,

n = order of reflections ~ 1,

λ = x-ray wavelength (for Cu~ 1.54 A^o),

d =interplanner spacing,

θ =diffraction angle,

a =lattice parameter,

hkl =planes,

ε =lattice strain and

β = FWHM (full width half maxima).

From **fig. 5.14**, shift in peak position is found by increasing the lead content. Lead atoms introduce the lattice disorder that can cause the shifting of peak due to the change in interplanner spacing of every reflection. The atomic radius of Al ~ 125 pm and Si ~117.6 pm is comparably similar but, Pb ~ 180 pm have higher atomic radius than Al and Si. Therefore, Pb atoms may create a disorder in Al-Si alloy. The presence of disorder influences the reflections and structural properties of the alloy. The effect of lead content on lattice parameter, lattice Strain and crystallite Size of Al are given in table 1.

Table 6.1: The effect of lead content on lattice parameter, lattice Strain and crystallite Size of Al.

Composition	Lattice parameter of Al (A^o)	Lattice strain (%)	Crystallite Size (nm)
Al-6Si-0Pb	4.053	0.869	37.83
Al-6Si-10Pb	4.041	1.003	39.84
Al-6Si-20Pb	4.046	1.009	40.50
Al-6Si-30Pb	4.037	0.989	40.90

The crystallite size is found to increases due to the shifting of peak position with respect to Pb addition in Al-6Si alloy. For Al-6Si-0Pb alloy, the crystallite size is ~ 37.83 nm, whereas for 10%, 20% and 30% Pb rich Al-6Si alloy, the crystallite size approaches to 39.84, 40.50 and 40.90 nm, respectively. **Table 6.1** indicates, the lattice parameter for Al reflections. However, data follows the same trend, but slight increase in lattice parameter for Al-6Si-20Pb alloy is observed. The increase in lattice parameter for Al-6Si-20Pb alloy is due to the increase in lattice strain. The increase in lattice strain is observed due to the non-uniform type (shifts of atoms from their ideal position and peak broadening) strain. Generally, this non-uniform type behavior is noticed due to the point defects (vacancies, site-disorder) or poor crystallinity. In this context, this slight change in lattice strain is observed because of the disorder created by Pb atoms in Al-Si matrix. Therefore, the lattice parameter is varied due to the lattice strain. From **fig. 5.14**, the relative intensities of reflections for Al-6Si-20Pb alloy are lower than Al-6Si-10Pb alloy. Those relative intensities of reflections are certainly decreases with increase of Pb content in the Al-Si alloy. For Al-6Si-0Pb alloy the relative intensities of reflections are found to be larger than the other Pb added Al-6Si alloy. The simplified reason for this context is accumulated Pb atoms and their electrons [8] take participation in the relative intensities and respective reflections.

The cold rolling process changes the crystallographic texture in Al-6Si-xPb alloy (**fig. 5.15**) there of impact on structural properties and other mechanical properties. The study is analyzed in **fig. 6.1** and **6.2**, respectively. The induced crystallographic texture by cold rolling is studied with the help of eq. 4 and 5. In this relation, texture coefficient of a hkl crystallographic plane is calculated and correlated with the rolling order,

$$TC_{(hkl)} = R_{exp(hkl)}/R_{theo(hkl)} \tag{6.4}$$

$$R_{(hkl)} = (I_{(hkl)}/\Sigma I_{(hikili)}) * 100 \tag{6.5}$$

Where $R_{exp(hkl)}$ is the experimental reflection plane of crystallographic plane (hkl) and $R_{theo(hkl)}$ is the theoretical reflection plane of the same crystallographic plane, $I_{(hkl)}$ is the intensity of (hkl) crystallographic plane and $\sum I_{(hikili)}$ is the sum of all intensities analyzed. In addition, $R_{exp(hkl)}$ is calculated from the experimental diffraction spectrum of aluminium alloy and eq. (5), whereas $R_{theo(hkl)}$ is calculated from the theoretical diffraction spectrum presented in ASM data and eq. (5).

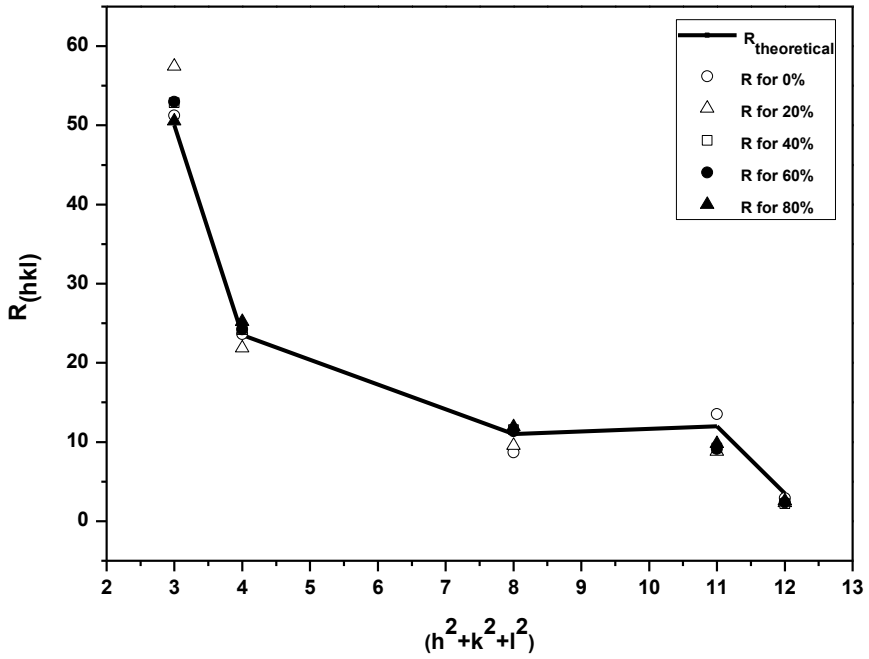

Fig. 6.1. Comparison between the theoretical reflection of crystallographic planes and experimental reflection of crystallographic planes for 0 to 80 % thickness reduction.

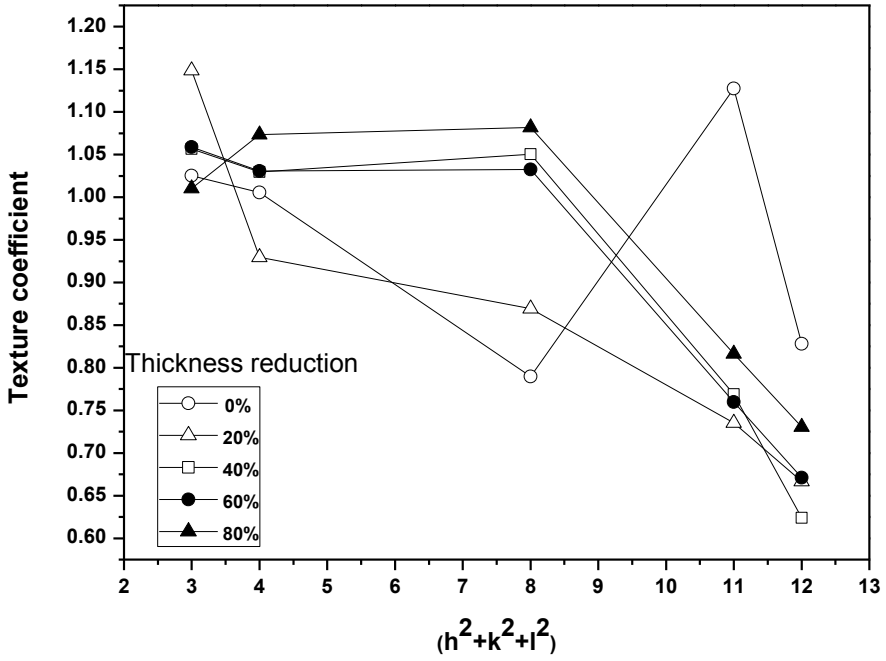

Fig. 6.2. Influence of thickness reduction on texture coefficient (crystallographic orientation) for a crystallographic planes.

Fig. 6.1 shows the comparison between the theoretical reflection of crystallographic planes and obtained experimental reflection of crystallographic planes for (0-80%) thickness reduction. For [(111), (220)], thickness reduction increases the R_{exp} reflection of crystallographic plane. The experimental results are compared with the standard ASTM XRD (R_{theo}) data for Al. For 0% thickness reduction, R_{exp} have almost similar values as that of R_{theo} for all planes, except for (220) plane. While, for 20%, 40%, 60% and 80% thickness reduction the results are comparable with the standard ASTM XRD (R_{theo}) data. To examine the reason behind this behaviour, the texture coefficient (TC) have been calculated by using eq. 4. The preferred orientations for texture development of 0% thickness reduction are [(111), (200) and (311)]. This is because the texture coefficient for these crystallographic planes has values greater than 1, which indicates preferred orientation. For 20% thickness reduction, the preferred orientations for texture development is (111). This might be because of cold rolling, which destroyed the crystalline order. This behaviour is also observed for other thickness reduction. For 40%, 60% and 80% thickness reduction, the preferred orientations for texture development are (111), (200) and (220). This developed texture can lead a significant increase of the hardness and mechanical properties of the alloy [8]. The influence of thickness reduction on texture coefficient (crystallographic orientation) for a crystallographic planes is shown in **fig. 6.2**.

6.3 Porosity development in preform

There are two types of porosity in the samples. One is originated during spray forming and the other one is originated during rolling. During spray forming, porosity can take place due to the dissolved gas evolution, insufficient melt to fill porosity, gas entrapment and solidification shrinkage while during rolling, porosity can take place due to the crack formation in the sample. Therefore, first one is called as casting porosity and the other one is called as crack porosity. In the present study, some remarkable features observed on porosity development were the decrease in porosity from centre to periphery of the deposit (**fig. 5.18**), the variation in porosity with thickness reduction (**figs. 5.20** to **5.23**) and the increase in porosity with the increase in lead content (**fig. 5.24**). However, porosity remains same along the thickness of the deposit (**fig. 5.17**).

As it was discussed in earlier section that the solidification rate remains same along the thickness of the deposit therefore porosity also remains the same. If the porosity increasing or decreasing with the increase in thickness, in that case one condition will arrive at which 0 or

100 % porosity occurs on the top surface of the deposit. Both of these events are not occurring. Hence, porosity remains same along the thickness of the deposit.

There can be two reasons due to which porosity decreases from centre to periphery of the deposit. First, the grains size decreases at periphery. It means that the grain size of Pb droplets also decreases. The interstitial voids generated due to the solidification of Al-rich phase were filled with these fine lead droplets and therefore, the porosity decreases at periphery. Second, the decrease in gas velocity at periphery as compare to that of the centre of the spray deposit. High gas velocity at the centre can lead to more entrapment of the gas in the deposit as compared to that of the periphery and hence more porosity formation at the centre of the deposit.

6.3.1 Porosity variation during rolling

During the rolling process, casting porosity of the material decreases and it is almost eliminated at 80% thickness reduction. But phase become hard with rolling and hard phase is more prone to crack due to which cracks generated in the material, these cracks forms the crack porosity. The total porosity of the sample is the combination of these two porosities (crack and casting). Total porosity increases if rate of increase in crack porosity is higher than the rate of decrease in casting porosity after rolling. In Al-6Si-0Pb alloy, porosity increases at 40% thickness reduction it means, at 40 % thickness reduction rate of increase in crack porosity is higher than the rate of decrease in casting porosity while in case of Al-6Si-20Pb and Al-6Si-30Pb alloys porosity increases at 60% thickness reduction it means, at 60 % thickness reduction rate of increase in crack porosity is higher than the rate of decrease in casting porosity. But there was continuous decrement in porosity up to 60 % thickness reduction for the composition Al-6Si-10Pb as observed from **fig. 5.21**. It means, rate of increase in crack porosity is lower than the rate of decrease in casting porosity up to 60 % thickness reduction. It was due to the presence of softer Pb phase in the grain boundary region. But as we further increase the composition of Pb in Al-6Si material there are two possibility for the Pb. The Pb may also occupy the interstitial position in the FCC structure of Al or may form individual bulk particulate in the matrix of Al-6Si. The interstitial position of Pb can be confirmed by the XRD analysis. There is observed shift in the peak positions (**fig. 5.14**) due to the change in interplaner spacing of the Al reflections. This may decrease the stability of the Al matrix, since a distorted structure have less stability as compared to a normal structure. So, the cracks porosity dominate in Al-6Si-

20Pb and Al-6Si-30Pb while not for Al-6Si-10Pb material. However, cracks get also filled by the same process as the pores fill in the samples and therefore porosity again decreases.

6.3.2 Effect of lead content on porosity

By increasing the lead content, surface tension of aluminum decreases [103] and hence the flow of aluminum should take place easily. Therefore, porosity of the preform should decrease by increasing the lead content. But it was found that porosity increases by increasing lead content. It can be due to the difference in solidification shrinkage of aluminum and lead. The solidification shrinkage of lead is higher than that of aluminum. There can be formation of shrinkage cavity around lead particles in the deposit because lead solidifies after the solidification of aluminum rich phase. Also, the fraction of melt (as Pb) increases on the deposition surface by increasing the lead content. More melt will give rise to more solidification shrinkage porosity. There can be significant dissolution of hydrogen in the Al-Si-Pb alloy. This hydrogen comes from the humidity and it can dissolve mainly in aluminum because in lead its solubility is very low [116]. Therefore, the increase in lead content should decrease the porosity but the reverse is true in the present study. Hence, the former reason of solidification shrinkage explained above dominates over this factor of gas dissolution.

6.4 Hardness

Hardness is going to increase continuously with the increase in thickness reduction (**figs. 5.27** to **5.30**) due to the development of texture orientation [90] (as explained earlier in section 6.2) and work hardening of the alloy. The number of dislocations per materials volume increases significantly during the forming processes of metallic materials [90]. Thus, the nucleation and movement of new dislocations is hindered by the existing dislocations, causing an increase of hardness. Although by increasing the Pb content, hardness decreases (**fig. 5.31**) due to the increase in porosity.

Hardness of the Al-Si-Pb alloy preform was recorded as a function of lead content (**fig. 5.31**), distance from centre to periphery (**fig. 5.32**) and with thickness reduction. A factorial design analysis [117, 118] was conducted to study the effect of different parameters, viz., lead content, distance from centre to periphery of the preform (R_s) and thickness reduction, which is as follows. The design matrix of these three variables is given in **table 6.2**.

Table 6.2 Design matrix for hardness study

Pb	R_s	Thickness reduction
-	-	-
+	-	-
-	+	-
-	-	+
+	+	-
+	-	+
-	+	+
+	+	+

Values of the required parameters for this design matrix are given below in **table 6.3**

Table 6.3 Values of various parameters as per design matrix.

Pb (%)	R_s (mm)	Thickness reduction (%)	Hardness
0	0	0	45.40
30	0	0	35.60
0	90	0	47.50
0	0	80	75.50
30	90	0	38.70
30	0	80	65.56
0	90	80	79.40
30	90	80	68.4

The calculated effect of all the parameters on hardness is given below in **table 6.4**.

Table 6.4 Effects of various parameters on hardness.

Parameters	Effects
Thickness reduction	60.8
Pb	- 19.8
R_s	6

From above table it can be seen that the effect of thickness reduction on hardness is much higher as compared to that of the distance from centre to periphery of the deposit and lead content. The influence of Pb content is more than that of the distance from centre to periphery (Rs). Negative sign indicates that hardness decreases by increasing the lead content.

It can also be verified from **fig. 6.3** which shows the plot between relative variation in hardness and relative variation of different parameters viz. Pb content, thickness reduction and distance from centre to periphery (R_s).

Both, porosity and grain size decreases with the increase in distance from centre to periphery of the deposit. Therefore, a small effect of the distance on hardness means that both porosity and grain size or any one of them has small effect on the hardness. Panagopoulos et. al [90] reported that the decrease of average grain size of aluminum alloy leads to the increase of its hardness. Hence, the increase in hardness with the increase in distance from centre to periphery of the preform is due to the decrease in porosity and grain size of the deposit.

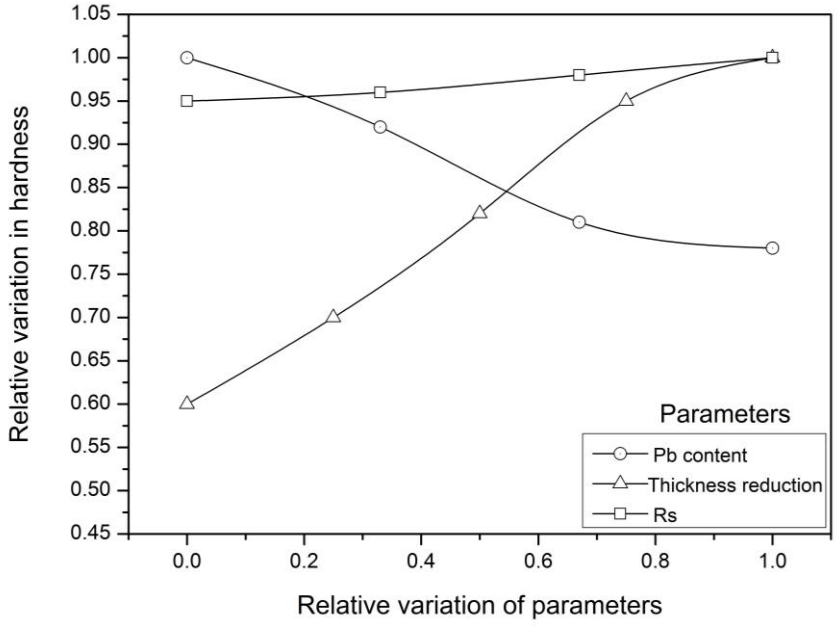

Fig. 6.3. Relative variation in hardness Vs relative variation of parameters.

Finally, it can be concluded that hardness increases drastically with the increase in thickness reduction. Also, porosity and grain size both have an effect on hardness and the decrease in hardness with the increase in lead content is attributed to the increase in soft phase (Pb rich) and the increase in porosity with the increase in lead content.

6.5 Wear characteristics

The effect of alloy composition, thickness reduction via rolling and load on wear rate of Al-6Si-(0-30%)Pb alloys have been investigated. The wear rate decreases and the load-bearing capacity of the alloy increases with increasing lead content. The nature of the wear process changes with applied load. There is still no clear agreement in the literature regarding the role of porosity distribution and thickness reduction on the wear resistance of Al-Si-Pb alloys. Therefore, the present work has been undertaken to investigate systematically the effect of thickness reduction over a wide range of composition on the wear resistance of Al-Si-Pb alloys. Further, the topography of the worn surfaces have been studied in detail to elucidate the wear mechanisms.

When two surfaces slide against each other under an applied load, repetitive welding and fracture through the weaker metal causes the wear [14]. Thus, it is obvious that as the load increases, the enhanced rate of fracture will result in a larger amount of wear. Moreover, as the load increases, the temperature attained by the specimen during sliding is also increases because of an increased amount of heat generation owing to friction. The increase in temperature causes the oxidation of the specimen. Hence, oxidative wear takes place at a lower applied load (10 to 30 N). Metal oxides present in debris confirms it (**fig. 5.47(a)**).

Wear rate versus load variation (**figs. 5.33** to **5.36**) can be divided into three distinct regions having different rate of increase in wear rate with the increase in applied load. Wear in these regions may be referred to as mild wear (oxidative), intermediate wear and severe wear (metallic). These wear regions are a function of applied load. Shivanath et al**.** [119] have identified at least two of the above types of wear regions in their work, but their wear rate depend on the composition. Dwarkadasa [120] and Kadhim [121] have also identified the mild and intermediate wear regions in their subsequent work on different materials and showed in each case a linear dependence of wear rate on applied load.

In order to investigate the wear mechanism, the surfaces of the worn samples were examined under SEM (**figs. 5.43** and **5.44**). In first region (at a lower load), the worn surface appears smooth and consisted with fine grooves. A white film formed over the surface of the specimen with the increase in applied load (**fig. 5.43 (a), (b)** and **(c)**). EDX was used to check the composition of worn surface, it showed that worn surface contains a certain amount of Fe and O, which indicates a typical oxidative wear [41, 61]. In this region, wear rate increases linearly with the increase in applied load because progressively more white film is available to wear with the increase in load. In second region, there is damage to the oxide film (white film)

as load is increased further (**fig. 5.43 (d), (e)** and **(f)**). As the surface oxide is removed, the fresh metal exposed is further oxidized. Since the amount of metal removed is confined to the thickness of the oxide layer, the wear loss observed in this region did not show much variation with the applied load. Therefore, the rate of increase in wear rate has decreased in this region as compared to that of the first region. In third region, deep black groove and more damage to oxide film (white film) appears with the increase in applied load (**fig. 5.43 (g), (h)** and **(i)**). As the applied load exceeds the yield strength of the material, the fracture occurs with the separation of large fragments of the metal. Therefore, the rate of increase of the wear rate in this region is higher than that of other two regions. It is due to the starting of metallic wear or delamination wear as revealed by XRD analysis of the debris (**fig. 5.47(b)**).

6.5.1 Influence of thickness reduction by cold rolling

Wear rate decreases for cold rolled spray deposited alloy as compare to that of spray deposited alloy (**figs. 5.37** to **5.40**). The wear rate is often considered to be inversely proportional to the hardness of the composite, according to the well-known Archard's law [122, 123]. Also, porosity in the as sprayed composite is a kind of serious microstructure defect that affects the wear resistance of materials [124, 125]. Cracks can be generated from these porosity during wear test. Therefore, the porosity is equal to crack sources. Thus, wear rate is a function of hardness and as well as of porosity. As we discussed in previous sections that the hardness and density of the alloy increases with thickness reduction therefore wear rate decreases with thickness reduction.

But, the trend of the wear plots is same as that of the porosity plots. **Fig 6.4** shows the wear rate variation of spray deposited Al-Si-xPb alloy with porosity for different Pb content. A linear relationship can be seen between porosity and wear rate. While there is no such type of relationship observed between hardness and wear rate as shown in **Fig 6.5**. It means that porosity is the predominant factor that affect the wear rate more as compare to the hardness.

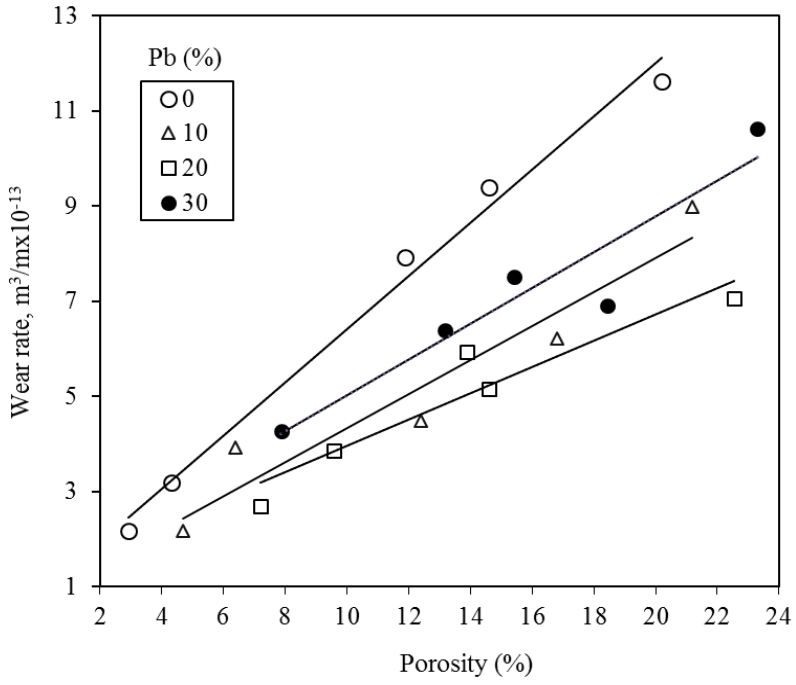

Fig 6.4: Wear rate variation of spray deposited Al-Si alloy with porosity for different Pb content.

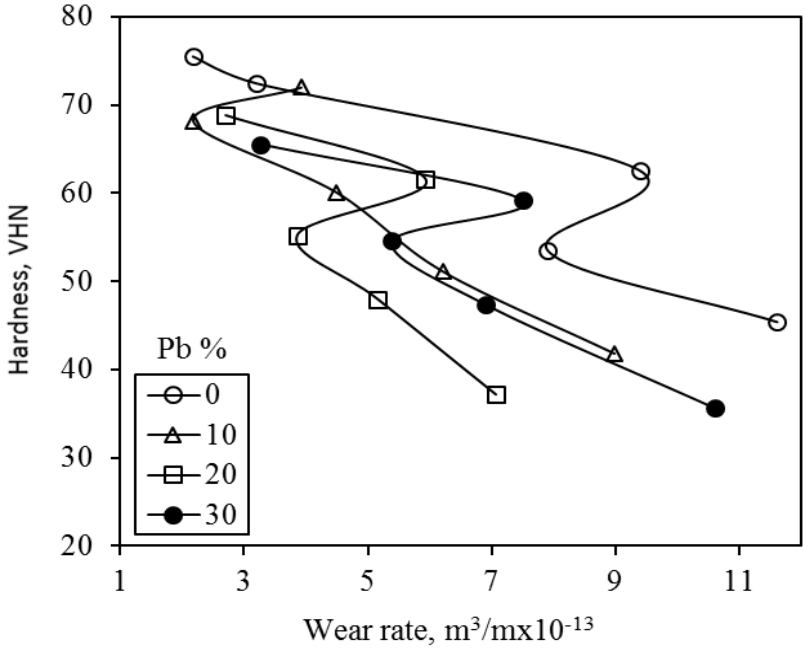

Fig 6.5: Wear rate variation of spray deposited Al-Si alloy with hardness for different Pb content.

At lower load, the wear rate of the as-sprayed alloy is near to that of the cold rolled spray cast alloy. In this condition, the pores beneath the worn surface remain stable and cannot propagate significantly. Therefore, at lower loads, the porosity in the as-sprayed alloy displays very small effects on the wear behavior. When the applied load is large enough so as to make the pores beneath worn surface become unstable then the porosity in the as-sprayed alloy would create a significant influence on wear rate.

6.5.2 Effect of Lead content

The lead metal, which has low hardness, low elastic modulus and low shear strength, spreads very easily between the mating surfaces to form the lubricating film. An easy spreading of lead makes it to cover complete sliding surfaces giving rise to uniform friction, low scatter and stable film that prevents adhesion of sliding matrix material. This results in decreased wear rate [28]. **Fig. 5.41** shows the variation in wear rate with lead content at different applied loads. At a given load, the wear rate decreases with increasing lead content in the alloy up to 20 % due to the wiping of a thin layer of lead over the Al matrix. The wiped area of lead in the matrix increases with lead content up to 20 % but beyond this, there is thickening of the wiped lead layer, resulting in the fragmentation of the lead layer [14]. Therefore the wear rate is increases at higher lead contents above 20 % in spray cast Al-Si-Pb alloy. Similar variations in wear behavior with film thickness has been observed by other workers [126, 127] for different soft metals when coated on hard substrate.

It has been explained in previous section that the porosity increases and hardness decreases with the increase in lead content. Both these factors (increment in porosity and decrement in hardness) increase the wear rate [128]. It means that lead layer is the predominant factor that affect the wear rate more as compared to that of the porosity and hardness, which finally resulting a decrease in the wear rate with an increase in the lead content up to 20 %.

6.6 Coefficient of friction

The coefficient of friction for the spray deposited Al-Si-Pb alloys appeared to decreases with increasing cold rolling deformation (**figs 5.48** to **5.51**). As, it was demonstrated earlier that the cold rolling process has lead to an increase of the surface hardness of spray deposited alloy and thus to the decrease of the coefficient of friction of the material [90]. A D Sarkar has also reported that friction depends on material properties such as hardness, strain, density, shear strength, modulus of elasticity, yield and ultimate tensile strength [129]. High hardness of cold rolled spray deposited alloy may also reduce the incidence of fracture and deformation of surface asperities and therefore real contact area may reduce. Hence, the above may be attributed to low coefficient of friction in sliding of cold rolled spray deposited alloy than that of spray deposited alloy [130].

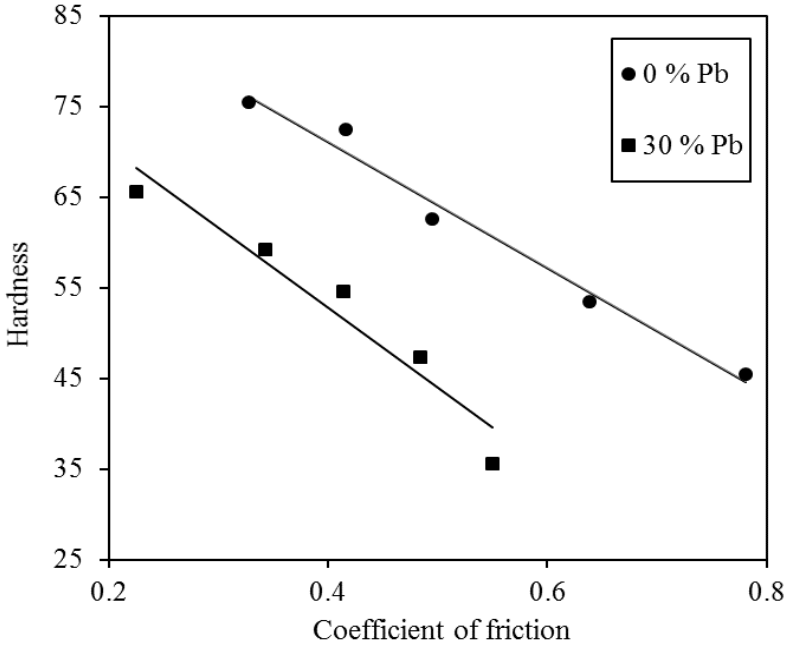

Fig 6.6: Hardness variation of spray deposited Al-Si alloy with coefficient of friction for different 0 and 30 % Pb content.

Fig 6.6 shows the hardness variation of spray deposited Al-Si alloy with coefficient of friction for different 0 and 30 % Pb content. A linear relationship can be seen between hardness and Coefficient of friction. While there is no such type of relationship observed between any other factor and Coefficient of friction. It means that hardness is the major factor that affect the coefficient of friction.

The lower coefficient of friction with Pb content is due to the smearing of the soft Pb on the sliding surfaces (**fig. 5.52**). The lubricating film of Pb at the interface of mating surfaces restricts metal-metal contact and hence resistance to friction is improved. The thickness of the lubricating film has the direct relationship with characteristics of friction of Al-Si-Pb alloy [82]. It has been well demonstrated that an optimum lubrication is obtained at thickness of about 1 μm [28]. Therefore, higher Pb content (beyond 20 %) will results in increase in coefficient of friction.

The coefficient of friction decreases very rapidly up to 30 N load and then it becomes almost constant (**fig. 5.53**). Panagoupoulos et al [131] also concluded that increasing the applied load resulted in a considerable decrease in the friction coefficient of 5083 aluminium alloy against stainless steel. However, the actual area of contact increases with increasing load [106], and accordingly, the coefficient of friction should increases. But, the decay in coefficient of friction is due to the formation and growth of an oxide film. Beyond 30 N load, metallic wear starts and there is no growth of the oxide film, therefore coefficient of friction remains constant. The nature of variation of the coefficient of friction is similar for all the alloys studied.

6.7 Corrosion behavior

The bulk materials have in- build tendency to undergo a high corrosion rate due to the appeared grain boundaries. Hereby, grain boundaries are more prone to intergranular corrosion and stress corrosion. Also, the presence of porosity, alloy elements and defect can influence the corrosion behavior. As we know that grain refinement occurs by spray deposition technique so number of grain boundaries increases in the material produced by spray deposition technique. Therefore, corrosion rate should increase in spray deposit material but, Moore et al have reported that the overall refinement of the microstructural scale provided by the spray deposition process did not have either a beneficial or detrimental effect on corrosion behavior [100]. Here, in this present investigation the role played by defects or disorder are expressed with the help of obtained results and tries to relate with the corrosion theories and other experimental observations.

Corrosion study of Al-6Si-(0-30)Pb alloy as a function of thickness reduction in 3.5% NaCl (Sea water environment) illustrate that the thickness reduction shows the pronounced effect on the corrosion behaviour (**fig. 5.55**). The trend of the graph is similar as that of porosity

graphs. It means porosity affect the corrosion rate. Corrosion rate decreases with the increase in thickness reduction however, it increases where porosity increases.

Form the graph, it can be seen that the initial value of corrosion rate decreases with increase in lead content. When Pb is added to the Al-Si alloys, a microgalvanic coupling cell is formed between Al and Pb [130], reducing the tendency of OCP (open circuit potential). Lee [132] reported that the addition of Pb to Al-Si alloys, does not affect the corrosion potential or corrosion current density, but reduces the anodic polarisation of the Al-Si alloys promoting passivation in the anodic potential direction. A passive film is expected to improve the resistance to a corrosion environment. Also, the oxidation potential of Pb is less than that of Al and corrosion rate is directly proportional to the oxidation potential. Therefore, corrosion rate decreases by increasing the Pb content.

Fig.5.57 shows the SEM morphologies of the corroded surface of the Al-6Si-20Pb alloys for 0 and with 80 % thickness reduction. The type of corrosion is pitting corrosion [133]. Pits initiate at flaws or porosity within the surface film. It is obvious that the without cold rolled sample has much more corroded spots on the surface and higher pitting tendency than others. With increasing the thickness reduction up to 80, the corroded spots of the sample become smaller in size and less in quantity.

CHAPTER -7

CONCLUSIONS

Al-Si-Pb alloys were prepared by spray deposition technique and then cold rolled to different percentage of thickness reductions. Microstructural characteristics, porosity, hardness, wear and corrosion rate of the samples were determined and discussed. The following conclusions can be made:

1. Fine equiaxed grain morphology with a uniform distribution of Pb and Si phase in an Al-matrix was observed.
2. The size of the Al- grains was lower at the peripheral region than that of the centre and top regions of the preform.
3. It was observed from the microstructures that the size of Pb particles increased with the increase in Pb content however it was lower at peripheral region.
4. Grains were observed to be elongated in the rolling direction after 60 and 80 % thickness reductions.
5. Aspect ratio of the Al-grains was increased with the increase in thickness reduction.
6. Pore size was decreased with the increase in thickness reduction and it was almost negligible after 80 % thickness reduction. However, it was increased with the increase in Pb content.
7. A shift in peak position of the XRD pattern was found by adding the Pb and the crystallite size was found to increase with the increase in Pb content.
8. The cold rolling process changed the crystallographic texture in Al-6Si-xPb alloy and the peak intensity for all the planes was found to decrease with the increase in thickness reduction of the sample.
9. Two types of porosity were found in the samples, one was called as casting porosity and the other as crack porosity.
10. The porosity was unaffected along the thickness of the deposit.
11. The porosity of the Al-Si-Pb spray deposited alloy was increased with the increase in Pb content and it was decreased from centre to periphery of the deposit.

12. The total porosity was decreased with the increase in thickness reductions however it was increased where the rate of increase in crack porosity was higher than the rate of decrease in casting porosity with the increase in thickness reduction.
13. Hardness of the deposit was increased from centre to periphery of the deposit and it was decreased with the increase in porosity of the deposit.
14. Hardness of the deposit was increased with the increase in thickness reduction and it was decreased with the increase in lead content.
15. Increase in wear rate with the increase in applied load has three stages, in the second stage rate of increase in wear rate was the lowest and in the third stage it was the highest.
16. The Wear rate was decreased linearly with the increase in Pb content up to 20%, after that it was increased.
17. The wear rate was decreased from centre to periphery of the deposit.
18. The wear rate was decreased with the increase in thickness reductions irrespective of Pb content however it was increased where the porosity was increased. A linear relationship was found between wear rate and porosity of the samples.
19. Coefficient of friction was decreased with the increase in thickness reduction. Also, it was decreased with the increase in Pb content up to 20 % and afterwards it was increased.
20. Coefficient of friction was decreased rapidly up to the load of 30 N and beyond this load it was almost constant.
21. A linear relationship was found between Coefficient of friction and hardness of the samples.
22. Corrosion rate was decreased with the increase in thickness reduction however it was increased where the porosity was increased.
23. Corrosion rate was decreased with the increase in Pb content and also from centre to periphery of the deposit.

CHAPTER-8

SCOPE FOR FUTURE WORK

1. Atomizer or nozzle design should be such that it could produce preform of uniform thickness.
2. Lead can be replaced by the tin or graphite.
3. Hot or warm rolling can be performed in place of cold rolling.
4. Other mechanical processing of the preform like forging, extrusion etc. can be done.

REFERENCES

1. Kingsbury G.R., “Friction and wear of sliding bearing materials”, 10th ed. In: Olson D, editor. ASM handbook, Materials Park (OH): ASM International, 18, 743-756 (1992).
2. Fang X. and Fan Z., “Rheo-diecasting of Al–Si–Pb immiscible alloys”, Scripta. Mater., 54, 789-793 (2006).
3. Mohan S., Agarwala V. and Ray S., “Friction characteristics of stir-cast Al-Pb alloys”, Wear, 157, 9-17 (1992).
4. Abramov V.O., Abramov O.V., Sommer F. and Orlov D., “Influence of Si addition on the microstructure and the properties of Al-Pb base alloys prepared under quasi-weightlessness condition”, Mater Lett., 29, 67-71 (1996).
5. J.Z. Zhao 1, S. Drees, L. Ratke, “Strip casting of Al–Pb alloys — a numerical analysis”, Mater. Sci. Eng. A, 282, 262–269 (2000).
6. Rudrakshi G.B., Srivastava V.C., Pathak J.P. and Ojha S.N., “Spray forming of Al-Si-Pb alloys and their wear characteristics”, Mater. Sci. Eng. A, 383, 30-38 (2004).
7. An J., Liu Y.B., Lu Y. and Zhang Q.Y., “The formation of reacted film and its influence on tribological properties of extruded Al-Si-Cu-20-25Pb alloy under dry sliding”, J. Mater. Sci., 38, 1975-1982 (2003).
8. Yu F., Dwarakadasa D.S. and Ranganathan S., “Microstructure and mechanical properties of spray-formed Al-Si-Pb alloys”, J. Mater. Process. Technol., 137, 164-167 (2003).
9. Singh R.N., Sommer F., “Segregation and immiscibility in liquid binary alloys”, Rep. Prog. Phys., 60, 57-150 (1997).
10. Ratke L. and Diefenbach S. “Liquid immiscible alloys” Mater. Sci. Eng., R15, 263-347 (1995).
11. An J., Liu Y.B., Lu Y., Zhang Q.Y. and Dong C., “Dry sliding wear behavior of hot extruded Al-Si-Pb alloys in the temperature range 25-200 0C”, Wear, 256, 374-385 (2004).
12. Suwas S. and Upadhyaya G.S., "Powder metallurgy processing of aluminide intermetallics", Met. Mater. Proces., 7, 225-250 (1995).

13. An J., Liu Y.B. and Lu Y., "The influence of Pb on the friction and wear behavior of Al-Si-Pb alloys", Mater. Sci. Eng. A, 373, 294-302 (2004).
14. Mohan S., Agarwala V. and Ray S., "The Effect of Lead Content on the Wear Characteristics of a Stir-Cast Aluminium-Lead Alloy", Wear, 140, 83-92 (1990).
15. Pathak JP, Tiwari SN, Malhotra SL. "Production of high-leaded aluminium by impeller mixing", Met. Technol., 6, 442-445 (1979).
16. Panwar R.S., Pandey O.P., "Analysis of wear track and debris of stir cast LM13/Zr composite at elevated temperatures", Mater. Character., 75, 200-213 (2013).
17. Mohan S., Agarwala V. and Ray S., "Microstructure of Stircast Al-Pb Metal-Metal Composites", Mater. Trans. JIM, 33, 1057-1062, (1992).
18. Agarwala V, Satyanarayana KG, Agarwala RC, Garg R. "A study on the development and wear characteristics of rheocast Al-5Cu-2Pb alloy and Al-5Cu/Pb-18Sn wire composites", Mater. Sci. Eng. A, 327, 186-202 (2002).
19. Liu Y.Q., Qian M. and Fan Z., "Microstructure and mechanical properties of a rheo-diecast Mg-10Zn-4.5Al alloy", Mater. Trans., 46, 2221-2228 (2005).
20. Dey A.K., Poddar P., Singh K.K. and Sahoo K.L., "Mechanical and Wear properties of Rheocast and Conventional Gravity Die cast A356 alloy", Mater. Sci. Eng. A, 435-436, 521-529 (2006).
21. Suh Y. C. and Lee Z. H., "Nucleation of liquid Pb-phase in hypermonotectic Al-Pb melt and the segregation of Pb-droplets in melt-spun ribbon", Scripta Metall. Mater., 33, 1231-1237 (1995).
22. Zhao J. Z., Drees S. and Ratke L., "Strip casting of Al–Pb alloys — a numerical analysis", Mater. Sci. Eng. A, 282, 262-269 (2000).
23. Mohan S., Agarwala V. and Ray S., "Liquid-Liquid Dispersion for Fabrication of Al-Pb Metal-Metal Composites", Mater. Sci. Eng. A, 144, 215-219 (1991).
24. Guang R., Jing E. Z., Shemgqi X. and Pengliang L., "Formation of nanocrystalline and amorphous phase of Al–Pb–Si–Sn–Cu powder during mechanical alloying", Mater. Sci. Eng. A, 416, 45-50 (2006).
25. Zhang Y., Hao Y., Liu Z. and Chen G., "Production of rapidly solidified Al-Pb-Cu alloy by liquid stirring, ultrasonic gas atomization and liquid dynamic compaction", Mater. Sci. Eng., 98,119-121 (1988).
26. Singer A.R.E., "The principle of spray rolling of metals", Met. Matter. 4, 246–261 (1970).

27. Ojha K. V., Tomar A., Singh D. and Kaushal G. C., "Shape, microstructure and wear of hypoeutectic Al-Si alloys" Mat. Sci. Engg. A, 487, 591- 596 (2008).
28. Rudrakshi G.B., Srivastava V.C. and Ojha S.N., "Microstructural development in spray formed Al-3.5Cu-10Si-20Pb alloy and its comparative wear behaviour in different environmental conditions", Mater. Sci. Eng. A, 457, 100-108 (2007).
29. Liang X. and Lavernia E.J., "Solidification and microstructure evolution during spray atomization and deposition of Ni_3Al", Mater. Sci. Eng. A, 161, 221-235 (1993).
30. Gupta M., Mohamed F.A. and Lavernia E.J., "Heat transfer mechanism and their effects on microstructure during spray atomization and co deposition of metal matrix composites", Mater. Sci. Eng. A, 144, 99-110 (1991).
31. Anand S., Srivatsan S., Wu Yue and Lavernia E.J., "Processing, microstructure and fracture behavior of a spray atomized and deposited aluminum-silicon alloy", J. Mater. Sci., 32, 2835-2848 (1997).
32. Liang X., Earthman J.C. and Lavernia E.J., "On the mechanism of grain formation during spray atomization and deposition", Acta metall. mater. 40, 3003-3016 (1992).
33. Srivastava A.K., Anandani R.C., Dhar A. and Gupta A.K., "Effect of thermal conditions on microstructural features during spray forming", Mater. Sci. Eng. A, 304-306, 587-591 (2001).
34. Sharma M. M., "Microstructure and mechanical characterization of various modified 7XXX series spray formed alloys", Mater. Charact., 59, 91-99 (2008).
35. Ferrarini C.F., Bolfarini C., Kiminami C.S., Botta F W.J., "Microstructure and mechanical properties of spray deposited hypoeutectic Al-Si alloy", Mater. Sci. Eng. A, 375–377, 577-580 (2004).
36. Gouthama, Rudrakshi G. B. and Ojha S. N., "Spray forming and wear characteristics of liquid immiscible alloys", J. Mater. Process. Technol., 189, 224-230 (2007).
37. Payne R.D., Moran A.L. and Cammarata R.C., "Relating porosity and mechanical properties in spray formed tubulars", Scripta metal.et. Mater., 29, 907-912 (1993).
38. Srivastava V.C., Mandal R.K., Ojha S.N. and Venkateswarlu K., "Microstructural modifications induced during spray deposition of Al-Si-Fe alloys and their mechanical properties", Mater. Sci. Eng. A, 471, 38-49 (2007).
39. Lavernia E.J. and Wu Y., "Spray atomization and deposition", John Wiley and Sons, Chichester, 57 (1996).

40. Muller H.R., Ohla k., Zauter R. and Ebner M., "Effect of reactive elements on porosity in spray formed copper alloy billets", Mater. Sci. Eng. A, 383, 78-86, (2004).
41. Gui M., Kang S.B. and Lee J.M., "Influence of porosity on dry sliding wear behavior in spray deposited Al-6Cu-Mn/ SiC_p composite", Mater. Sci. Eng. A, 293, 146-156 (2000).
42. Goudar D.M. , Raju K., Srivastava V.C., Rudrakshi G.B., "Effect of copper and iron on the wear properties of spray formed Al–28Si alloy", Mater. Des., 51, 383-390 (2013).
43. Raju K., Harsha A.P., Ojha S.N., "Evolution of microstructure and its effect on wear and mechanical properties of spray cast Al–12Si alloy", Mater. Sci. Eng. A, 528, 7723-7728 (2011).
44. CAI Yuan-hua, LIANG Rui-guang, S U Zhan-pei, ZHANG Ji-shan, "Microstructure of spray formed Al-Zn-Mg-Cu alloy with Mn addition", Trans. Nonferrous Met. Soc. China, 21, 9-14 (2011).
45. Chaudhury S.K., Singh A.K., Sivaramakrishnan C.S., Panigrahi S.C., "Wear and friction behavior of spray formed and stir cast Al–2Mg–11TiO2 composites", Wear, 258, 759–767 (2005).
46. XiongBaiqing, Zhang Yongan, Wei Qiang, Shi Likai, XieChangan, Shang Chengjia, He Xinlai, "The study of primary Si phase in spray forming hypereutectic Al–Si alloy", J. Mater. Process. Technol.,137, 183–186 (2003).
47. Woo-Jin Kim, J.H. Yeon, J.C. Lee, Superplastic deformation behavior of spray-deposited hyper-eutectic Al–25Si alloy, J. Alloys Compd. 308, 237–243 (2000).
48. Srivastava V.C., Ghosal P., Ojha S.N., "Microstructure and phase formation in spray-deposited Al–18%Si–5%Fe–1.5%Cu alloy", Mater. Lett., 56, 797–801 (2002).
49. Whitton E.D.M., Stone I.C., Jones J.R., Grant P.S., Cantor B., "Isothermal grain coarsening of spray formed alloys in the semi-solid state", Acta Materialia, 50, 2517–2535 (2002).
50. Fuxiao Y., Jianzhong C., Ranganathan S., Dwarakadasa E.S., "Fundamental differences between spray forming and other semisolid processes", Mater. Sci. Eng. A, 304–306, 621–626 (2001).
51. Ha T.K., Park W.J., Ahn S., Chang Y.W., "Fabrication of spray-formed hypereutectic Al–25Si alloy and its deformation behaviour", J. Mater. Process. Technol., 130–131, 691–695 (2002).

52. Raghukiran N., Kumar R., “Processing and dry sliding wear performance of spray deposited hyper-eutectic aluminum–silicon alloys”, J. Mater. Process. Technol., 213, 401-410 (2013).
53. Kumar A., Ghosh S. and Dhindaw B.K., “Simulation of Cooling Rate of Alloy Drops during Spray Casting”, Trans. Indian Institute of Metals, 60, 2-3, (2007).
54. Shukla P., Mandal R.K. and Ojha S.N., “Microstructural Modifications Induced by Spray Forming of Al-Cu Alloys”, Mater. Sci. & Eng., 304, 583-586 (2001).
55. Shukla P., Mandal R.K. and Ojha S.N., “Non-equilibrium Solidification of Under cooled Droplets during Spray Atomization”, Bull. Mater. Sci., 24, 547-554 (2001).
56. Majumdar A.K., Shah H., Shukla P. and Barnwal J.P., “Effect of operating variables on shape of “Fish-hook” curves in cyclones”, Min. Eng., 20, 204-206 (2007).
57. Liu P., Dunlop G.L. and Arnberg L., “Microstructural development in a rapidly solidified Al-5Mn-2.5Cr alloy”, Mater. Sci. & Eng., 98, 437-441, (1988).
58. Grant P.S., “Spray forming”, Progr. Mater. Sci., 39, 497–545 (1995).
59. Zhang J.G., Shi H.S., Sun D.S., “Research in spray forming technology andits applications in metallurgy”, Mater. Process Technol., 138, 357–360 (2003).
60. Lavernia E.J., Grant N.J., Spray deposition of metal: a review, Mater. Sci. Eng. 98, 381–394 (1988).
61. Wang F., Ma Y., Zhang Z., Cui X., Jin Y., “A comparison of the sliding wear behavior of a hypereutectic Al–Si alloy prepared by spray-deposition and conventional casting methods”, Wear, 256, 342–345 (2004).
62. Sundaram K., Babu N.H., Scamans G.M., Eskin D.G. and Fan Z., “Solidification behaviour of an AA5754 Al alloy ingot cast with high impurity content”, Int. J. of Mater. Rese., 103, 1228-1234 (2012).
63. Singh K.K. and Mishra R.R., “Minimizing the casting defect using casting simulation-A case study of an industrial casting”, Indian Foundry Journal, 57, 49-52 (2011).
64. Singh K.K., Patrudu B.V. and Upadhyaya R., “Indentification and Control of Micro Porosity for Al-Alloy wheel castings”, Int. J. of Eng. Rese. & Technol., 3, 5, (2014).
65. Gibbons G.J. and Hansell R.G., “Down-Selection and Optimisation of Thermal-Sprayed Coatings for Aluminium Protection and Upgrade”, J. Therm. Spray Tech., 15, 340, 1059-9630 (2006).
66. Gibbons G.J. and Hansell R.G., “Thermal-Sprayed Coating on Aluminium for Mould Tool Protection and Upgrade” J. Mater. Process. Technol., 204, 184-191 (2008).

67. Wimpenny D.I. and Gibbon G.J., "Metal spray tooling for composite forming", J. Mater. Process. Technol., 138, 443-448 (2003).
68. Hariprasad S, SastrySML, Jerina KL and Lederich RJ "Microstructures and mechanical properties of dispersion-strengthened high-temperature Al-8.5Fe-1.2V-1.7Si alloys produced by atomized melt deposition process", Metall. Trans. 24, 865-873 (993).
69. Rizzi P., Habib A., Castellero A. and Battezzati L., "Constrained deformation of an Al based amorphous alloy by cold rolling", J. Alloys Compd., 5095**,** 5275-5278 (2011).
70. Singh D., Nageswara R. P. and Jayagandhan R., "Effect of deformation temperature on mechanical properties of ultrafine grained Al-Mg processed by rolling", Mater. Des., 50, 646-655 (2013).
71. Machado R., Kasama A. H., Jorge Jr A. M., Kiminami C. S., BottaFo W. J., Bolfarini C., "Evolution of the texture of spray formed Fe-6.5 wt%Si-1.0 wt% Al alloy during warm rolling", Mater. Sci. Eng. A, 449-451, 854-857 (2007).
72. Wang X.F, Zhao J.Z, HE J, Zhuang H.Q, "Hot rolling characteristics of spray formed AZ91 magnesium alloy", Trans. Nonferrous Met. Soc. China 17, 238-243 (2007).
73. Panigrahi S.K., Jayaganthan R., "Effect of rolling temperature on microstructure and mechanical properties of 6063 Al alloy", Mater. Sci. Eng. A 492, 300–305 (2008).
74. Gholinia A., Humphreys F. J., Prangnell P. B., "Production of ultra-fine grain microstructures in Al–Mg alloys by coventional rolling", Acta Materialia 50 4461–4476 (2002).
75. Zhana M., Chen Z., Yan H., "Two novel rolling processes of porous metal preforms prepared by spray deposition technique using conventional rolling mill", J. Mater. Process. Technol., 202, 269–274 (2008).
76. Ghosh S., Gabane P., Bose A. and Chakraborti N., "Modeling of Recrystallization in Cold Rolled Copper using Inverse Cellular Automata and Genetic Algorithms", Computational Mater. Sci., 45, 96-103 (2009).
77. Sahoo S. and Ghosh S., "Effect of rolling speed on microstructure of Al-33wt. % Cu alloy strip prepared by twin roll strip casting", Mater. Sci. Forum, 710, 192-196, (2012).
78. Jianjun Z., Yimin G., Jiandong X., Xiaowei W., Shengqiang M. and Baohua C., "Effect of Hot Forging on Microstructure and Abrasion Resistance of Fe-B Alloy", Tribol. Trans. 56, 461-468 (2013).

79. Rao P.N., Singh D., Jayagandhan R., Mechanical properties and microstructural evolution of Al 6061 alloy processed by multidirectional forging at liquid nitrogen temperature, Mater. Des., 56 97-104 (2014).
80. Dayanand M. Goudar, K. Raju b, V.C. Srivastava, G.B. Rudrakshi, "Effect of secondary processing on the microstructure and wear behaviour of spray formed Al–30Mg2Si–2Cu alloy", Mater. Des., 47 489-496 (2013).
81. Godinho H. A., Beletati A. L. R., Giordano E. J., Bolfarini C., "Microstructure and mechanical properties of a spray formed and extruded AA7050 recycled alloy", J Alloys Compd. 586, 139-142 (2014).
82. An J., Dong C., Zhang Q. Y., "Improvement of the wear behaviour of stircast Al-Si-Pb alloys by hot extrusion", Tribol. Int., 36, 25-34 (2003).
83. Mazzer E.M., Afonso C.R.M., Bolfarini C. and Kiminami C.S., "Microstructure study of Al 7050 alloy reprocessed by spray forming and hot extrusion and aged at 121 ^{0}C", Intermetallics, 43, 182-187 (2013).
84. Mazzer E.M., Afonso C.R.M., Galano M., Kiminami C.S. and Bolfarini C., "Microstructural evolution and mechanical properties of Al-Zn-Mg-Cu alloy reprocessed by spray forming and heat treated at peak aged condition", J. Alloys Compd., 579, 169-173 (2013).
85. Liu J., Backmark U., Arnberg L., Bäckström N., Grinder O. and Savage S., "Hot extrusion and mechanical properties of rapidly solidified Al and Cu alloy powders", Mater. Sci. Eng., 98, 419-423, (1988).
86. Deshmukh A.R., Sundararajan T., Dube R.K., Bhargava S., "Analysis of cold densification rolling of a sintered porous metal strip", J. Mater. Process. Technol., 84, 56-72 (1998).
87. Tripathy M.R., Dube R.K. and Koria S.C., Rolling behaviour of steel backed spray deposited Al–Snstrip, J. Mater. Process. Technol., 190**,** 342-349 (2007).
88. Zhan M.Y., Chen Z.H., Yan H.G., Xia W.J., "Deformation behaviors of porous 4032 Al alloy perform prepared by spray deposition during hot rolling", J. Mater. Process. Technol., 182, 174–180 (2007).
89. Louaisil K., Dubar M., Deltombe R., Dubois A., Dubar L., "Analysis of interface temperature, forward slip and lubricant influence on friction and wear in cold rolling", Wear, 266, 119-128 (2009).

90. Panagopoulos C.N. and Georgiou E.P., “Cold rolling and lubricated wear of 5083 aluminium alloy”, Mater. Des., 31, 1050-1055 (2010).
91. Zhen L., Chen J., Yang S., Shao W., Dai S., “Development of microstructures and texture during cold rolling in AA 7055 aluminum alloy”, Mater. Sci. Eng. A, 504, 55–63 (2009).
92. Wang D., Ma Z.Y., Gao Z.M., “Effects of severe cold rolling on tensile properties and stress corrosion cracking of 7050 aluminum alloy”, Mater. Chem. Phys., 117, 228–233 (2009).
93. Liu W.C., Man C.-S., Raabe D., “Effect of strain hardening on texture development in cold rolled Al–Mg alloy”, Mater. Sci. Eng. A, 527, 1249–1254 (2010).
94. Narayanan P.R., Suwas S., Sreekumar K., Sinha P.P. and Ranganathan S., "Influence of Crystallographic Texture on Mechanical Properties in Cold Rolled 7XXX Series Al Alloys Used in Space Applications", Mater. Sci. Forum, 710, 539-544 (2012).
95. Gurao N.P., Kumar P., Bhattacharya B., Haldar A. and Suwas S., "Evolution of Crystallographic Texture and Microstructure during Cold Rolling of Twinning-Induced Plasticity (TWIP) Steel: Experiments and Simulations", Metall. Mater. Trans. A, 43, 5193-5201 (2012).
96. Srivastava V.C., Mondal R.K. and Ojha S.N., “Microstructure and mechanical properties of Al-Si alloys produced by spray forming process”, Mater. Sci. Eng. A, 304-3006, 555-558 (2001).
97. Kaur K. and Pandey O.P., “Microstructural characteristics of spray formed Zr sand reinforced LM13 composite”, J. Alloys Compd., 503, 410-415 (2010).
98. Anil M., Srivastava V.C., Ghosh M.K., Ojha S.N., “Influence of tin content on tribological characteristics of spray formed Al-Si alloys”, Wear 268, 1250-1256 (2010).
99. Wang F., Liu H., Ma Y., Jin Y., “Effect of Si content on the dry sliding wear properties of spray-deposited Al-Si alloy”, Mater. Des., 25, 163-166 (2004).
100. K.L. Moore, J.M. Sykes, S.C. Hogg, P.S. Grant, ‘Pitting corrosion of spray formed Al-Li-Mg alloys’, Corros. Sci., 50, 3221-3226 (2008).
101. W.d. Cai, E.J. Lavernia, ‘Modeling of porosity during spray forming’, Mater. Sci. Eng. A, 226-228, 8-12 (1997).
102. Tomar A. and Singh D., “Porosity in disk shape spray formed Al-Si-Pb alloy preform”, Powder Metall. Min., 2, 1-4 (2012).

103. Candan E., “Effect of alloying additions on the porosity of SiCp preforms infiltrated by aluminium”, Mater. Lett., 60, 1204-1208 (2006).
104. Hamid A.A., Ghosh P.K., Jain S.C. and Ray S., “Influence of particle content and porosity on the wear behaviour of cast in situ Al(Mn)-Al2O3(MnO2) composite”, Wear, 260, 368-378 (2006).
105. Zhang Lin, QU XuanHui, Duan Bo Hua, He Xin Bo, Qin Ming Li, ‘Effect of porosity on wear resistance of SiCp/Cu composites prepared by pressure less infiltration’, Trans. Nonferrous Met. Soc. China 18, 1076-1082 (2008).
106. Mervin A.H., Maiti R., Mitra R. and Chakraborty M., “Wear behaviour of cast and mushy state rolled Al-4.5Cu alloy and in-situ Al4.5Cu-5TiB2 composite”, Wear, 265, 1606-1618 (2008).
107. Mondal D.P. and Das S., “High stress abrasive wear behaviour of Al hard particles composites: Effect of experimental parameters, particle size and volume fraction”, Tribol. Int., 39, 470-478 (2006).
108. Bauri R. and Surappa M.K., “Sliding wear behaviour of Al-Li-SiCp composites”, Wear, 265, 1756-1766 (2008).
109. Barbucci A., Delucchi M., Panizza M., Sacco M. and Cerisola G., “Electrochemical and corrosion behaviour of cold rolled AISI 301 in 1 M H_2SO_4”, J. Alloys Compd., 317-318, 607-611 (2001).
110. Ramachandra M. and Radhakrishna K., “Effect of reinforcement of flyash on sliding wear, slurry erosive wear and corrosion behaviour of Al-matrix composite”, Wear, 262, 1450-1462 (2007).
111. Ahlatci H., “Wear and corrosion behaviour of extruded Al-12Si-XMg alloys”, Mater. Lett., 62, 3490-3492 (2008).
112. Hamilta de Oliveria Santos, Fernando Morais dos Reis, Clarice Teruiunioshi, JesualdoLuiz Rossi, Isolda Costa, “Corrosion performance of Al-Si-Cu hypereutectic alloys in a synthetic condensed automotive solution”, Mater. Rese., 8(2) 155-159, (2005).
113. Osorio W.R., Garcia L.R., Goulart P.R. and Garcia, “Effect of eutectic modification and T4 heat treatment on mechanical properties and corrosion resistance of an Al-9 Wt% Si casting alloy”, Mater. Chem. Phys., 106, 343-349 (2007).

114. Heiberg G. and Arnberg L., “Investigation of the microstructure of the Al-Si eutectic in binary aluminum-7 wt% silicon alloys by electron backscatter diffraction”, J. Light Metals, 1, 43-49 (2001).
115. Mervin H A, Sankar C, Mitra R, and M Chakraborty The Minerals, Metals and Materials Society and ASM International 2110 (2007).
116. Sahu K.K., Dube R.K. and Koria S.C., “Aspects of porosity formation in spray deposited thin aluminium strip”, Powder Metall., 52, 135-144 (2009).
117. Evans M., “Optimization of manufacturing processes: A Response Surface Approach”, Maney Publishing, London, 29 (2003).
118. Pariona M.M., Bolfarini C., Santos R.J.D., Kiminami C.S., “Application of mathematical simulation and the factorial designmethod to the optimization of the atomization stage in thespray forming of a Cu±6% Zn alloy”, J. Mater. Process. Technol., 102, 221-229 (2000).
119. Shivnath R., Gupta P.K.S. and Eyre T.S., Br. Foundryman, 77 349 – 356. and ASTM Source Book on Wear, ASTM, Philadelphia, PA, 1979, 185, (1970).
120. Yaseen R.S. and Dwarkadasa E.S., “Wear of aluminium under dry sliding conditions”, Wear, 84, 375-379 (1983).
121. Kadhim M.J. and Dwarakadasa E.S., “Some studies of wear of an AI-22wt.%Si alloy under dry sliding conditions”, Wear, 82, 377-380 (1982).
122. Rohatgi P. K., Riu Y. and Ray S., “Friction, Lubrication and Wear Technology”, American Society for Metals, Metals Park, OH, 85, (1992).
123. Zhenhua C., Jie T., Gang C., Dingfa F. and Hongge Y., “Effect of the silicon content and thermomechanical treatment on the dry sliding wear behavior of spray-deposited Al–Si/SiCp composites”, Wear, 262, 362–368 (2007).
124. Bindumadhavan P.N., Chia T.K. and Chandrasekaran M., “Effect of particle porosity clusters on tribologicalbehavior of cast aluminum alloy A356–SiCp metal matrix composites”, Mater. Sci. Eng. A 315, 217–226 (2001).
125. Lee H.L., Lu W.H. and Chan S.L.I., “Abrasive wear of powder metallurgy Al alloy 6061-SiC particle composites”, Wear, 159, 223–231 (1992).
126. Jahanmir S., Abrahamson E. P., II, and Suh N. P., "Sliding Wear Resistance of Metallic Coated Surface," Wear, 40, 75-84 (1976).
127. Jahanmir S., Suh N. P. and Abrahamson E. P., II, "The Delamination Theory of Wear and the Wear of a Composite Metal Surface," Wear, 32, 33-49 (1975).

128. Gui M., Kang S.B. and Lee J.B., “Influence of porosity on dry sliding wear behavior in spray deposited Al–6Cu–Mn:SiCp composite”, Mater. Sci. Eng., A293, 146–156 (2000).
129. Dwivedi D.K., “Wear behaviour of cast hypereutectic aluminium silicon alloys”, Mater. Des., 27, 610-616 (2006).
130. Sarkar A.D. and Clarke J., “Friction and wear of aluminium-silicon alloys”, Wear, 61, 157-167 (1980).
131. Panagopoulos C.N. and Georgiou E.P., “Wear behaviour of 5083 wrought aluminium alloy under free corrosion conditions”, Mater. Surface & Interf., 1, 161-164 (2007).
132. Lee C. K., “Effects of Pb and Cu additives on microstructure and wear corrosion resistance behaviour of PM Al–Si alloys”, Powder Metall., 49, 334-344 (2006).
133. Panagopoulos C.N., Georgiou E.P. and Gavras A.G., “Corrosion and wear of 6082 aluminum alloy”, Tribol. Int., 42, 886-889 (2009).

APPENDIX-A

Measured and theoretical density determination

Measured density of sample (ρ_{sample}) can be calculated by Archimedes method:-

Weight of sample in water(w_2) + weight of water displaced = weight of sample in air (w_1)

Weight of water displaced = $w_1 - w_2$

$$\rho_w . V_{sample} = w_1 - w_2 \quad (1)$$

where, ρ_w is density of water

$$\text{Or,} \quad V_{sample} = \frac{w_1 - w_2}{\rho_w} \quad (2)$$

Now,

$$\rho_{sample} = \frac{w_1}{V_{sample}} \quad (3)$$

From equations (2) and (3) measured density of sample is given by

$$\rho_{sample} = \left(\frac{w_1}{w_1 - w_2} \right) \rho_w$$

Now, Theoretical density of sample was determined by two methods and it was found to be having the same value.

Method-1

The density was measured from the sample prepared by hot rolling at 550 K to 70 % thickness of the same composition but casted alloy as reported in reference [48].

Method-2

$$Theoretical\ density = \frac{total\ weight}{total\ volume}\ gm/cc \quad (4)$$

Assuming the total volume of the alloy equal to the sum of volumes of alloying elements (as both are almost insoluble in aluminum) the theoretical density of an alloy (for example Al-6Si-15Pb) can be determined as follows:-

Let, total weight of alloy = 100 gm

So, $total\,volume = \frac{79}{2.7} + \frac{6}{2.33} + \frac{15}{11.34}$

$= 33.16\ cm^3$

Using these values in equation (5) theoretical density of Al-6Si-15Pb alloy is given by

$Theortical\ density = \frac{100}{33.16}$

$\approx 3.02\ gm/cc$

APPENDIX-B

Calculation of d-spacing, lattice parameter and crystallite size

Table 1: Calculation of d-spacing, lattice parameter and phases of Al-6Si alloy.

Peak number	**2θ**	**θ**	**Sinθ**	**$(Sin\theta)^2$**	**N = $(Sin\theta)^2$/ $(Sin\theta)^2_{min}$ x 3 (odd integer)**	**N**	**hkl**	**Phases Si or Al**	**d-spacing (A^o)**	**Lattice parameter (A^o)**
1	28.398	14.199	0.24516	0.06010	2.99	3	111	Si	3.142	5.442
2	38.435	19.217	0.32899	0.10823	3	3	111	Al	2.342	4.056
3	44.694	22.347	0.38003	0.14442	4.0029	4	200	Al	2.027	4.054
4	47.288	23.644	0.40086	0.16069	8.0200	8	220	Si	1.922	5.436
5	56.119	28.059	0.47038	0.22126	11.043	11	311	Si	1.638	5.432
6	65.106	32.553	0.53807	0.28952	8.0248	8	220	Al	1.432	4.050
7	78.191	39.095	0.63061	0.39767	11.022	11	311	Al	1.222	4.052
8	82.386	41.193	0.65859	0.43375	12.022	12	222	Al	1.17	4.052
9	88.001	44.000	0.69466	0.48255	24.084	24	422	Si	1.109	5.432
10	99.032	49.516	0.76058	0.57849	16.033	16	400	Al	1.013	4.052

For d-spacing (2θ = 38.435),

$$n\lambda = 2d.Sin\theta$$

$$d = 1x1.54/ (2 \times 0.3289)$$

$$d = 2.342$$

For lattice parameter (2θ = 38.435),

$$a = d. (h^2+k^2+l^2)^{1/2}$$

$$= 2.342 \times (1 +1+1)^{1/2}$$

$$= 4.056$$

Table 2: Calculation of interplanner spacing and FWHM.

hkl plane	Peak position, d spacing & FWHM											
	Al-6Si			Al-6Si-10Pb			Al-6Si-20Pb			Al-6Si-30Pb		
	θ	β	d	θ	β	d	θ	β	d	θ	β	d
[111]Si	28.398	0.227	3.142	28.603	0.227	3.120	28.517	0.227	3.130	28.670	0.227	3.113
Pb	-	-	-	31.458	0.227	2.843	31.353	0.227	2.853	31.509	0.227	2.839
Pb	-	-	-	36.443	0.227	2.465	36.345	0.227	2.471	36.496	0.227	2.462
[111]Al	38.435	0.227	2.342	38.652	0.227	2.329	38.556	0.227	2.335	38.710	0.227	2.326
[200]Al	44.694	0.227	2.027	44.900	0.227	2.018	44.812	0.303	2.022	44.962	0.227	2.016
[220]Si	47.288	0.227	1.922	47.464	0.227	1.915	47.398	0.227	1.918	47.548	0.227	1.912
Pb	-	-	-	52.428	0.303	1.745	52.324	0.227	1.748	52.475	0.227	1.743
[311]Si	56.119	0.303	1.638	56.286	0.303	1.634	56.224	0.303	1.636	56.364	0.303	1.632
Pb	-	-	-	62.344	0.227	1.489	62.249	0.227	1.491	62.389	0.303	1.488
[220]Al	65.106	0.303	1.432	65.297	0.227	1.429	65.212	0.227	1.430	65.356	0.227	1.427
[311]Al	78.191	0.378	1.222	78.387	0.378	1.219	78.303	0.303	1.221	78.421	0.378	1.219
[222]Al	82.386	0.303	1.170	82.574	0.378	1.168	82.488	0.378	1.169	82.624	0.378	1.167
[422]Si	88.001	0.303	1.109	88.329	0.303	1.106	88.157	0.454	1.108	88.274	0.303	1.107
[400]Al	99.032	0.227	1.013	99.197	0.303	1.012	99.130	0.227	1.012	99.247	0.227	1.011

For FWHM (2θ = 38.435),

Step 1: Half of the peak height.

Step 2: X1 and X2 position calculation from X-axis (i.e. 2 θ)

Step 3: X2-X1 gives FWHM

Step 4: For calculation convert this values into radian by multiplying the factor of 3.14/180

For hkl planes (2θ = 38.435),

$$N = (\sin\theta)^2/(\sin\theta)^2_{min} \times 3 \text{ (odd integer)}$$

$$N = 0.10823/ 0.10823 = 1 \times 3 = 3$$

$$N = 3 = (111)$$

For crystallite size (2θ = 38.435),

$$D = (0.94 \times \lambda)/(\beta \times \cos\theta)$$

$$= (0.94 \times 1.54) / (0.227 \times (3.14/180) \times 0.9442)$$

$$= 387.16 \times 10^{-10}$$

$$= 38.71 \text{ nm}$$

APPENDIX-C

Calculation of texture coefficient

Table 3: The effect of rolling (% thickness reduction) on experimental reflection plane of crystallographic plane (hkl).

	Peak intensity and peak intensity ratio									
hkl	**0%**	**R exp**	**20%**	**R exp**	**40%**	**R exp**	**60%**	**R exp**	**80%**	**R exp**
111	51919.93	51.25	27836.88	57.43	24943.53	52.83	24988.88	52.95	20995.36	50.51
200	23937.19	23.63	10589.12	21.84	11421.35	24.19	11432.08	24.22	10485.22	25.22
220	8797.86	8.685	4634.52	9.56	5455.41	11.55	5360.47	11.35	4945.96	11.90
311	13704.77	13.52	4276.76	8.82	4356.56	9.228	4303.07	9.118	4071.02	9.795
222	2935.97	2.898	1131.07	2.33	1031.1	2.184	1108.33	2.348	1062.77	2.557
$\sum I_{(hikili)}$	101295.7		48468.35		47207.95		47192.83		41560.33	

Table 4: The effect of rolling (% thickness reduction) on texture coefficient of a hkl crystallographic plane.

Al reflections	$h^2+k^2+l^2$	R theoretical [90]	TC (0%)	TC(20%)	TC(40%)	TC(60%)	TC(80%)
(111)	3	50	1.025116	1.148662	1.056751	1.059012	1.010356
(200)	4	23.5	1.005575	0.929681	1.029519	1.030817	1.073571
(220)	8	11	0.789575	0.869268	1.050557	1.032605	1.08188
(311)	11	12	1.127456	0.735318	0.769037	0.759838	0.816287
(222)	12	3.5	0.828119	0.66675	0.624047	0.671004	0.730621

$$TC_{(hkl)} = R_{exp(hkl)} / R_{theo(hkl)} \quad (1)$$

$$R_{(hkl)} = (I_{(hkl)} / \sum (I_{(hikili)}) \, x \, 100 \quad (2)$$

For R_{hkl} calculation (hkl -111)

$$R_{(hkl)} = (I_{(hkl)} / \sum (I_{(hikili)}) \, x \, 100$$

$$= (51919.93/101295.7) \times 100$$

$$= 51.25$$

For Al-6Si, Texture coefficient (TC) calculation (hkl - 111),

$$TC_{(hkl)} = R_{exp(hkl)} / R_{theo(hkl)}$$

$$= 51.25/50$$

$$= 1.02511$$

APPENDIX-D

Some publications from this work

1. Dry sliding wear behavior of spray formed ZrSio4 reinforced Al-Si-Sn alloy.
   Rashmi Mittal, Devendra Singh
   Adv. Mater. Lett. 2012, 3(1), 38-43.

2. Thickness uniformity and microstructure of disk shape spray formed Al-Si-Pb alloys.
   Rashmi Mittal, Aruna Tomar, Devendra Singh
   Adv. Mater. Lett. 2012, 3(1), 55-63.

3. Effect of cold rolling on the mechanical properties of spray cast Al-6Si-20Pb alloys.
   Rashmi Mittal, Devendra Singh
   Adv. Mater. Rese. 2012, 585, 402-406.

4. Wear Behavior of Disk Shape Spray Formed Al-Si-Pb Alloy Preform.
   Rashmi Mittal, Aruna tomar and Devendra singh
   J. Mater. Eng. Process. 2014, 23, 975–981.

5. Dry sliding wear behaviour of cold rolled Spray cast Al-6Si alloy.
   Rashmi Mittal, Devendra Singh
   Trans. Indian Ins. Metals. 2014, 67(4), 551-557

6. Strength and Elongation of Spray Formed Al-Si-Pb Alloy.
   Aruna Tomar, **Rashmi Mittal**, Devendra Singh
   Int. J. Min. Met. Mat. (**Accepted 2014**).

7. **Rashmi Mittal**, Devendra Singh. "Effect of Secondary Processing on the Microstructure and Wear Performance of Spray cast Al-6Si-20Pb Alloy", International Conference on Smart Technologies for Mechanical Engineering - (STME), New Delhi, India, October 25-26, 2013.

8. **Rashmi Mittal**, Devendra Singh. “Tribology Characteristics of Cold Rolled Spray Cast Al–6Si–20Pb Alloy”, Proceedings of International Conference on Advances in Tribology and Engineering Systems, Springer India 2014, 431-439.